Fall 12-14-2021

The Timing of Smectite-To-Illite Transformation in Cretaceous Rocks of Powder River Basin

Benard O. Uruowhe
Georgia State University

The Timing of Smectite-To-Illite Transformation in Cretaceous Rocks of Powder River Basin

by

Benard Uruowhe

Under the Direction of W. Crawford Elliott, Ph.D.

A Thesis Submitted in Partial Fulfillment of the Requirements for the Degree of

Master of Science

in the College of Arts and Sciences

Georgia State University

2021

ABSTRACT

Mixed-layer illite/smectite (I-S) is an important semi-quantitative geothermometer for the study of thermal histories of sedimentary basins. The purpose of this research is to examine the relationship between smectite illitization and hydrocarbon formation and migration in the Cretaceous Mowry shale of the Wyoming Powder River Basin. The I-S ($R \geq 1$) and the measured K-Ar ages of I-S ranging from 49 Ma to 64.9 Ma were observed in the clay fractions of the Mowry Shale. The measured ages of I-S correspond to burial temperatures ~110 C. While maximum burial occurred later in the Miocene Epoch for the Mowry Shale. The extent of illitization in the Mowry Shale bentonites was limited by the availability of potassium.

INDEX WORDS: Cretaceous, Bentonites, I-S mixed layer, K-Ar age, X-ray diffraction, Mowry Shale, Powder River Basin.

The Timing of Smectite-To-Illite Transformation in Cretaceous Rocks of Powder River Basin

by

Benard Uruowhe

Committee Chair: W. Crawford Elliott

Committee: Hassan A. Babaie

Daniel Gebregiorgis

J. Marion Wampler

Electronic Version Approved: December 2021

Office of Graduate Services

College of Arts and Sciences

Georgia State University

December 2021

DEDICATION

I dedicate this study to the Almighty God, the source of wisdom and knowledge, as well as to my late father, Pa Daniel Uruowe, who sacrificed everything to make my dream a reality.

ACKNOWLEDGEMENTS

I would like to convey my heartfelt appreciation to Dr. Crawford Elliott, my mentor and adviser, for his encouragement, motivation, and unwavering efforts in ensuring the success of my M.S. Degree Program at GSU. His correction, patience, and guidance were invaluable in the completion of my thesis.

I would like to express my gratitude to Devon Energy company for granting me the privilege and chance to access the company's data collection for this project. My collaborator, Dr. Marion Wampler, deserves special thanks for sharing his knowledge of K-Ar geochronology with me and not forgetting his spirited efforts in ensuring the completion of the K-Ar analysis aspect of this study.

It is with pleasure that I appreciate Dr. Daniel Gebregiorgis for taking time to teach me about the XRD analysis equipment used in my research and for agreeing to serve on my committee. I am grateful to Dr. Hassan Babaie, whom in spite of the short notice agreed to serve as a member of my research committee. Special thanks to Georgia State University and the Geosciences Department at large, for providing a conducive research environment and for the financial support in the form of stipends every semester.

To my fiancée, Faith Kirkland, I can’t thank you enough for your prayers, moral and emotional support throughout the period of writing this report, my story is incomplete without you.

My deepest gratitude goes to God for his extravagant grace, infinite mercy, and great love for me. All glory to my lord and savior, who is the reason I've gotten this far.

TABLE OF CONTENTS

ACKNOWLEDGEMENTS ..... **V**

LIST OF TABLES ..... **IX**

LIST OF FIGURES ..... **X**

LIST OF ABBREVIATIONS ..... **XII**

1 INTRODUCTION **1**

1.1 Smectite, Illite, and the Smectite-to-Illite Reaction **1**

1.2 Previous Studies on Smectite to Illite Transformation **3**

1.3 Kinetics of Smectite-Illite Transformation **6**

1.4 Significance of Smectite-to-Illite Transformation and Relation to Hydrocarbon Exploration **11**

1.5 Powder River Basin **13**

1.6 Study Objectives **18**

2 METHODS AND METHODOLOGY **19**

2.1 Sample Collection, Location, and Description of Samples. **19**

2.2 Sample Preparation for Clay Mineral Identification and K-Ar Geochronology **20**

2.2.1 Soaking and Disaggregation of Soil Sample ***20***

2.2.2 Sample Treatment and Removal of Carbonate Cements, Gross Organic Matter, and Iron (III) Oxides ***20***

2.2.3 Separation of Clay, Silt, and Sand Fraction ***21***

2.2.4 Oriented Mount Clay and X-Ray Diffraction Analyses 22

2.2.5 X-ray Diffraction Analyses 23

2.2.6 Mineral Identification 25

2.3 K-Ar Geochronology 28

2.3.1 Extraction and measurement of ^{40}Ar from clay 29

2.3.2 Potassium determination 32

2.3.3 K-Ar Age Calculation 33

3 RESULTS 34

3.1 Clay Fraction Mineralogy 34

3.1.1 Bentonites XRD Results 34

3.1.2 Reworked Bentonites XRD Result. 38

3.2 K-Ar Geochronology 40

4 DISCUSSION 42

5 CONCLUSION 50

REFERENCES 52

APPENDICES 62

Appendix A: X-ray Analyses 62

Appendix A.1 Method: Sample Preparation and Procedure 62

Appendix A.2 X-Ray Diffraction Patterns. 64

The patterns were labeled with specific d-spacings (Glycol Solvated, Air Dried and Heated). X-Ray Diffraction Patterns for the Mowry Bentonites Samples. 64

Appendix A.3: X-Ray Diffraction Patterns for the Mowry Reworked Bentonites. 89

Appendix B: K-Ar Method 104

B1 Sample Preparation and Procedure for K-Ar Analyses 104

B 2: Extraction and measurement of argon from clay 105

Setup Checklist 105

Argon Extraction and Cleanup 106

ARGON TRANSFER 108

USUAL ARGON TRANSFER 108

ALTERNATIVE ARGON TRANSFER 108

ISOTOPIC ANALYSIS OF ARGON 109

EXTRACTION LINE SETUP 109

MASS SPECTROMETER SETUP 110

B 3 Extraction Line Daily Startup 110

B 3 Extraction Line Daily Shutdown 112

LIST OF TABLES

Table 1-1 Showing estimated percentage illite, temperatures for changes in mixed- layer illite/smectite (I-S) in Hoffman and Hower and short- life geothermal I-S geothermometry models. Modified from Pollastro (1993). 12

Table 2-1 Showing Devon's rock samples and their corresponding depth in the cretaceous Mowry shale, Powder River Basin. 19

Table 2-2 Specifications of XRD Scan. Adapted from (Murshed, 2021)..... 24

Table 2-3 Observed mineral diagnostic diffraction d-spacing values (d_{hkl}). 26

Table 2-4 Adapted from Moore and Reynolds, table 8.3., The position (CuKα) of useful reflection for estimating percent illite in illite/EG-smectite 26

Table 3-1 Mineralogy of < 2-micron fraction of Bentonites. 37

Table 3-2 Mineralogy of < 2-micron fraction of Reworked Bentonites. 39

Table 3-3 Result of K-Ar Dating 41

LIST OF FIGURES

Figure 1-1 Schematic diagram of the proposed neoformation mechanism for the conversion of smectite to illite in bentonites. From Nadeau et a. (1985). 5

Figure 1-2 Schematic diagram illustrating the transformation mechanisms as proposed by Altaner and Ylagan (1997). Image source: (Bauluz,2007). 5

Figure 1-3 Pictorial view of the mixed-layer transformation mechanism. Chemical exchange of reactant and product species occurs through the hydrous interlayer region. Source: Altaner and Ylagan (1997)..... 9

Figure 1-4 Stacking order of mixed-layer I-S represented as a MacEwan crystallite and as an aggregate of fundamental particles. From Altaner and Ylagan (1997). 10

Figure 1-5 X-ray powder diffraction patterns of ethylene glycol-saturated mixed-layer I-S with different expandability and Reichweite (R) ordering calculated with the modeling program NEWMOD. From Pollastro (1993)..... 12

Figure 1-6 The connection between changes in mixed-layer I-S and oil generation temperature, diagenesis, and vitrinite reflectance. Figure from (Jiang, 1979)..... 13

Figure 1-7 Location map of the Powder River Basin. From Lynds (2013). 15

Figure 1-8. Generalized cross section of the Powder River Basin. From Lichtner et al. (2020).. 15

Figure 1-9 : Map showing the study area and stratigraphic fill of the Powder River Basin. Arrow points to the Mowry Shale. Figure modified from SHALE EXPERTS, Powder River Basin Overview..... 17

Figure 1-10. Stratigraphic column and succession intervals of Lower Cretaceous strata in the Powder River Basin including identification of the Mowry Total Petroleum System (TPS). From Anna (2009). 17

Figure 2-1 Basic stages in sample preparation for clay mineral identification..... 22

Figure 2-2 Percentage of illite layers vs. 002($_{10Å}$)/003($_{17Å}$) d-spacing (Å)..... 27

Figure 2-3 Photograph of argon extraction line showing the placement of the liquid nitrogen, used to trap condensable gases, and the MS 10 mass spectrometer (left). 30

Figure 2-4 Aspects of extraction and measurement of ^{40}Ar from clay. 31

Figure 2-5. Perkin Elmer 3110 atomic-absorption spectrophotometer (left) and Mettler M-220 analytical balance (right)..... 32

Figure 3-1 X-ray diffraction pattern of oriented, ethylene glycol-solvated Iberlin < 2-µm clay. 36

Figure 3-2 X-ray diffraction pattern of oriented, ethylene glycol-solvated Cross Creek < 2-µm clay. 36

Figure 4-1 The connection between changes in mixed-layer I-S and oil generation, temperature, diagenesis, and vitrinite reflectance. Figure modified from Jiang (2012) by the addition of arrow showing the link of the R ≥ 1stacking order of I-S with the temperature observed of the "oil generation window" in Cretaceous rocks. 45

Figure 4-2 Burial history of the Powder River Basin at the State Wright well location. Image source: Devon Energy Corporation. 46

Figure 4-3 Burial history of the Powder River Basin at the Tillard well location. Image source: Devon Energy Corporation. 47

LIST OF ABBREVIATIONS

Å	Ångstrom
Al^{+3}	Aluminium ion
Ar	Argon
β^{-}	radioactive decay by electron emission
C	Carbon
Ca	Calcium
CaCl	Calcium chloride
CsCl	Cesium chloride
CBD	Sodium citrate, sodium bicarbonate, and sodium dithionate
ºC	Degree Celsius
DI	Deionized
EG	Ethylene glycol
ft	feet
Fe	Iron
G	gram
>	greater than
I-S	illite-smectite
I	illite
K^{+}	Potassium ion
K	potassium
K-Ar	Potassium-Argon
<	less than
Ma	million years
Mg	Magnesium
m	meter
mi	mile
mm	millimeter
ml	milliliter
mg	milligram
µm	micrometer
M	molarity
Na	Sodium
NaAc	Sodium acetate
NaAc-HAc	Sodium acetate-acetic acid buffer
O	Oxygen
PRB	Powder River Basin
%	percent
$^{40}Ar_{rad}$	radiogenic argon
RPM	Rotations per minute
R	Reichweite
S	Smectite
Si^{+4}	Silicon ion
SST	Solid state transformation
t	time

Θ	theta
λ	wavelength of X-rays (Ångstrom), decay constant
λ_b	partial decay constant for decay by electron emission (β^-)
λ_e	partial decay constant for decay by electron capture
XRD	X-ray diffraction

1 INTRODUCTION

The study of diagenetic minerals in petroleum source and reservoir rocks is necessary to understand the processes that lead to the generation and accumulation of sizeable amounts of crude oil and natural gas in sedimentary basins. Traps, petroleum source and reservoir rocks, and fractures have been imaged utilizing 3D seismic methods (Cartwright and Huuse, 2005; Dolson et al., 2017). These seismic methods have been helpful to predict the timing of the generation and the movement of hydrocarbon without expensive drilling of wildcat and exploration wells (Soares and Webb, 2018; Mao and Journel, 1999).

Mineralogical studies provided important information toward understanding the generation and accumulation of crude oil and natural gas in source and reservoir rocks. For example, the mineralogical and K-Ar geochronologic study of source-rock diagenetic minerals (illite, the focus of this work) have been used to establish a connection between the generation of crude oil and natural gas and the transformation of smectite to illite from some major oil and gas producing basins of the world (Pollastro, 1993; Pevear, 1999). The object of the present study was diagenetically formed illite in illite-smectite (I-S) of the Cretaceous Mowry Shale in the Powder River Basin, USA. This study was done to understand further the time-temperature history of the Mowry Shale in the Powder River Basin. It was done also to study the connection of the smectite-to-illite transformation and the timing of hydrocarbon generation and migration in the Powder River Basin.

1.1 Smectite, Illite, and the Smectite-to-Illite Reaction

Smectite is a group of expandable dioctahedral and trioctahedral phyllosilicate mineral species of low layer charge (Moore and Reynolds, 1997). Smectite forms primarily from the alteration of silica-rich glass in volcanic ash (e.g. Zielinski, 1983). Smectite can also form by the

alteration of volcanoclastic sediments (e.g., Kadir et al., 2021; Elliott et al., 2021). It can also form as precipitates from pore fluids containing Si, Fe, Al, Mg, Na, and Ca.

The most useful and well-known species of the smectite clay group are montmorillonite, nontronite, beidellite, hectorite, and saponite (Odom, 1984). Smectite is found in argillaceous rocks such as shale and bentonite. Bentonites are argillaceous rocks that consist mainly of smectite, predominantly montmorillonite. In many cases, smectite in bentonite has been subsequently converted to illite or I-S during diagenesis. Potassium bentonites are composed mainly of diagenetically formed I-S whose percentage of illite layers is > 50% (Huff, 1962; Pevear, 1999).

Illite has been thought as a "field" term for a dioctahedral, high layer charge phyllosilicate mineral (Newman and Brown, 1987). The term illite has been used to represent a non-expandable, dioctahedral, 2:1 aluminosilicate clay mineral that is structurally like mica. Illite has been found frequently in soils and sedimentary rocks (Brigatti et al., 2006; Pevear, 1999). Illite was considered to have formed as a weathering product of muscovite in both soils and weathered rocks (Pevear, 1999). Illite is formed from the alteration of smectite (montmorillonite) in a reaction controlled by kinetics (temperature, potassium availability, and time) as mentioned in the next paragraph.

In burial diagenetic settings, which involve the physical and chemical changes in sediments caused by increasing temperature and pressure with increasing depth in the Earth's crust, smectite in argillaceous sediments has been observed to transform to (or react to form) illite within the temperature range of 60°C–140°C. This temperature range is similar to the temperature range for the generation of crude oil and natural gas from kerogen materials (Ge, 2019). Additionally, the release of interlayer water from smectite during the transformation of smectite to illite (via I-S intermediates) has created zones of overpressure (Magara, 1975; Bruce, 1984; Burst, 1969) in

petroleum source rocks. The generation of overpressure in these source rocks is believed to help move crude oil and natural gas from source rocks to reservoir rocks and to aid in long distance petroleum migration (Lynch, 1997). The expulsion of connate waters from deep crustal rocks has been linked to the long-distance migration of crude oil and natural gas in foreland basins (Oliver, 1986). As crude oil and natural gas are generated, smectite reacts to form illite through a progression of mixed-layer I-S intermediates (Eslinger and Peaver 1988). This process has been referred to as smectite illitization informally. The rate of illitization and percentage of illite in the I-S has been found to proceed as a function of temperature, ion activity of potassium (K^+), presence of other cations (Ca^{2+}, Na^+, and Mg^{2+}), and time (e.g. Elliott and Matisoff, 1996). This process has been modelled as a kinetic process (Pytte and Reynolds, 1989; Elliott and Matisoff, 1996; Huang et al, 1983; Eslinger and Pevear, 1988; Boles and Franks, 1979; Stefanov, 2018; Huertas, 2007). Kinetic models provide a way to predict the timing and extent of the smectite-to-illite reaction where the time-temperature history is known (e.g., Elliott and Matisoff, 1996).

1.2 Previous Studies on Smectite to Illite Transformation

The smectite-to-illite transformation is one feature of clay mineralogy that has received considerable attention from academics all around the world (Cuadros and Linares, 1996). The transition mechanisms and kinetics of the smectite-to-illite reaction in argillaceous sedimentary rocks have been studied by Hower et al. (1976), Whitney and Northrop (1988), Nadeau et al. (1985), Pytte (1982), and Elliott et al. (1999). Due to the complexity of the reaction mechanism and the crystal structure of the interstratified I-S, these investigations have sparked debate (e.g. Nadeau et al., 1985). There are two primary mechanisms for smectite-illite transition that have been established: 1) the layer-by-layer transition proposed by Hower et al., (1976) and 2) dissolution-precipitation, also known as the neoformation process or fundamental illite concept

(Figure 1-1, Nadeau et al., 1985). The neoformation process entails converting smectite to illite in a process in which illite grows as the smectite dissolves in sedimentary rocks at diagenetic temperatures. The disparities in transformation hypotheses, according to Cuadros and Linares (1996), are attributable to the nature and presence of the intermediate products, and mixed-layer I-S. However, one generally accepted concept is that smectite is transformed to illite through mixed-layer I-S intermediates in many geological settings at diagenetic temperatures (Bauluz, 2007).

For the transformation of smectite to illite, Bauluz et al. (2000) investigated two reaction pathways using electron microscopy. The first is the solid-state transformation (SST), also known as "layer-by-layer transformation." The SST reaction involves the gradual replacement of smectite by illite, resulting in an increase in the number of illite layers in the original structural framework. The dissolution-crystallization process (DC) is defined as the full dissolution of the smectite phase followed by the precipitation of illite, with the resultant mineral (illite) having a different structural framework than the smectite parent mineral (Altaner and Ylagan, 1997).

After comparing data from X-ray diffraction and scanning electron microscopy (SEM) analysis for both bentonites and sandstones from North America and the North Sea, Nadeau et al. (1985) concluded that the neoformation mechanism (dissolution-precipitation) in smectite-to-illite transformation was operative not only in sandstones but also in bentonites. Researchers today believe that, depending on the external conditions, both solid-state transition and dissolution crystallization methods have occurred; nevertheless, an increase in temperature and pore fluids drives the dissolution-precipitation mechanism (Cuadros and Linares, 1996).

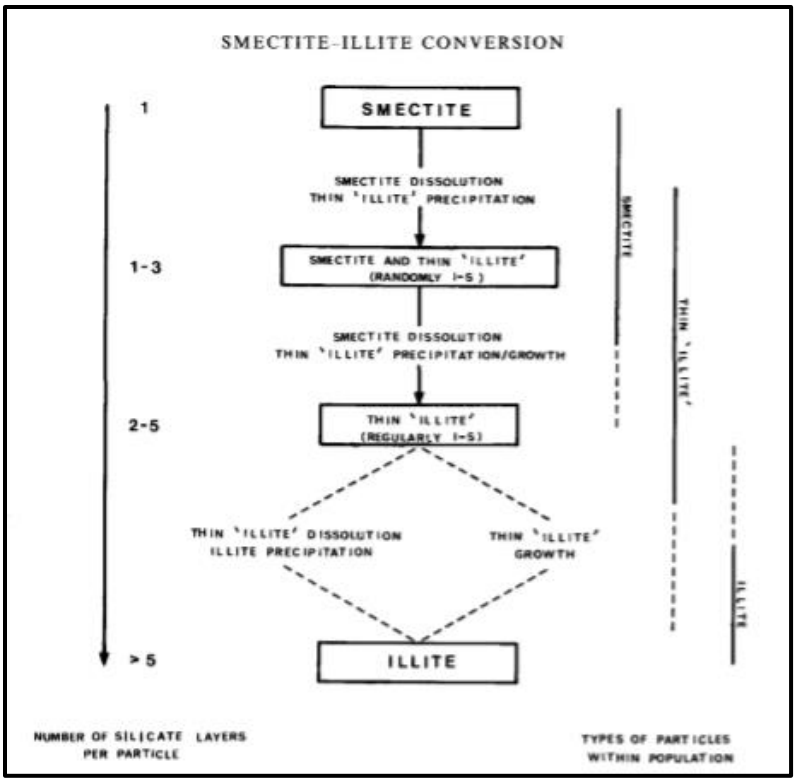

Figure 1-1 Schematic diagram of the proposed neoformation mechanism for the conversion of smectite to illite in bentonites. From Nadeau et a. (1985).

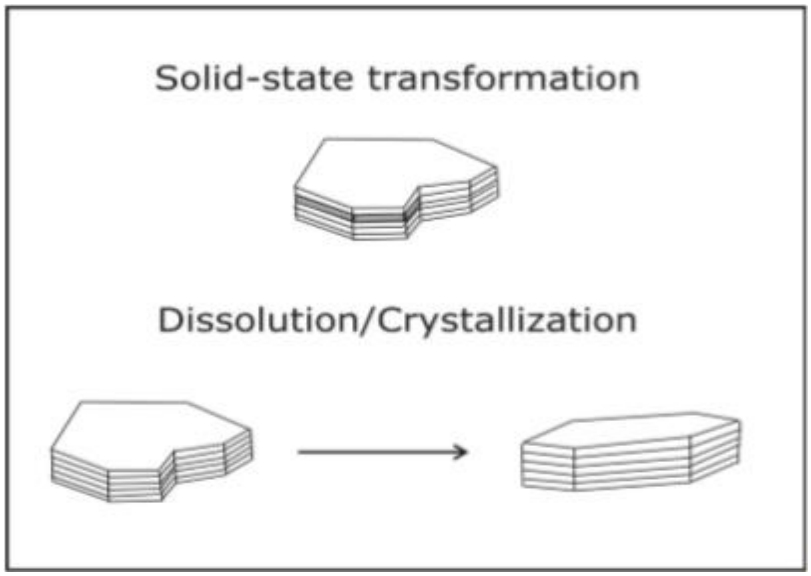

Figure 1-2 Schematic diagram illustrating the transformation mechanisms as proposed by Altaner and Ylagan (1997). Image source: (Bauluz,2007).

1.3 Kinetics of Smectite-Illite Transformation

Many researchers have conducted extensive work on the kinetics of the smectite-to-illite transformation, both in natural geological environments and in controlled laboratory experiments (Elliott and Matisoff, 1996.; Cuadros and Linares, 1996; Huang et al., 1993; Elliott et al. 1999). Elliott et al. (1999), for example, examined the degree of smectite-to-illite transition in Cretaceous bentonites at various distances from the Cerro Negro volcanic neck. The timing and extent of this transition would serve as a way to see whether heat from the intrusion impacted the microbial communities in the Cretaceous shales enclosing these bentonites. This research revealed that randomly ordered I-S was the predominant clay mineral in the bentonites. K-Ar ages spanning from 36 Ma to 48 Ma for the randomly ordered I-S were discovered to agree with a kinetic model estimate of the change of smectite to illite caused naturally by increasing burial. The findings of this investigation revealed that illite production and rate were solely linked to temperature from gradual burial, except perhaps for the samples from closest to the intrusion. It could not be determined whether the intrusion of the volcanic neck had any impact on smectite illitization or on the microbiology communities in these shales.

While the rate of smectite-to-illite transformation is strongly influenced by the ion activity of potassium, other cations ($Ca^{2+,}$ Na^{+}, and Mg^{2+}, Figure 1-3) also impact the rate of smectite illitization (Eslinger and Pevear, 1988; Elliott and Matisoff, 1996). Ge (2019) considered the effect of time on the extent of the reaction, given the fundamental rate-governing factors (temperature and potassium concentration in the pore fluid). The duration of the transformation can be estimated at various temperatures using mathematical modeling and the Arrhenius rate law (eq. 1). The duration of smectite illitization has been observed to decrease with increasing temperature (Pytte 1982; Pytte and Reynolds 1988; Elliott et al. 1991).

$$-\left(\frac{dsmectite}{dt}\right) = \quad k\,(smectite) \qquad\qquad k = Ae^{-\frac{Ea}{RT}}$$

Equation 1

where A is the pre-exponential constant (t^{-1}), Ea is the activation energy (kcal/mol), R is the gas constant, and T is absolute temperature.

Eslinger and Pevear (1988) described three distinct ways to express the reaction of smectite to illite. The layer-by-layer transformation theory is supported by the first reaction. Al and K from dissolved K-feldspar are both substituted in this reaction, whereas Si, Mg, and Fe from the smectite are liberated to create chlorite and quartz. The reaction's chemical form is as follows:

$4.5\ K^{+} + 8\ Al^{+3}$ + Smectite = Illite + $3\ Si^{+4}$ + Cations and Water. (Transformation Reaction).

The second reaction concentrates Al (from the initial smectite) in the tetrahedral sheet of the illite layer, which is formed by dissolving and removing part of the parent smectite's silica. Al is conserved in this reaction.

$2.5\ K^{+}$ + Smectite = 0.64 Illite + $15.7\ Si^{+4}$ + Cations and Water.

The neoformation (dissolution and crystallization of a new mineral) of mixed-layer I-S is the third reaction, which produces two moles of illite for every mole of parent smectite reacted.

$16.6\ K^{+} + 24\ Al^{+3} + 32\ Si^{+4}$ + Smectite = 2 Illite + cations and water. (Neoformation). (Eslinger and Pevear 1988).

The R-descriptor Reichweite, translated as “reach back”, has been used to describe the stacking order of different minerals in a mixed layered structure, such as illite or smectite in I-S (Altaner and Bethke 1988). The layer ordering types can range from random, to short-range ordered to long-range ordered. For example, the I-S with R=0 stacking order is called random ordered I-S. This

arrangement is characterized by 50% illite or 50% smectite layers such that no Illite layers were placed on top of one another. An ordered R≥1 I-S describes an alternating illite and smectite strata layered arrangement termed "short range" order. R≥ 3 I-S is the term for mixed-layer I-S having over 80% illite layers and is classified as long-range ordered (Figure 1-5). In this last type of arrangement, there is usually no less than a three illite layers stacked before a smectite layer (Moore and Reynolds 1997).

Ge (2019) showed that the diagenetic conversion of smectite to illite occurs in three stages at temperatures ranging from 60°C to 140°C at shallow burial depths in the Gulf of Mexico. The initial stage in the transformation process of smectite to illite, with a higher percentage of parent smectite layer, is marked by the presence of the randomly ordered mixed-layer I-S with a stacking order R = 0. With a rise in the percentage of illite layers, the stacking order changes from a randomly ordered I-S (R=0) to an ordered mixed-layer I-S (R≥ 1). Illite becomes the predominant layer in the later stages of this process (Ge, 2019). This relationship was simplified by Eslinger and Pevear (1988) into three stages, as illustrated below:

Smectite (parent mineral) ⟹ I/S randomly ordered (R=0) ⟹ I/S ordered (R≥1) ⟹ I/S ordered (R≥3) ⟹ Illite (1Md) ⟹

Illite (1M) => Mica ($2M_1$).

R=0 is the randomly ordered smectite with 0-60% illite content represented as SSSISSSISSIISSSSSSISSISISSIS, wherein these layers are stacked parallel to the c-axis. Smectite layer cannot be followed by another smectite layer.

R≥1 is ordered with 65-85% illite content: ISISISIS, wherein these layers are stacked parallel to the c-axis. Each smectite is followed by one or more illite layers.

Those with 85-100% illite concentration are defined as R=3 ordered: ISIIISIIISIII, wherein the layers are stacked parallel to the c-axis and smectite is followed by no fewer than three illite layers. The solid-state conversion is shown in Figure 1-2. The two mechansims (solid-state transformation) and dissolution/precipitation are thought to result in the formation of MacEwan crystallites and fundmental particles respectively. These representations are shown together in Figure 1-4.

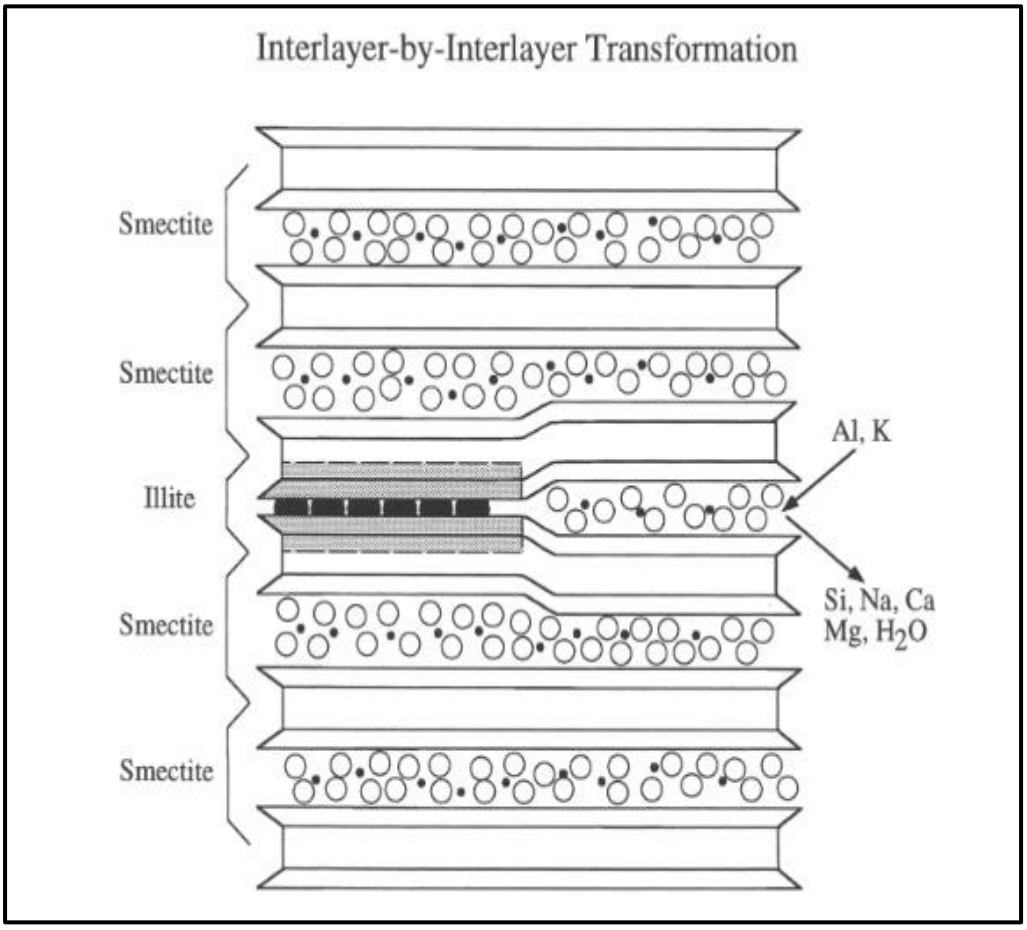

Figure 1-3 Pictorial view of the mixed-layer transformation mechanism. Chemical exchange of reactant and product species occurs through the hydrous interlayer region. Source: Altaner and Ylagan (1997)

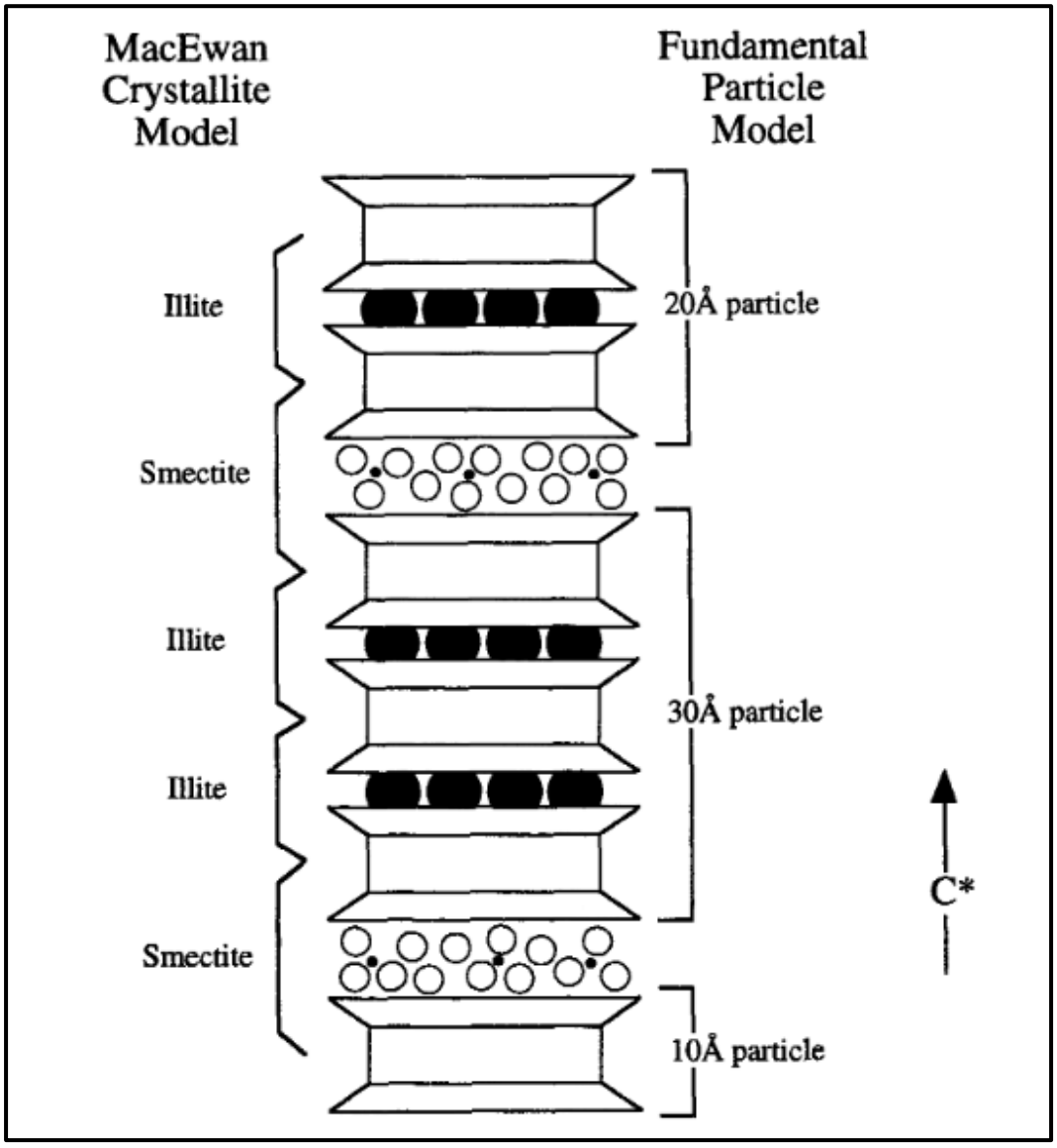

Figure 1-4 Stacking order of mixed-layer I-S represented as a MacEwan crystallite and as an aggregate of fundamental particles. From Altaner and Ylagan (1997).

1.4 Significance of Smectite-to-Illite Transformation and Relation to Hydrocarbon Exploration

The importance of the diagenetic smectite-illite to the petroleum industry is not only due to the complexity of the transformation mechanism (producing overpressures) or the nature of the intermediate products (I/S), but also due to its use as a paleo-thermometer for basin heating and oil generation window. Pollastro (1993) discussed the utility of clay minerals as a source of information on the temperature and burial histories of sedimentary rocks in hydrocarbon exploration. This research emphasized on the diagenetically-generated mixed-layer I-S as a semi-quantitative geothermometer to show thermal maturity of source rocks. The transition from random I-S (R = 0) to ordered I-S (R ≥ 1), according to Pollastro (1993), was regarded as the most essential relationship of I-S to hydrocarbon exploration (Figure 1-6). According to the Hoffman and Hower (1979), a change in the stacking order of I-S from R = 0 to R ≥ 1 corresponds to the temperature observed of the "oil generation window" in Cretaceous rocks at a temperature range of 100° - 110°C.

Elliott et al. (1991) also mentioned that the stacking order of the I-S mixed layer is useful in determining the maximum burial temperature. The age of the diagenetic I-S can be used to predict the time of maximum temperature due to burial (Hoffman and Hower, 1979; Elliott et al., 1991; Pollastro, 1993). The K-Ar ages of I-S mixed-layer and diagenetic illite can also be used to determine the timing of basin-wide fluid migrations and petroleum formation (Lee, 1985; Elliott and Aronson, 1987). Changes in the amount of illite, smectite, and ordering of these minerals, as determined by X-ray powder diffraction (XRD) profiles, are related to temperature changes caused by increased burial (Pollastro, 1993).

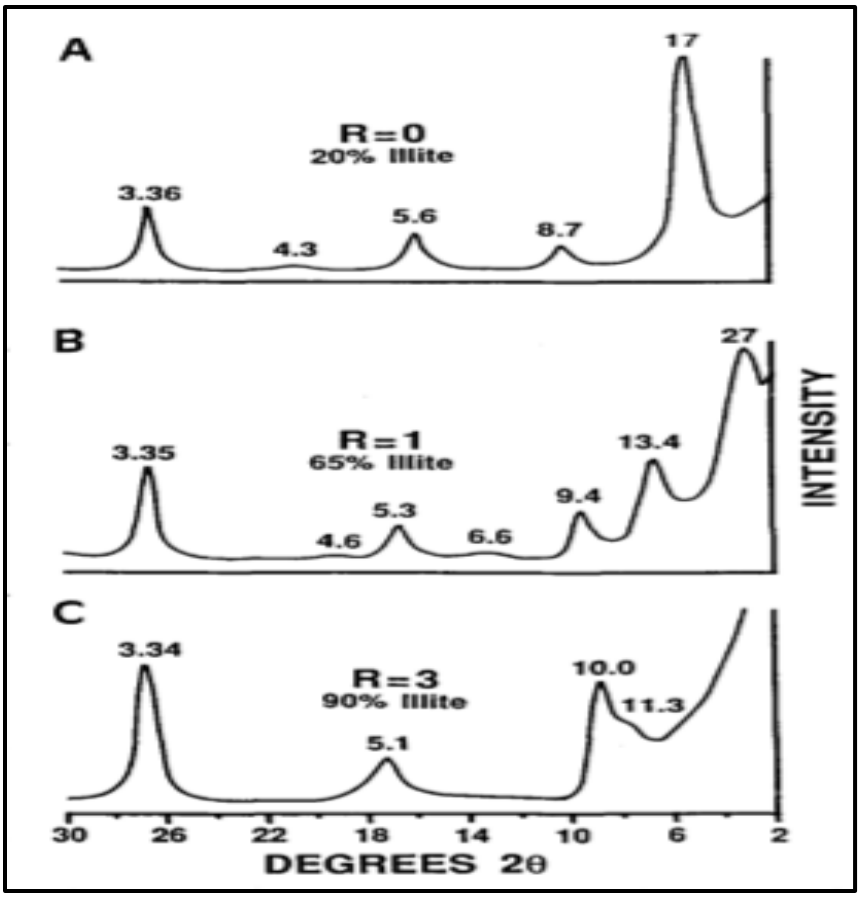

Figure 1-5 X-ray powder diffraction patterns of ethylene glycol-saturated mixed-layer I-S with different expandability and Reichweite (R) ordering calculated with the modeling program NEWMOD. From Pollastro (1993)

Table 1-1 Showing estimated percentage illite, temperatures for changes in mixed- layer illite/smectite (I-S) in Hoffman and Hower and short- life geothermal I-S geothermometry models. Modified from Pollastro (1993).

Changes in Illite/Smectite	Hoffman and Hower model (5-300 m.y)	Short term geothermal model (< 3 m.y)	% illite layer
Starting smectite – R = 0 I-S	50°- 60°C	variable	0 - 60%
R = 0 to R ≥ 1	100°- 110°C	120°C - 140°C	65 – 85 %
R = 1 to R ≥ 3	170°- 180°C	170°- 180°C	90 – 100%

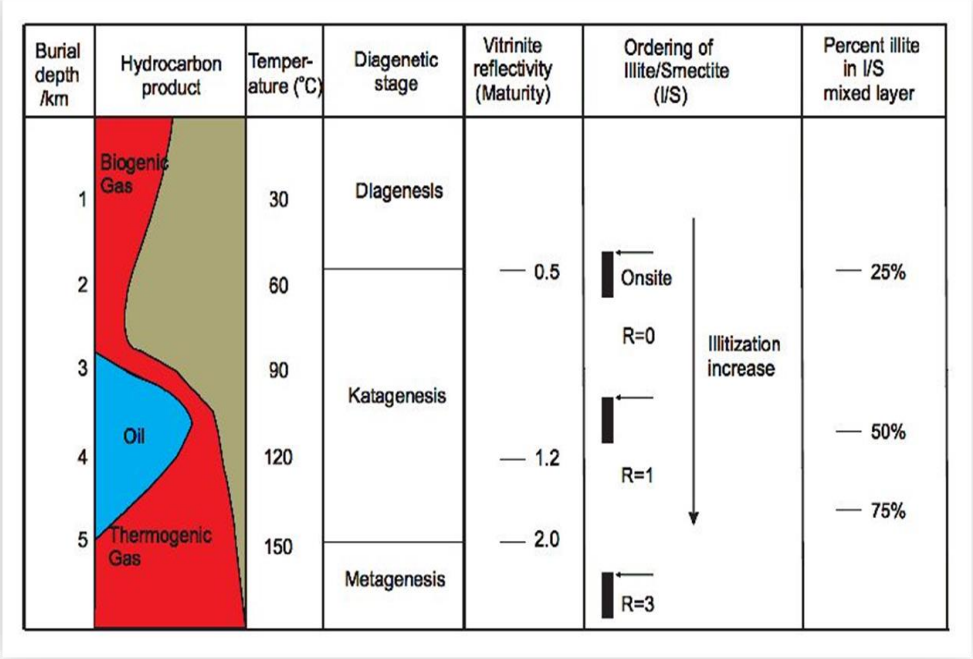

Figure 1-6 The connection between changes in mixed-layer I-S and oil generation temperature, diagenesis, and vitrinite reflectance. Figure from (Jiang, 1979).

1.5 Powder River Basin

The Powder River Basin (PRB) covers 20,000 square miles in southeastern Montana and northeastern Wyoming in the United States (Figure 1-7). The Casper Arch, Black Hills, Laramie Mountains, and Bighorn Mountains, respectively, border the basin in the southwest, east, south, and west (Beikman, 1962; Lynds, 2013). The PRB, which encompasses a large portion of the northern Rocky Mountain region, extends over approximately 100 to 150 miles from east to west and nearly 200 miles from north to south (Craddock et al., 2012). The basin axis is located toward the western margin and is oriented in a northwest-southeast direction. The basin has an asymmetric shape, and approximately 17,000 ft of sediment is found at the basin axis (Anna, 2009). During the Laramide Orogeny late in the Cretaceous, the Powder River Basin was formed by the

separation of the Bighorn Mountains and the Black Hills monoclines, forming an uneven syncline now known as the Powder River Basin (Sharp and White, 1956). The basin dips about 100 ft/mi to the west on the east flank, and rises to at least 500 ft/mi through the Black Hill monocline limbs (Figure 1-8). There is however a decrease in the dip on the western side to about 50 ft/mi towards the Wyoming-Montana northern boundary. Numerous structures presently visible in the PRB at the surface are due to faults or zones of weakness in the Precambrian basement that were reactivated during the Laramide orogeny (Anna, 2009).

The PRB, which was part of the larger foreland basin east of the Sevier orogenic belt prior to Laramide deformation, is composed of Cambrian to Eocene sedimentary deposits (Beikman, 1962; Lichtner et al., 2020). The maximum thickness of the sedimentary fill was calculated to be about 5,500 m (18,000 ft) (Beikman, 1962). The Cretaceous stratigraphic fill of the basin is made up of a succession of intercalated shallow-marine, deltaic, and coastal sediments. The Cretaceous sediments were deposited as a result of the changing sea level and supply of sediment.

Among the Wyoming basins, the PRB ranks first and second in oil and gas production respectively, (Lichtner et al., 2020). The first discovery of oil and gas deposits was made in the Lower Cretaceous Newcastle Sandstone on the east flank of the basin in 1887. Hydrocarbons have been subsequently found in structural and stratigraphic traps within Mississippian to Late Cretaceous reservoirs. A recent geologic assessment of undiscovered oil and gas potential emphasizes the Powder River Basin's rich hydrocarbon history and found it probable that roughly 600 million barrels of oil and 16,000 billion cubic feet of gas remain undiscovered (Anna, 2009).

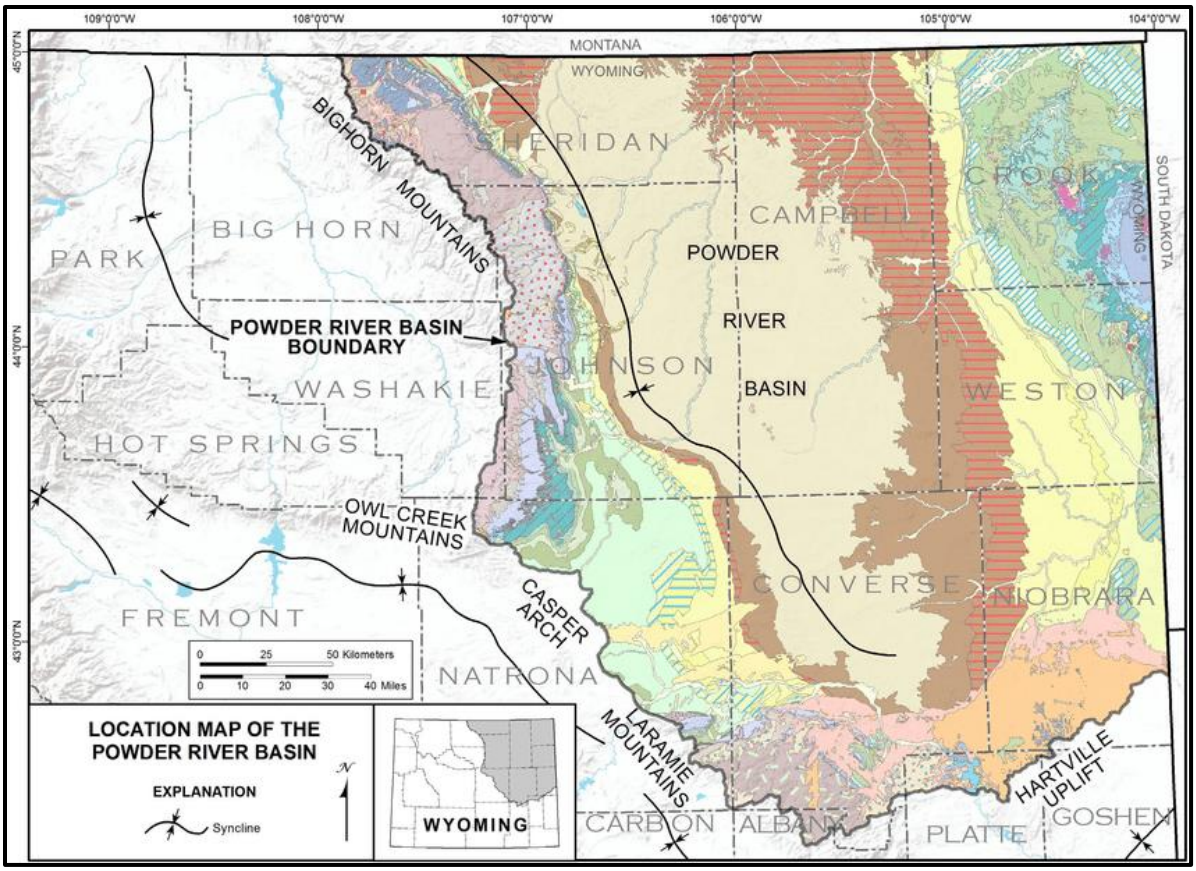

Figure 1-7 Location map of the Powder River Basin. From Lynds (2013).

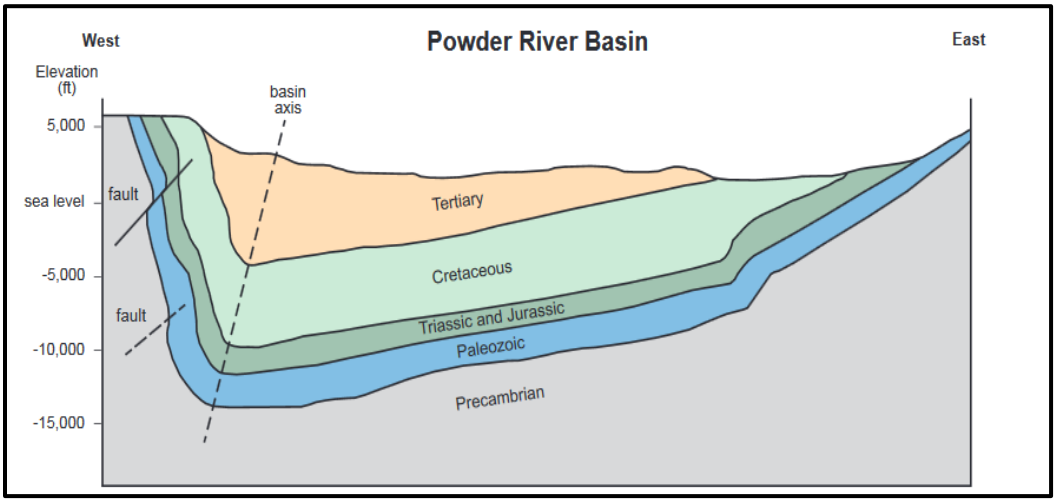

Figure 1-8. Generalized cross section of the Powder River Basin. From Lichtner et al. (2020).

The Mowry Shale is a dark brownish gray siliceous shale that was deposited during a period of maximum marine transgression that spanned the last part of the Lower Cretaceous Albian stage and the beginning of the Upper Cretaceous Cenomanian stage (Anna, 2010). It is composed of a lower unit of 200 feet of dark shale with bentonite inter-beds and an upper unit of 350 feet of siliceous shale (Lichtner et al., 2020). As a result of anoxic conditions and the absence of detrital silt, the shale has a high organic content due to the retention of organic material. Several bentonite markers were observed to split the unit into time stratigraphic intervals allowing for the mapping of three depositional units within the Mowry, hence the Mowry units are regionally persistent and lithologically distinctive (Anna, 2009). In the upper part of the Mowry Shale, bentonite beds are most prevalent, but they only account for a minor percentage of the total thickness of the Cretaceous rocks in the area (Rubey, 1927). Smectite-to-illite transformation, kaolinite-to-chlorite transformation, and the ordering of the mixed-layer 1-S clays are the three primary diagenetic processes in the PRB of Wyoming Laramide Basin (Surdam, et al. 2010). Rubey (1927) described the Mowry as a relatively thin member of hard platy shale in the lower part of the Upper Cretaceous series (Figure 1-9), found throughout the northern Rocky Mountain States, where it is known as the Mowry Shale. He noted that the peculiar lithologic characteristics of the shale are primarily due to its hardness, which is caused by the presence of a significant amount of silica in the rock.

The Mowry Shale is regarded as the primary source of hydrocarbons for Cretaceous reservoirs in the PRB, however minor quantities of hydrocarbons may be found in the Lower Cretaceous Skull Creek Shale and Fuson Shale (Figure 1-10). Additionally, the Mowry is conformably overlain by the Belle Fourche Formation in the Eastern PRB, and by the member of the Frontier Formation in the Western PRB. The Mowry Shale is being developed as a non-conventional reservoir (Anna, 2009; Lichtner et al., 2020).

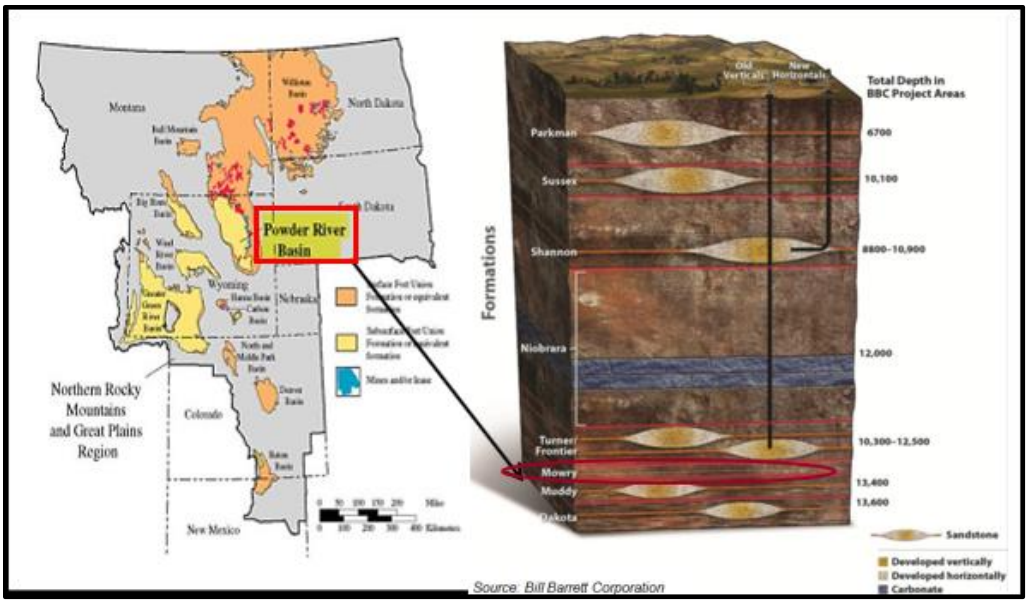

Figure 1-9 : Map showing the study area and stratigraphic fill of the Powder River Basin. Arrow points to the Mowry Shale. Figure modified from SHALE EXPERTS, Powder River Basin Overview.

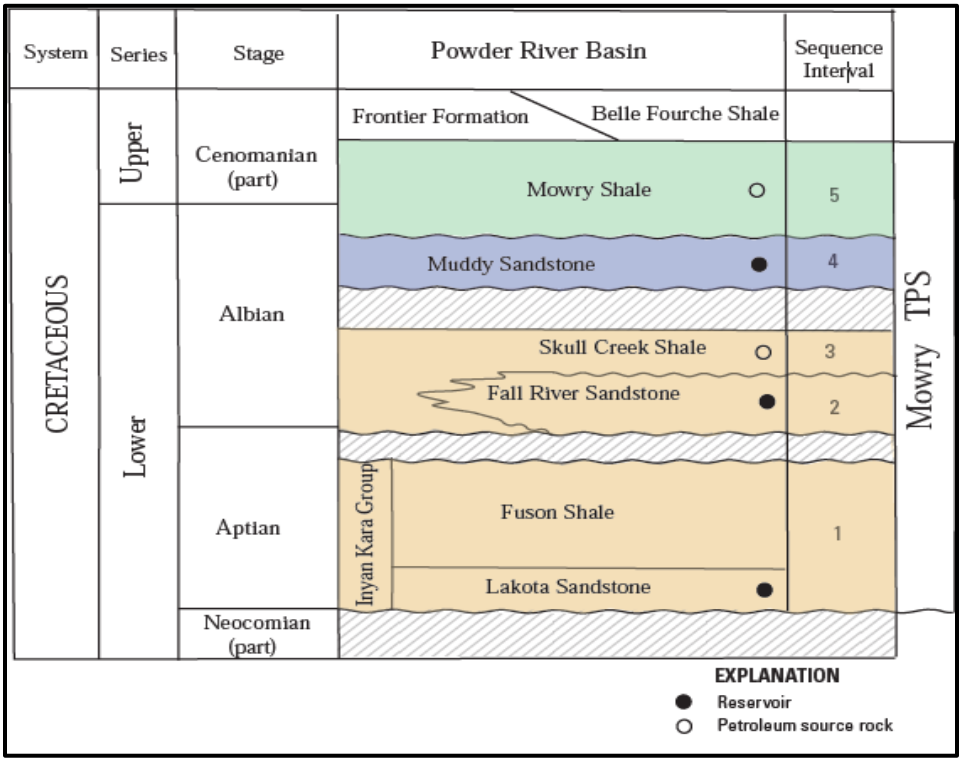

Figure 1-10. Stratigraphic column and succession intervals of Lower Cretaceous strata in the Powder River Basin including identification of the Mowry Total Petroleum System (TPS). From Anna (2009).

1.6 Study Objectives

This study evaluates the relationship between the illitization of smectite and generation and possibly the migration of hydrocarbons in the Cretaceous Mowry Shale of the Powder River Basin, Wyoming United States. In this study, bentonites collected from the Mowry formation were analyzed to determine the presence of I-S and the stacking order and percentage of illite in the I-S. K-Ar geochronology was used to determine the timing of I-S formation in these bentonites. The mineralogical and K-Ar geochronological analyses of the bentonites were used to establish a basis for connecting hydrocarbon generation and smectite-to-illite transformation. This connection was achieved by determining: (1) The extent of illitization and percentage of illite in the mixed-layer I-S from the X-ray diffraction analyses, and (2) the K-Ar age values of I-S to find the timing of illitization in the bentonites. These findings will inform models for the thermal maturation of Cretaceous rock in the Powder River Basin.

2 METHODS AND METHODOLOGY

2.1 Sample Collection, Location, and Description of Samples.

Twenty samples in total were collected from five cored wells through the Cretaceous Mowry Shale in the Powder River Basin (Figure 1-7) by Jess Parrish (Devon Energy) for this study. The samples consisted of eight bentonites, five reworked/pyritized bentonites, and seven regular mud rocks. The drill cores sampled were the State Wright, Tillard, Ponderosa, Iberlin, and Cross Creek wells from the Powder River Basin. The positions of these samples in these cores were noted by Devon Energy personnel (Table 2).

Table 2-1 Showing Devon's rock samples and their corresponding depth in the cretaceous Mowry shale, Powder River Basin.

S/N	Core/Well	Depth (ft.)	Rock Type	Stratigraphic Unit	Weight Received (g)
1	Cross Creek	10463.90	Bentonites	Mowry	40.08
2	Cross Creek	10475.15	Pyritized bentonite	Mowry	50.11
3	Cross Creek	10476.40	Reworked bentonite	Mowry	62.20
4	Iberlin	13254.25	Reworked bentonite	Mowry	81.88
5	Iberlin	13254.75	Bentonite	Mowry	72.35
6	Iberlin	13225.20	Reworked bentonite	Mowry	77.49
7	State Wright	11108.50	Bentonite	Mowry	27.38
8	State Wright	11110.00	Bentonite	Mowry	52.97
9	Tillard	12106.40	Reworked bentonite	Mowry	36.39
10	Tillard	12107.25	Bentonite	Mowry	41.60
11	Tillard	12110.65	Bentonite	Mowry	36.73
12	Ponderosa	13005.20	Bentonite	Mowry	125.38
13	Ponderosa	13005.90	Bentonite	Mowry	87.09

2.2 Sample Preparation for Clay Mineral Identification and K-Ar Geochronology

The preparation of the samples for X-Ray diffraction and K-Ar geochronological analyses was carried out following a procedure suitable for the separation of < 2-micron clay fraction from bentonites and the carbonaceous Mowry Shale. The samples were well-lithified bentonites and shale. They were subjected to various sample preparation techniques as described below (Moore and Reynolds, 1997; Jackson, 1979). The primary goal of these techniques was to separate the clay fraction while avoiding the incorporation of coarse-grained silts and sand into the clay fraction (Moore and Reynolds, 1997).

2.2.1 Soaking and Disaggregation of Soil Sample

The samples (20-30 grams) were soaked in 200 ml of deionized (DI) water for two weeks. The bentonite-water mixtures were gently stirred and crushed in a mortar and pestle with DI water. This technique was done to reduce large bentonite clumps so that it could be poured into centrifuge bottles. This disaggregation likely detached clay from other sand and silt minerals.

2.2.2 Sample Treatment and Removal of Carbonate Cements, Gross Organic Matter, and Iron (III) Oxides

The disaggregated material from Section 3.2.1 was treated with 75 ml, 1*M* sodium acetate-acetic acid buffer ($CH_3COOH + CH_3COONa$, NaAc-HAc buffer) of pH = 5 at 50°C four hours to remove carbonate cement. The treated bentonite was centrifuged using the floor centrifuge (Varifuge 3.0). The natant was discarded and the treated sample was disaggregated in 30 ml of NaAC buffer and centrifuged again. This washing removed soluble ions that might reform into cement (Ca). The carbonate free treated material was reacted with 10 ml of 30% hydrogen peroxide (H_2O_2) to remove gross organic matter at room temperature. It was then heated at 50°C

for 30 minutes. The organic free material was washed two times in NaAc-HAC buffer and once in methanol. Removal of Iron (III) oxide (Fe_2O_3) from bentonite was accomplished by adding 40 ml of 0.3 M sodium citrate ($Na_3C_6H_5O_7$), 5 ml of 0.3 M sodium bicarbonate ($NaHCO_3$), and 3 g sodium dithionite ($Na_2O_4S_2$) at 50°C for 15 minutes following the CBD method (Jackson, 1979). Exchangeable cations and salts remnant were removed by washing them three times with 20 ml, of NaAc-HAC buffer (Jackson, 1979; Edenfield, 1998). The chemical treatments were carried out at 50 °C to prevent radiogenic argon loss from bentonite minerals (Elliott, 1988; Edenfield, 1998).

2.2.3 Separation of Clay, Silt, and Sand Fraction

The separations of sand (> 50 µm), silt (20-50 µm), fine silt (2-20 µm), and clay fractions (< 2 µm) were carried out by the timed settling method (Jackson, 1979). The sand fraction (> 50 µm) was separated using a 4-inch tall 200 ml beaker. This solution was settled for 40 seconds after which the < 50 µm fraction was carefully decanted from the settled sand. This settling was repeated four times. The settled sand free from clay was dried in a laboratory oven at 50°C. The silt fraction (20 – 50 µm) was then separated by settling a 4-inch-tall volume of the less than 50 µm silt fraction solution for 5 minutes in a 400 ml beaker. The settled coarse silt was dried in the laboratory oven at 50°C. The less than 20 µm material was settled (four inches of solution for eight hours) yielding the fine silt fraction (2-20 µm) and the dispersed clay (< 2 µm). The < 2 clay µm fraction was centrifuged in a Sorval Tabletop Centrifuge to obtain a concentrated clay for X-ray diffraction analyses. Some stages in the sample preparation for clay mineral identification are shown in Figure 2-1.

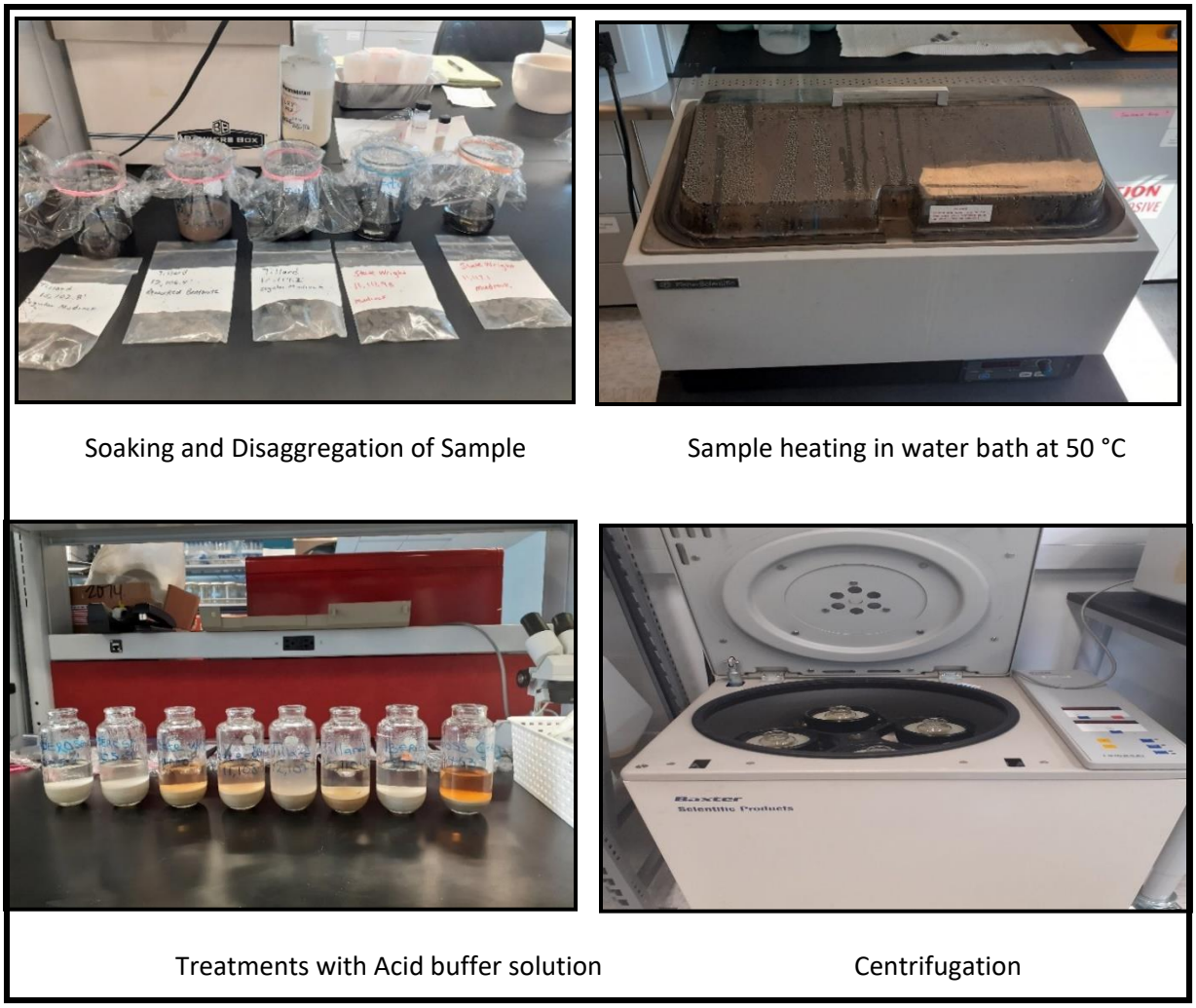

Figure 2-1 Basic stages in sample preparation for clay mineral identification

2.2.4 Oriented Mount Clay and X-Ray Diffraction Analyses

Using a disposable 4 ml pipette, the 3 ml of the less than 2-micron clay was dropped onto a petrographic glass slide for X-ray diffraction (XRD) analysis. This mounting technique produced an oriented mount whereby the *h-k* (*hkl*) planes of the phyllosilicate minerals laid flat onto the glass slide. X-rays are diffracted by only the *00l* planes from this mounted material (Moore and Reynolds, 1997).

Oriented clay mounts were scanned using a Panalytical X'Pert Pro X-ray Diffractometer using Ni-filtered Cu radiation (45 kV, 40 mA). Air-dried, ethylene glycol vapor solvated, and heated oriented mounts were prepared for each clay fraction. These oriented mounts were scanned from 2-40 degrees 2Θ at a speed of 1-degree 2Θ per two minutes. The oriented mounts were solvated in ethylene glycol vapor for 24 hours at room temperature. The oriented mounts were heated to 550 °C for an hour before scanning using an X-ray Diffractometer. The d-spacing values observed were determined for each diffraction peak using the Panalytical software. The observed d-spacing values were interpreted using data from two primary sources (Moore and Reynolds, 1997; Hower, 1981)

2.2.5 X-ray Diffraction Analyses

X-ray powder diffraction (XRD) was used to identify the minerals in the clay fraction. X-ray diffraction is the coherent and constructive scattering of X-ray radiation through the interior crystalline structure of a material. The use of Bragg's Law allows for the determination of the distance between the planes of the atoms that make up the sample when an X-ray beam strikes it and is diffracted. When applied to X-rays, Bragg's Law is given by the equation: $n\lambda = 2d(\sin\theta)$ (Moore and Reynolds 1997), where n is the order of diffracted light, λ is the wavelength of the incident monochromatic X-ray beam (Ni-filtered, Cu-Kα radiation), d is the distance between consecutive planes of atoms (also known as d-spacing), and θ is the angle of incidence of the X-ray beam. The d-spacing for a diffraction peak is computed using Bragg's Law. One of the benefits of X-ray scanning is that the observed d-spacing values comprise a unique "fingerprint" of the minerals present in the sample. The observed d-spacing values can be compared to s-spacings of known minerals (e.g. Flohr, 1997; Moore and Reynolds, 1997). This investigation

utilized a Panalytical X-Pert Pro diffractometer. In the XRD analyses, the specifications are listed in Table 2-2.

Table 2-2 Specifications of XRD Scan. Adapted from (Murshed, 2021)

Instrument Settings		Oriented Scans	060 Scans
	X-ray Tube	Empyrean Cu LFF HR (99430 033 7310x)	
	Voltage	45 kV	45 kV
	Current	40 mA	40 mA
	Scan Time	68 mins	68 mins
	Scan Range	3.0˚ - 60.0˚	59.0˚ - 63.0˚
	Step Size	0.0262˚	0.0131˚
	Sample Stage	PW3071/xx Bracket	Reflection-Transmission Spinner PW 3064/60
	Sample Changer	n/a	Changer PW 3065/12
Incident Beam	Soller Slit		Changer PW 3065/12
	Programmable Divergence Slit (PDS)	1/32˚	1/8˚
	Fixed Incident Beam Mask	10 mm	10 mm
	Anti-scatter slit	Fixed 1/16˚	Fixed 1/4˚
	Beam Attenuator	None	None
Diffracted Beam Optics	Beta Filter	Ni	Ni
	Programmable Anti-Scatter Slit (PASS)	Fixed 1/32˚	Fixed 1/8˚
	PIXcel1D detector: Active length (2˚ Theta)	2.009˚	3.347˚

	Number of active channels	153	255
	Soller Slit	0.04 rad	0.04 rad

2.2.6 Mineral Identification

The diffraction patterns generated in this study are given in Appendix A. The minerals in the clay fractions were identified by the use of the XRD diffraction data (Table 2-3). Between 15.8 and 17.39 degrees *2θ*, the position of $002_{10Å}/003_{17Å}$ reflection corresponding to I-S from ethylene glycol-treated orientated clay was used to calculate the fraction of illite layers in I/S. (Moore and Reynolds, 1997, Table 2-4, Figure 2-2). The position of the 001 peak after ethylene glycol solvation was used to determine the stacking order for the samples (Hower, 1981). Stacking order of illite or smectite in mixed layered I-S has been expressed using the Reichweite, known as the R-descriptor (Moore and Reynolds, 1997). A stacking order of R = 0 indicated that the layers of I (illite) and S (smectite) were stacked in a random order. S followed by I and I was not followed by I was represented by that stacking order. For R≥1 in this case, smectite is followed by one or more illite layers. In the R≥3 stacking sequence, S was followed by at least three I layers. The R≥1 stacking order was recognized by the first peak being between 12.5 and 14Å in the glycol solvated patterns. The R≥3 stacking order was recognized by the first diffraction peak being 10-12Å in the glycol solvated patterns (Moore and Reynolds, 1997; Hower, 1981). The percentage of illite in I-S mixed-layer was determined from the plot of percentage of illite layers vs. $002_{(10)}/003_{(17)}$ d-spacing (Figure 2-2).

Table 2-3 Observed mineral diagnostic diffraction d-spacing values (d_{hkl}).

d-spacing			Minerals
$001_{10Å}/002_{17Å}$	$002_{10Å}/003_{17Å}$	*hkl*	
17 Å 14 Å – 12.5 Å 12.51 Å – 10 Å	5.33 – 5.25 Å		I-S
		7.1 Å – 7.18 Å 3.57 Å – 3.58 Å	Kaolinite
		4.25 Å	Quartz
		4.48 Å – 4.49 Å	Phyllosilicates

Table 2-4 Adapted from Moore and Reynolds, table 8.3., The position (CuKα) of useful reflection for estimating percent illite in illite/EG-smectite

		001/002		002/003		
% Illite	Reichweite	d(Å)	° 2θ	d(Å)	° 2θ	°Δ2θ
10	0	8.58	10.31	5.61	15.80	5.49
20	0	8.67	10.20	5.58	15.88	5.68
30	0	8.77	10.09	5.53	16.03	5.94
40	0	8.89	9.95	5.50	16.11	6.16
50	0	9.05	9.77	5.44	16.29	6.52
60	1	9.22	9.59	5.34	16.60	7.01
70	1	9.40	9.41	5.28	16.79	7.38
80	1	9.64	9.17	5.20	17.05	7.88
90	3	9.82	9.01	5.10	17.39	8.38

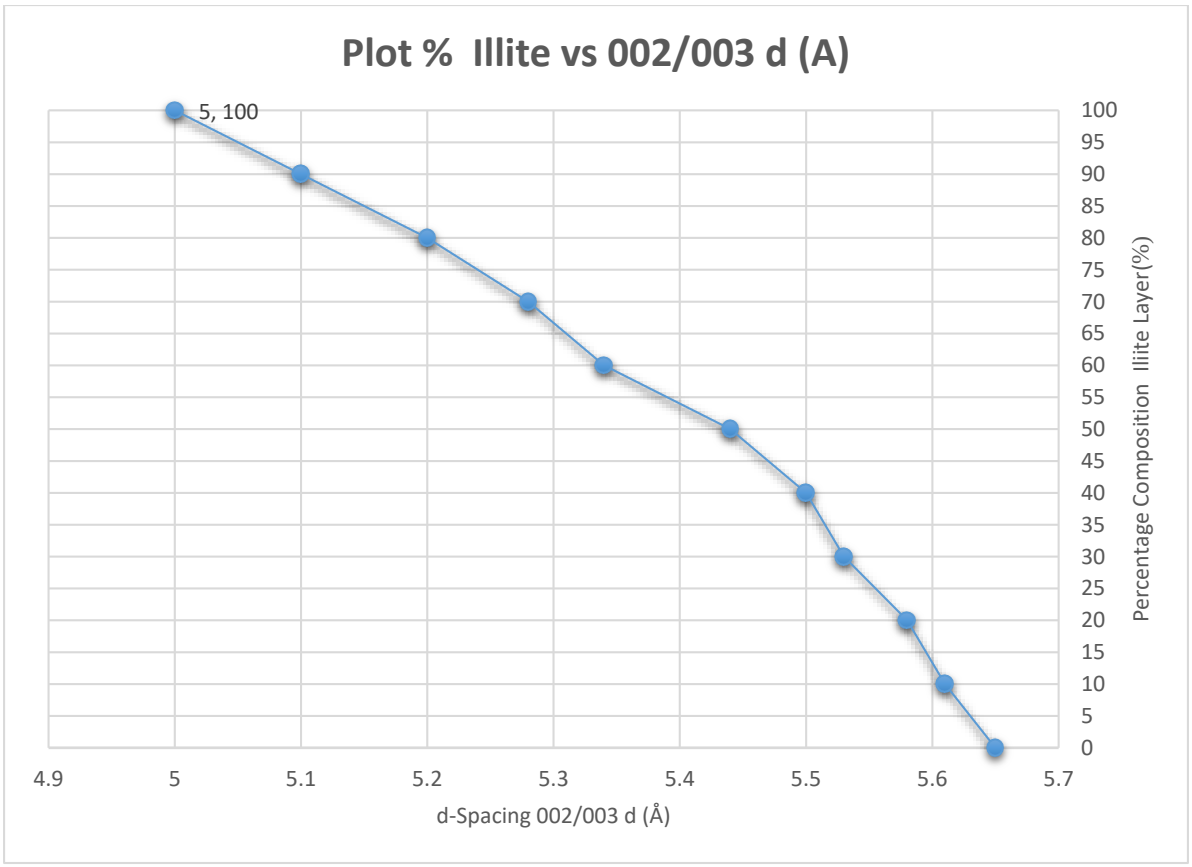

Figure 2-2 Percentage of illite layers vs. 002(10Å)/003(17Å) d-spacing (Å).

2.3 K-Ar Geochronology

Geochronologic ages of mixed-layer I-S in clay fractions were determined using conventional K-Ar geochronology. The decay of a naturally occurring potassium isotope, ^{40}K, to an isotope of argon, ^{40}Ar, provides the basis for K-Ar dating (Kelley, 2002; Faure and Mensing, 2005). There are three naturally occurring isotopes of potassium: ^{39}K, ^{40}K, and ^{41}K. ^{40}K undergoes branched decay to ^{40}Ca (by electron emission where $\lambda_b = 4.962\ 10^{-10}\ yr^{-1}$) and to ^{40}Ar (by electron capture where $\lambda_e = 0.581\ 10^{-10}\ yr^{-1}$). The value of the total decay constant λ is the sum of λ_e and λ_b. About 10.48% of radioactive ^{40}K decays to ^{40}Ar by electron capture, whereas, 89.52% of ^{40}K decays to ^{40}Ca by electron emission (β^- decay) to ^{40}Ca (Faure and Mensing, 2005). Potassium isotopes ^{41}K and ^{39}K are not measured in conventional K-Ar geochronology. The fractionation of these isotopes (e.g. $\delta^{41}K$) has been only recently addressed for diagenetic systems (Zheng et al., 2020). The calculation used to derive K-Ar ages is described in Section 2.3.3.

The K-Ar geochronologic dating method involves the measurement of accumulated radiogenic argon (^{40}Ar) rocks or minerals from the natural decay of potassium (^{40}K) (Gillot et. al., 2006; Faure and Mensing, 2005). The K-Ar analyses of bentonite clay fractions were performed following a one-weigh-out procedure for K-Ar age determination in the clay mineralogy laboratory at Georgia State University under the supervision of Professor Crawford Elliott and Professor Marion Wampler (Stephens et al., 2007; De Man et al., 2010). ^{40}Ar was extracted from test portions of clay samples by heating in vacuum. A spike of ^{38}Ar, whose amount and argon isotopic composition are known, was added to the extracted gases. The mixture of extracted argon and spike was cleaned of condensable and reactive gases by cold trapping and reaction with heated titanium metal and then isotopically analyzed with a MS-10 mass spectrometer connected to the high vacuum extraction line (Figure 2-3). The procedures for the K-Ar analyses are similar to those

used by Trevor Stoker and Andrea Edenfield in their master's theses (Edenfield, 1998; Stroker, 2009; Elliott et al., 1999; Stroker et al., 2013). The steps for meaurement of potassium and argon isotopic composition are given in Appendix B.

2.3.1 Extraction and measurement of ^{40}Ar from clay

Test portions, 16–27 mg, of powdered, < 2-micron clay fractions of bentonites were weighed using a Denver Instrument M-220 analytical balance (Figure 2-4). This analytical balance has 0.1 mg sensitivity. Each test sample was weighed into a capsule made of copper foil. The capsules containing the test portions were placed in vacuum overnight to remove adsorbed moisture. These test materials were then re-weighed, after which they were loaded into the extraction line and held under vacuum overnight. Argon was extracted by heating the samples to 1000 °C (in the presence of an added amount of ^{38}Ar of known amount and isotopic composition) with an external wire-wound heater. CO_2 and H_2O extracted with the argon were systematically trapped and removed by liquid nitrogen, and other gases were removed by reaction with heated titanium (Elliott et. al., 1999; Edenfield, 1998). The cleaned mixture composed of the added spike and the argon extracted from the test sample were released into the MS-10 mass spectrometer for isotopic analysis. The mass spectrometry was done in the static mode. Ion-beam currents of the argon isotopes were measured, and the data were recorded and saved as a text file on a computer.

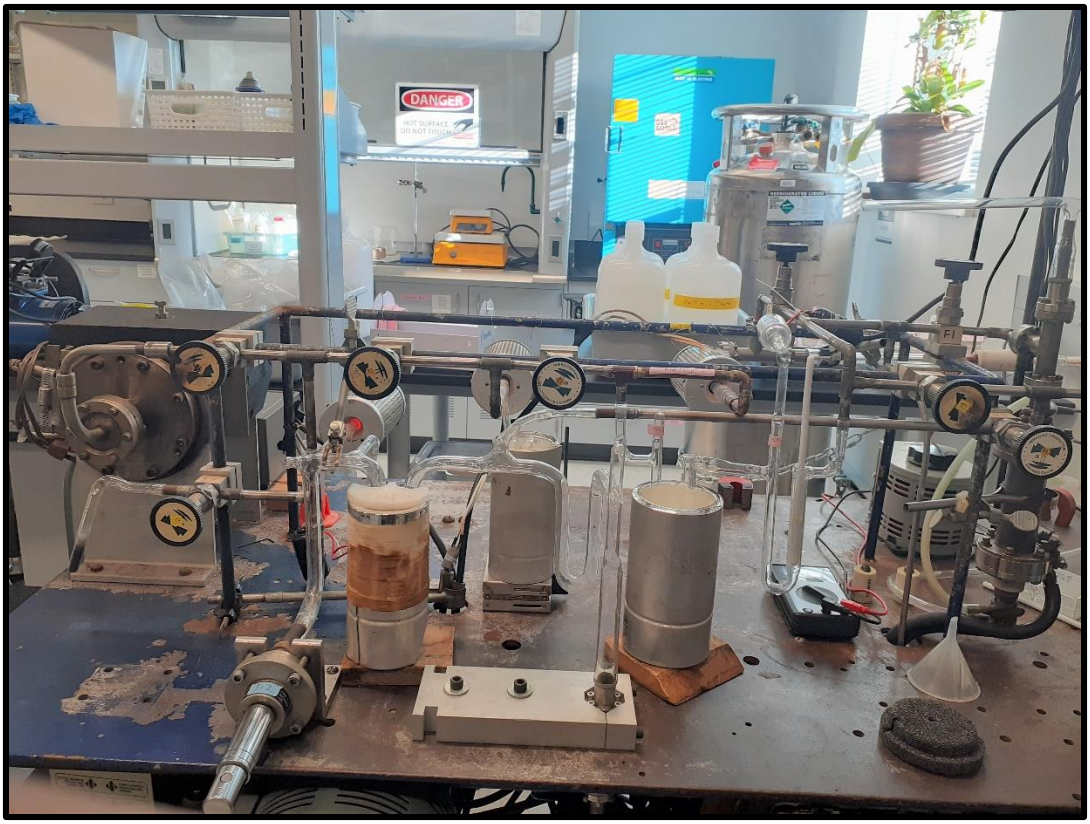

Figure 2-3 Photograph of argon extraction line showing the placement of the liquid nitrogen, used to trap condensable gases, and the MS 10 mass spectrometer (left).

Samples loaded into the extraction line

MS-10 Mass spectrometer controller

Traces of CO_2 and H_2O trapped by liquid nitrogen.

Copper capsules used to contain powdered clay fraction.

Figure 2-4 Aspects of extraction and measurement of ^{40}Ar from clay.

2.3.2 Potassium determination

For potassium determination, test portions in capsules retrieved after the completed argon extractions and isotopic analyses were dissolved in a solution of mixed concentrated hydrofluoric and nitric acids in a closed Savillex® fluorocarbon reaction vessel. This vessel was then heated overnight at near 100 °C on a hotplate inside a fume hood rated for hydrofluoric acid usage. The lid was removed and the solutions were evaporated to dryness in this fume hood at a higher hot-plate temperature. The dried nitrate salts were then dissolved in a weak nitric acid solution containing CsCl. These solutions were diluted prior to analyses on a Perkin Elmer 3110 atomic-absorption spectrophotometer (Figure 2-5). The procedures used were similar to those in past thesis research at GSU (Edenfield, 1998; Osborn, 2006)

Figure 2-5. Perkin Elmer 3110 atomic-absorption spectrophotometer (left) and Mettler M-220 analytical balance (right).

2.3.3 K-Ar Age Calculation

The K-Ar age can be calculated using the decay formula (Equation 2) based on the following assumptions.

1. The geologic material has been and remains in a closed system, such that, all radiogenic ^{40}Ar in the sample are those from the natural decay of radioactive potassium ^{40}K only. There were neither appreciable gains nor losses of parent or daugther nuclides.

2. Only the isotope ^{40}K (with a known decay constant) decayed to produce daughter isotopes ^{40}Ar in the mineral.

3. The measured argon isotope ratios were corrected knowing the corresponding atmospheric argon ratios. Mass spectrometer discrimination was measured to correctly calculate the fraction of radiogenic argon in these samples by measuring a sample of air.

4. The measured amount of ^{36}Ar can be used to correct the measured amount of ^{40}Ar to correct for contaminating ^{40}Ar from the atmosphere, leaving the correct amount of radiogenic ^{40}Ar.

The K-Ar age equation is as shown below (Faure and Mensing, 2005):

$$t = \frac{1}{\lambda} \ln\left(\frac{^{40}\mathrm{Ar}}{^{40}\mathrm{K}} \frac{\lambda}{\lambda_e} + 1\right) \qquad \text{Equation 2}$$

where: t = age;

λ = total decay constant of ^{40}K (t^{-1}),

λ_e = decay constant of ^{40}K to ^{40}Ar (constant decay for electron capture, t^{-1}),

^{40}Ar = content (mol kg^{-1}) of radiogenic ^{40}Ar produced by decay of ^{40}K, and

^{40}K = content (mol kg^{-1}) of radioactive ^{40}K.

3 RESULTS

3.1 Clay Fraction Mineralogy

The clay fraction minerals were identified using diffraction peaks observed in the air-dried, glycol-solvated, and heat-treated oriented mounts of the clay fractions from the bentonite and reworked bentonites (Tables 3.1, 3.2, Appendix A). The d-spacing values were derived from their positions (2θ) using Bragg's Law (Section 2.2.5). Overall, the clay fractions were composed of illite-smectite (I-S) with R≥1 stacking order. The presence of mixed layer I-S was determined from the expansion of the 12.5 Å peak to 12.9 Å and higher (13.3 Å) after solvation in ethylene glycol vapor. Kaolinite and quartz were identified on the XRD patterns at d_{001}=7.13Å, and d_{001}=4.25Å respectively (Figure 3-1, and 3-2). Heating the sample at 550^{o}C for an hour prior to the scan confirmed the presence of kaolinite. Table 3-1 and Table 3-2, contain the minerals, d-spacing and percentage of illite in I-S determined in this study.

3.1.1 Bentonites XRD Results

I-S mixed layer was the predominant clay mineral phase in the clay fractions of all the bentonites. The percentages of illite layers in I-S were from 63 % to 75 %. Trace amounts of kaolinite was found in the bentonite clay fractions of the Cross Creek, Iberlin, the State Wright's, and Tillard cores. The observed peak at 4.48 Å-4.49 Å is an hkl reflection denoting the presence of phyllosilicate minerals (i.e. a generic peak for phyllosilicate minerals). Both the generic phyllosilicates and kaolinite mineral were found together in all samples except the Ponderosa core bentonites. (Tables 3-1). The Iberlin bentonite at 13,254.75 ft was the deepest bentonite studied of the eight bentonites collected from Mowry Formation. This bentonite contained 70 % illite in I-S per the $002_{10Å}/003_{17Å}$ d-spacing at 5.27Å. This clay fraction had traces of kaolinite (d_{001}=7.13Å), and quartz (d_{001}=4.25Å) (Figure 3-1). The shallowest samples were observed from the Cross Creek

core. These bentonites were collected at depths of 10463.9 ft. These bentonites contained I-S with 63 % illite (d($002_{10Å}/003_{17Å}$) = 5.25Å). Kaolinite (d_{001}=7.17Å), and phyllosilicates (d_{hkl}=4.48Å), are the other identifiable minerals found in trace amount in these bentonites (Figure 3-2).

The bentonites from the Tillard core contained I-S with 66% (d ($002_{10Å}/003_{17Å}$) = 5.31Å) and 73% (d($002_{10Å}/003_{17Å}$) = 5.27Å) illite at depth 12107.25 ft. and 12110.65 ft. (Table 3-1). Both bentonites contained traces of kaolinite (d_{001}=7.15Å), and phyllosilicates (d_{hkl} =4.48Å) minerals (Appendix A.2). The State Wright bentonite (11110 ft.) with 75 % illite in the I-S layer shows traces of kaolinite and phyllosilicate on the XRD pattern at 7.18 Å and 4.49 Å d_{001} spacing and position. The other sample from the State Wright bentonite (11108.5 ft.) contained I-S with 71% illite in I-S per the position of the $002_{10Å}/003_{17Å}$ peak, as well as kaolinite (d_{002}=3.52 Å) and phyllosilicates (d_{001}=4.49 Å). The Ponderosa bentonites contains I-S mixed layer and the phyllosilicates minerals only. The percent illite in I-S layers in these bentonites are 71 % and 73 % at 13005.2 ft. and 13005.9 ft. respectively (Table 6). The phyllosilicates were observed at d_{001}= 4.49 Å for both samples. (Appendix A.2).

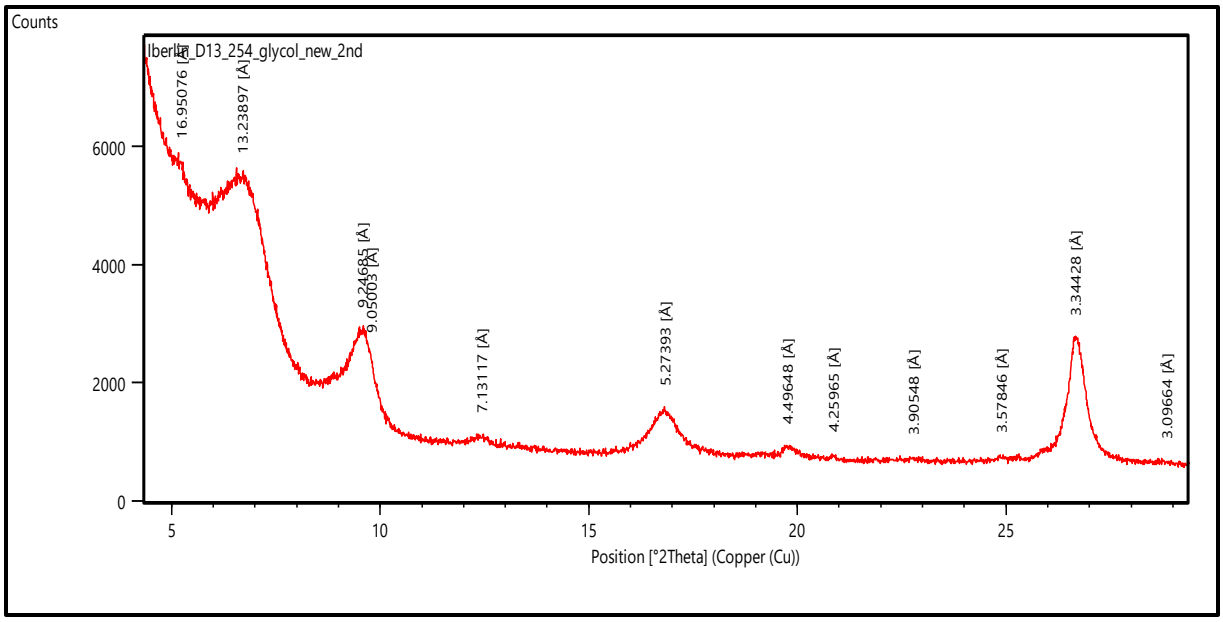

Figure 3-1 X-ray diffraction pattern of oriented, ethylene glycol-solvated Iberlin < 2-µm clay.

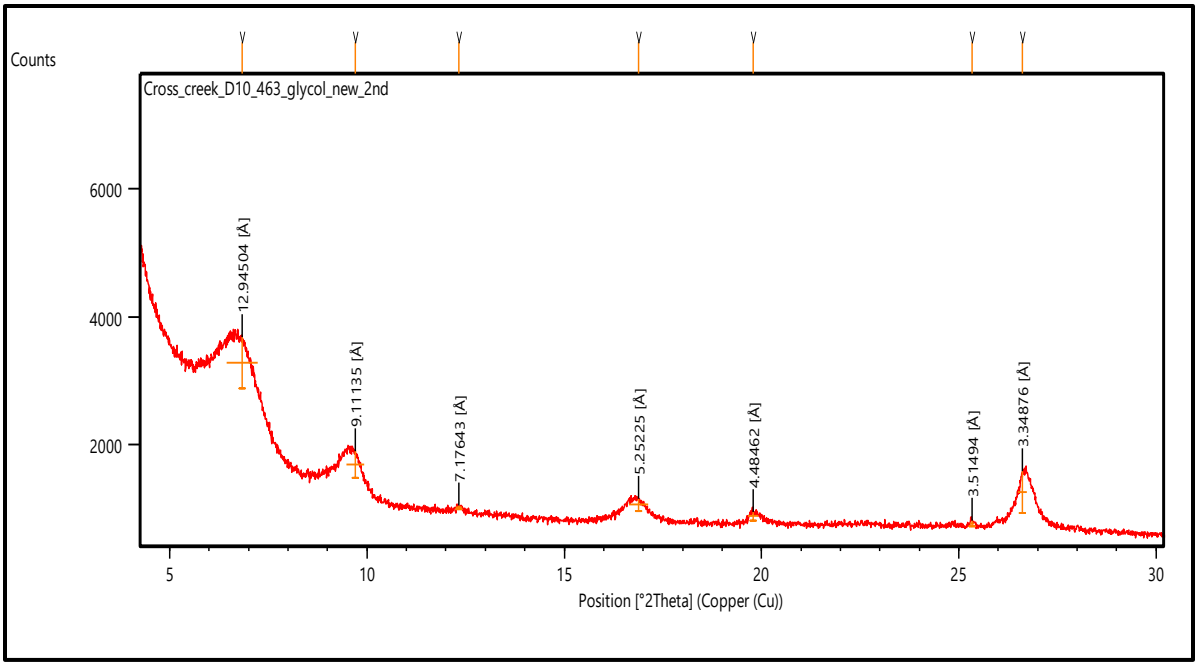

Figure 3-2 X-ray diffraction pattern of oriented, ethylene glycol-solvated Cross Creek < 2-µm clay.

Table 3-1 Mineralogy of < 2-micron fraction of Bentonites.

Core	Depth	Size Fraction	$002_{10Å}/003_{17Å}$ d-spacing and position		Mineralogy
	(ft)	(μm)	d-spacing (Å)	% Illite	(I/S, Kaolinite, Quartz, Phyllosilicates)
Cross Creek	10463.9	< 2	5.332	63	I/S, Kaolinite, Phyllosilicates
Iberlin	13254.75	< 2	5.274	70	I-S, Kaolinite, Quartz, Phyllosilicates
Ponderosa	13005.2	< 2	5.274	71	I-S, Phyllosilicates
Ponderosa	13005.9	< 2	5.250	73	I/S, Phyllosilicates
State Wright	11108.5	< 2	5.277	71	I/S, Kaolinite, Phyllosilicates
State Wright	11,110	< 2	5.252	75	I-S, Kaolinite, Phyllosilicates
Tillard	12110.65	< 2	5.277	73	I-S, Kaolinite, Phyllosilicates
Tillard	12107.25	< 2	5.318	66	I-S, Kaolinite, Phyllosilicates

3.1.2 Reworked Bentonites XRD Result.

The remaining five bentonites collected from the core of Cross Creek, Iberlin and Tillard are reworked and pyritized bentonites. These are bentonites that have been disturbed or mixed with pyrites. The result of the XRD analyses for the reworked bentonites are summarized in Table 3-2 and patterns can be found in Appendix A.3. The reworked bentonites have a varying percentage of illite in the I-S layers from 59 % to 70% and depict a short-ranged stacking ordered, except for the Cross Creek sample at depth 10476.4 ft, that exhibited a long range ordered structure ($R \geq 3$) with > 90 percent illite. All reworked bentonites analyzed for this study contain trace amount of kaolinite (d_{001}=7.16Å), quartz (d_{100}=4.25Å), and phyllosilicates (d_{hkl}=4.47Å). Bentonites collected from the lower part of the Cross Creek core at depths of 10475.15 ft and 10476.40 ft contained visible pyrite. These bentonites appeared to be reworked. They were composed of I-S with a range of illite layers (59 -100 %) per the $002_{10Å}/003_{17Å}$ peaks. The Cross Creek sample collected at depth 10476.4 ft appear to be long range ordered with > 90% illite in I-S layer. The sample from the Tillard core at depth 12106.4 contained I-S with 70% illite per $002_{10Å}/003_{17Å}$. The two Iberlin samples collected at similar stratigraphic depth (13255.2 ft and 13255.25 ft) have the same percentage illite (70 %) in I-S layer.

Table 3-2 Mineralogy of < 2-micron fraction of Reworked Bentonites.

Core	Depth	Size Fraction	$002_{10Å}/003_{17Å}$ d-spacing and position		Mineralogy
	(ft.)	(µm)	d-spacing (Å)	% Illite	(I/S, Kaolinite, Quartz)
Cross Creek	10475.15	< 2	5.368	59	I-S, Kaolinite, Quartz, Phyllosilicates
Cross Creek	10476.4	< 2	4.971	100	I-S, Kaolinite, Quartz, Phyllosilicates
Iberlin	13255.2	< 2	5.274	70	I-S, Kaolinite, Quartz, Phyllosilicates
Iberlin	13254.25	< 2	5.270	70	I-S, Kaolinite, Quartz, Phyllosilicates
Tillard	12106.4	< 2	5.276	70	I-S, Kaolinite, Quartz, Phyllosilicates

3.2 K-Ar Geochronology

The K-Ar geochronologic dating method was employed in determining the age of I-S for the eight bentonites that were not reworked bentonites. The K-Ar age values of the I-S are lower age than the stratigraphic age of the Mowry, indicating a diagenetic origin of the I-S in these bentonites. The ages of the I-S range from 49 ± 5 Ma to 64 ± 5 Ma. There was one outlier age. The measured age of I-S from the Ponderosa well at 13005.2 feet was 75 Ma. That bentonite was considered reworked per Devon Resources (Table 3.3; Appendix). The State Wright bentonites at a depth of 11110 ft. and 11108.5 ft. have K-Ar age values of 49 ± 5 Ma and 56 ± 5 Ma. The age of I-S from the Tillard core at depths of 12107.3 ft and 12110.7 ft are 55 ± 1 Ma and 59 ± 1 Ma respectively. The Ponderosa I-S at a depth of 13005.9 ft has a K-Ar age of 53 ± 1 Ma. The K-Ar age of I-S from the Cross Creek bentonite at 10463.9 ft (49.5 ± 5 Ma) is similar to the K-Ar age of the State Wright I-S at a depth of 11110 ft. The K-Ar age of the Iberlin I-S, from 13254.75 ft, is 64.9 ± 5 Ma.

The clay fractions contain kaolinite and quartz. These phases dilute measured K and Ar isotopic measurements but they do not contain K or Ar. As long as the I-S was closed to additions or losses of K and $^{40}Ar_{rad}$ and the kaolinite and quartz do not have K and $^{40}Ar_{rad}$, then the presence of quartz and kaolinite do not impact the measured K-Ar age.

Table 3-3 Result of K-Ar Dating

Core	Depth	Size Fraction	Potassium	Radiogenic Argon		K-Ar Age
	(ft)	(μm)	(% by mass)	(%)	(nmol kg^{-1})	10^6 Ma ± 5
State Wright	11110.0	< 2	3.34	75.3	288	49.0
Ponderosa	13005.2	< 2	2.49	81.7	331	75.2
Tillard	12110.7	< 2	2.89	76.3	302	59.4
Ponderosa	13005.9	< 2	3.58	80.3	335	53.2
Tillard	12107.3	< 2	3.35	75.6	327	55.5
Cross Creek	10463.9	< 2	3.92	80.5	341	49.5
Iberlin	13254.8	< 2	3.41	86.9	391	64.9
State Wright	11108.5	< 2	3.37	86.0	340	56.7

4 DISCUSSION

The I-S in the clay fractions of undisturbed bentonites from the Cretaceous Mowry Shale exhibited short-range ordered (R≥1) stacking of illite and smectite layers based on X-ray diffraction measurements. The percentage of illite layers in the I-S varied from 63 to 75% in these bentonite clay fractions. As postulated by Hower et al. (1976), the occurrence of mixed layer I-S implies that smectite illitization occurred as a result of a continuous transformation of smectite layers to illite, a process also known as layer-by-layer transformation. It was suggested by the percentage of illite layers in I-S and the observed stacking order that the transformation from randomly ordered to short-range ordered I-S took place at temperatures in the range of 100 ^{o}C to 130 ^{o}C (Figure 4-1; Jiang, 2012). This temperature range is known to correspond to the temperatures needed to generate crude oil and natural gas in petroleum source rocks (i.e. the “oil window") such as the Mowry Shale in the Powder River Basin. The Mowry Shale is the primary source rock for the Cretaceous hydrocarbon reservoirs in the Powder River Basin. The Mowry has one of the highest average total organic carbon contents of Cretaceous shales in the region, making it a valuable source rock for both Lower and Upper Cretaceous reservoirs (Lichtner et al., 2020; Anna, 2010). Furthermore, the range of maximum burial temperature of the Mowry formation (88 °C to 138 °C) inferred by Roberts et al. (2007) and Green et al. (2020) is consistent with the known maximum temperatures for the Mowry Shale from depth-of-burial curves for the State Wright (Figure 4-2), Tillard (Figure 4-3), Iberlin, and Cross Creek wells. The XRD analyses results showed that most of the reworked bentonites contain between 59% and 70% illite layers in the I-S, and that the stacking order is short-range. The stacking order exhibited by these reworked bentonites is also consistent with the estimated maximum burial temperature range of 100 ^{o}C to 130 ^{o}C. However, as stated in section 3.1.1, the Cross Creek sample at depth 10476.4 ft, showed a

long-range ordered structure (R≥3) with > 90 percent illite in the I-S (Table 3-2). The R≥3 stacking order of this sample indicates the bentonite contained detrital illite from the Mowry Shale.

The dark brownish gray siliceous Mowry Shale was deposited during a period of maximum marine transgression that spanned the last half of the Lower Cretaceous Albian (97 Ma) Stage to the beginning of the Upper Cretaceous Cenomanian (93 Ma) Stage (e.g. Anna, 2009; Merewether, 1996). Except for the anomalous age value of the Ponderosa clay from depth 13005.2 ft (75 ± 5 Ma), the I-S clays in the bentonites featured K-Ar ages from 49 ± 5 Ma to 64 ± 5 Ma. This range was lower than the depositional ages of these bentonites in the Mowry. At first approximation, the Mowry appears to have reached a maximum depth relative to mean sea level in the early Tertiary, per Figures 4-2 and 4-3. Hence, the formation of diagenetic illite appears to be a response to increased temperature from due to increased burial. The increased burial is associated with the formation of the PRB basin in the early Tertiary. This analysis reiterated that the K-Ar age of I-S is a time-integrated age (Aronson and Hower, 1976). The correlation of the ages to an apparent maximum burial depth and temperature are discussed in the paragraph below.

According to Nixon (1973), the post-depositional thermal history in a sedimentary basin is a function of the burial depth, time, and geothermal gradients. Where geothermal gradients and burial depths over time are known, the formation of diagenetic minerals (I-S) and the generation of crude oil and natural gas can be understood in the context of the burial history of a sedimentary basin. The K-Ar measured age values of the bentonite clay fractions from two cores were plotted on burial-history charts provided by Devon Energy Corporation (Figures 4-2 and 4-3). According to these charts, the age values determined for I-S in the State Wright bentonites (49 ± 5 Ma and 56 ± 5 Ma) and the Tillard bentonites (55 ± 1 Ma and 59 ± 1 Ma), correspond approximately to burial depths in the Paleocene of 11,000 to 12,000 feet (3353 to 3658 m) and temperatures near 110°C.

The burial history charts indicate that the thickness of sediment overlying the Mowry Shale increased through the Cenozoic Era to the Miocene Epoch, so burial depth of the Mowry Shale is interpreted as having increased until about 10 Ma, when maximum burial temperatures near 130°C were reached. Similar inferences can be made for the bentonites from the Iberlin and Cross Creek wells, because the now-deepest Iberlin bentonite should have been the first to reach a burial depth near 3500 m and a temperature near 110°C, at about 65 Ma, while the Cross Creek bentonite should have been the last to reach those conditions at about 50 Ma. Again, one measured age from the Ponderosa well (75 ± 5 Ma) is considered an outlier. This bentonite appeared to be mixed with other rock.

According to the burial curves as shown in the Figures 4-2 and 4-3, burial depth, and thus also temperature, in the south-central part of the Powder River Basin increased rapidly until about the end of the Paleocene. Illitization may have begun at a temperature well below 110°C, but the data of Pytte and Reynolds (1989) indicate a rate about 50 times greater at 110°C than at 80°C. Consequently, the burial histories and K-Ar age values of I-S suggest that most of the illite in the Mowry bentonites of the Powder River Basin formed rapidly at temperatures near 110°C. By this reasoning, where the sampled Mowry bentonite was (and still is) most deeply buried, at the Iberlin well, peak illitization occurred near the beginning of the Paleocene (K-Ar age of illite = 64 Ma, ~ 11,000 feet burial depth). At the Cross Creek well, the sampled bentonite reached a burial depth and temperature for illitization later in time (K-Ar age of illite = 49.5 Ma). The formation of diagenetic illite is a kinetic response to the timing and extent of burial in the PRB. Although the Mowry Shale was buried even more deeply until the Miocene Epoch, the illitization process was likely limited by the availability of K^+ (e.g. Aronson and Hower, 1976).

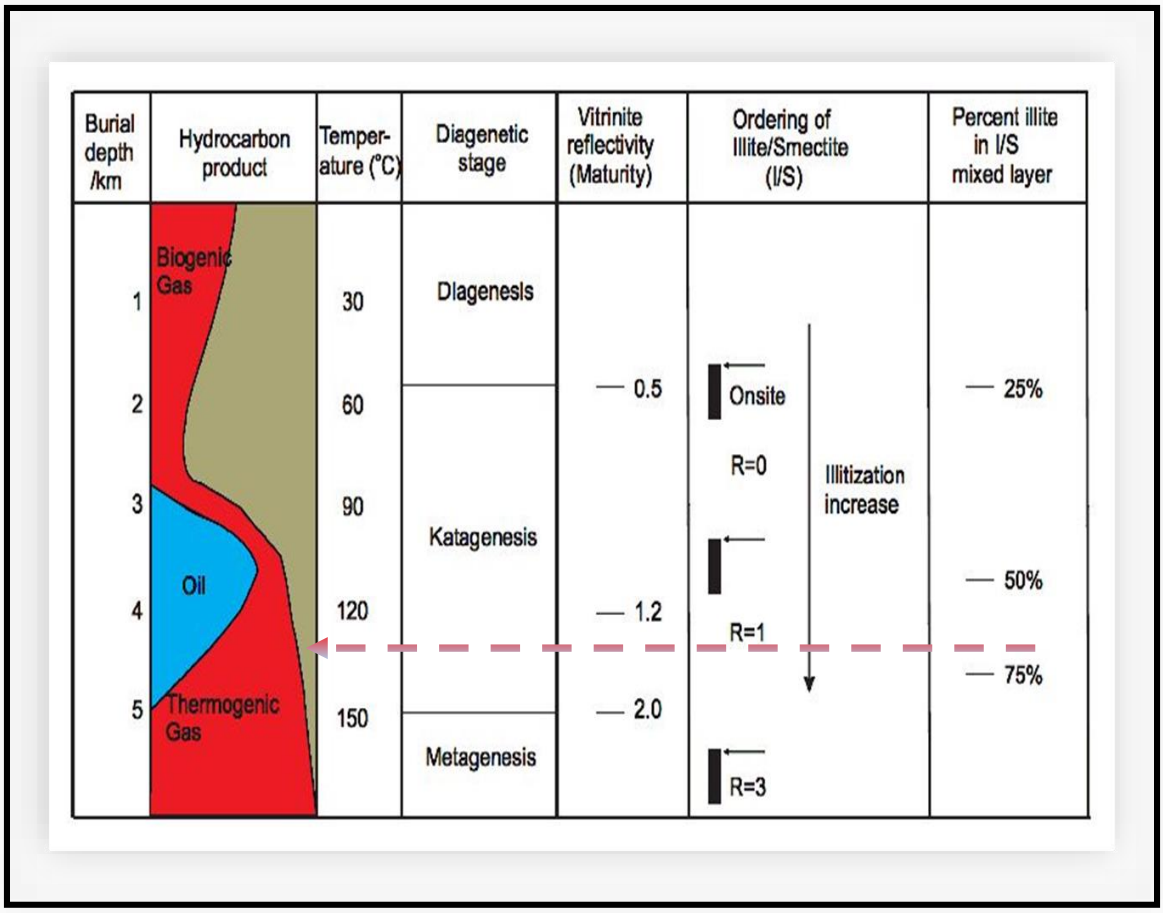

Figure 4-1 The connection between changes in mixed-layer I-S and oil generation, temperature, diagenesis, and vitrinite reflectance. Figure modified from Jiang (2012) by the addition of arrow showing the link of the R ≥ 1stacking order of I-S with the temperature observed of the "oil generation window" in Cretaceous rocks.

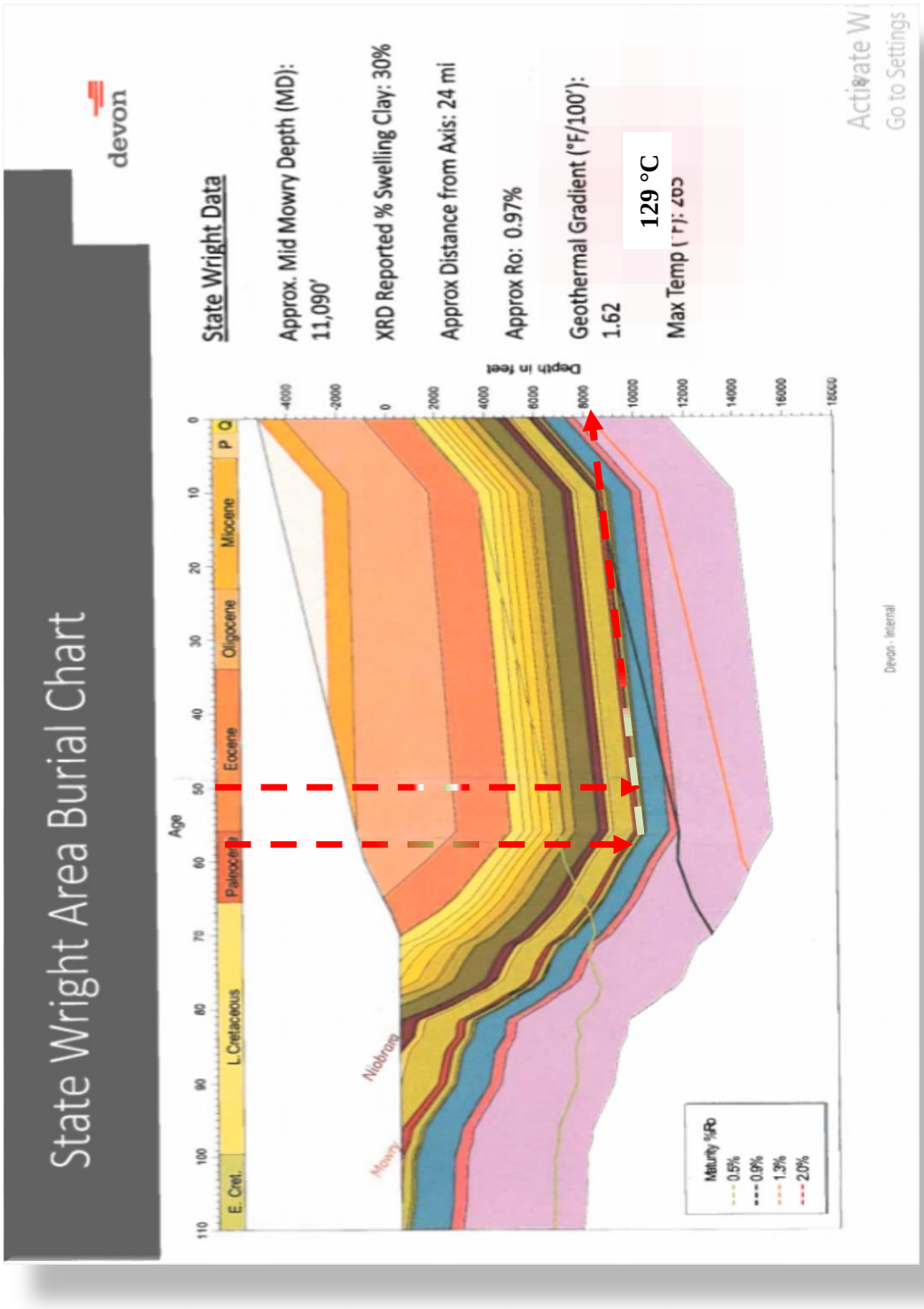

Figure 4-2 Burial history of the Powder River Basin at the State Wright well location. Image source: Devon Energy Corporation.

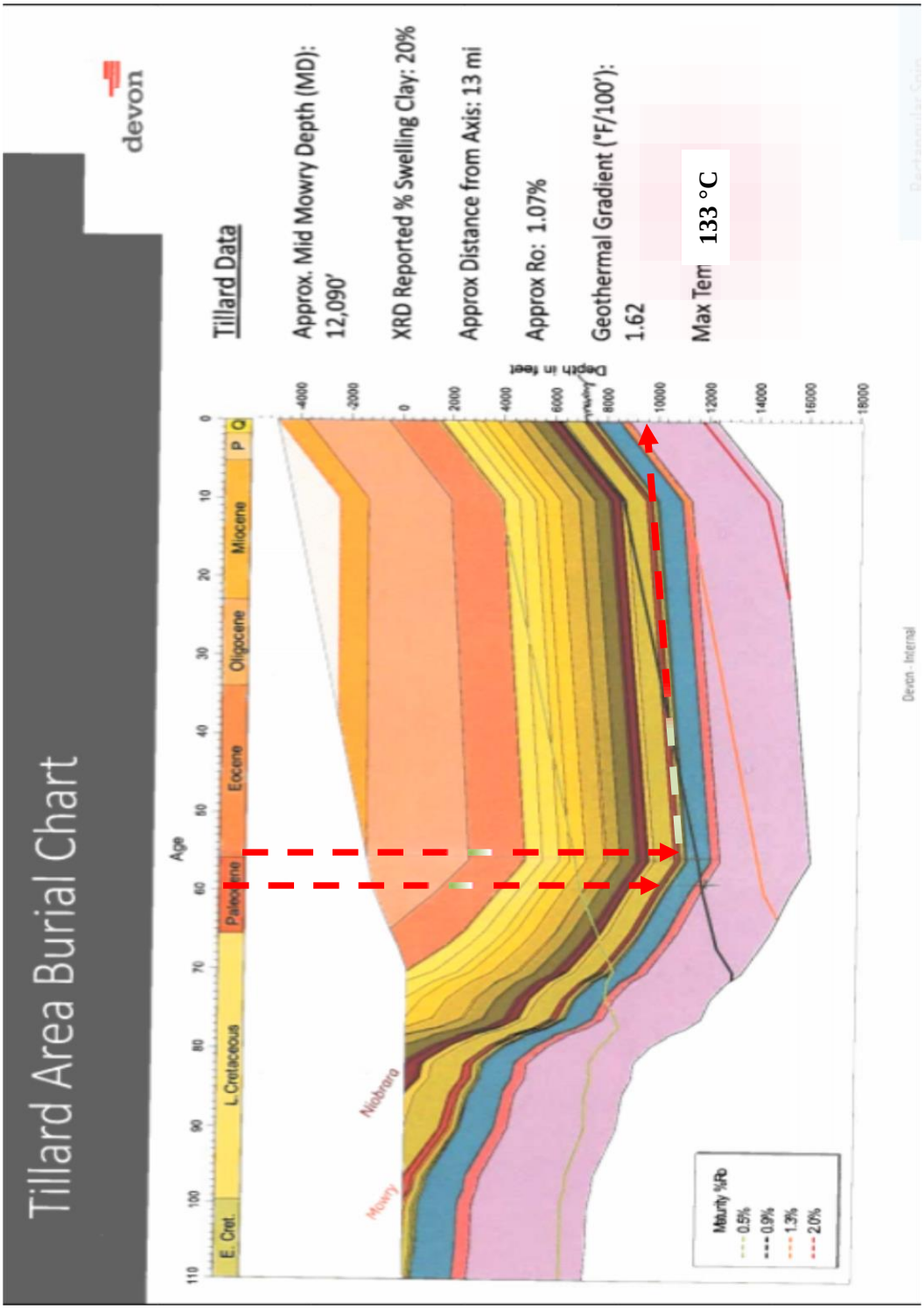

Figure 4-3 Burial history of the Powder River Basin at the Tillard well location. Image source: Devon Energy Corporation.

Bentonite deposits are the product of volcanic fallout into sea water. Volcanic ash is deposited to form a layer rich in volcanic glass, which is weathered in place to produce bentonite (e.g. Finn, 2021; Jiao and Surdam 1993). The bentonite beds in the Skull Creek and Mowry Shales are largely the product of volcanism in western Wyoming and Idaho (Jiao and Surdam, 1993). The origin of the Upper Cretaceous Mowry shale bentonites studied herein were volcanic ash that erupted frequently throughout the Cretaceous period. This interpretation is consistent with the work of Beikman (1962), who indicated that volcanic ash in the Mowry was converted to bentonite. This ash was likely produced by a long series of volcanic eruptions. These eruptions were located in Idaho, from which air-borne ash was moved, mostly eastward, and deposited in the Cretaceous Interior Seaway. Pyritized and reworked bentonites were seen in the core of Cross Creek at depth 10476.4 ft. The clay fractions of one of these bentonites contained long-range ordered I-S ($R \geq 3$) with > 90 percent illite layers in the I-S. This clay is interpreted as detrital clay reworked from the surrounding Mowry Shale.

The origin of the I-S in the Mowry bentonites studied herein, may also have been influenced by heat from volcanic activities accompanying the Laramide orogenic event (Rahman et al., 2016; Clayton and Ryder, 1984). However, the diagenetic temperatures responsible for the illitization in these bentonites are due largely to progressive burial by overlying strata. The Laramide orogeny was a Late Cretaceous to Paleocene orogenic event that resulted in the Laramide block uplifts in the United States between 80 Ma and 55 Ma. (e.g., English and Johnston, 2004). Basin subsidence due to Laramide tectonic activity was responsible for the deep burial of the shale and bentonites in the Mowry in the basin regions of Wyoming, Colorado, and Utah (Nixon, 1973). The rebuilt thickness of strata directly overlying the Mowry interval can approximate the burial depth. Although the structural configuration of the Mowry was altered by this orogeny, Nixon

(1973) described the state of the Mowry formation during and after deposition to be stable. Thus, the formation of the I-S in the bentonites of the Mowry shale was primarily as result of progressive burial and time.

In the Powder River basin, the Mowry Shale and other organic-rich sections of the Cretaceous stratigraphic layer have long been known as a prolific hydrocarbon source rocks. Formation of the diagenetic I-S clay was temperature dependent and may have been related to regional hydrocarbon production (Surdam et al., 2010). Conventionally, the timing of illitization is correlated with the timing of the production of crude oil and natural gas from shale formations (Figure 4-1). The results from our XRD analyses and K-Ar age determinations are consistent with I-S formation when thermal maturity in the oil generation range was reached in the Mowry Shale. The K-Ar age of illite provides the date of thermal maturation. Kinetic models can be used to determine the timing and amount of illitization in other Wyoming Laramide basins given a burial curve.

5 CONCLUSION

The following conclusions are derived from the result of this study:

1. From our analyses, the presence in bentonites of ordered mixed-layer I-S with R≥1 and percentage of illite layers ranging from 63% to 75% signifies temperature sufficient to generate crude oil and natural gas in the Mowry shale. Also, our results show traces of kaolinite and quartz in the samples. These phases dilute measured K and Ar isotopic contents but do not influence the calculated ages.
2. Except for the K-Ar age of the Ponderosa, which is about 75 Ma, the measured K-Ar ages range from 49 Ma to 65 Ma. The age values are lower than the stratigraphic age of the Cretaceous Mowry shale, which indicates that the illite is diagenetic and not a detrital mineral that was transported from another source into the basin. What this means is that the transformation of smectite to illite occurred *in-situ*.
3. The measured K-Ar ages, when plotted on the burial curves, correspond to when these bentonites reached temperatures of approximately 110^{o}C. This indicates that illitization started before maximum burial was reached in the Miocene. The illitization process was limited in duration because of a limited source of potassium. The K-Ar age value of I-S is a time integrated age for the formation of I-S and reflective of the kinetic processes needed to form illite.
4. As in the Denver basin, the results of the XRD analyses and the K-Ar ages of the I-S from the Mowry bentonites indicate that the timing of illitization (looking at the percentages of illite and burial temperatures) coincides with the timing of crude oil and natural gas generation in the Powder River Basin.

REFERENCES

Altaner, S., & Bethke, C. (1988)). Interlayer order in illite/smectite. *American Mineralogist, 73,*, 766-774.

Altaner, S.P., and Ylagan, R.F. (1997). Comparison of structural models of mixed-layer illite/smectite and reaction mechanisms of smectite illitization. *Clays and Clay Minerals 45 (4):* , 517–533.

Anna, L. (2009). *Geologic assessment of undiscovered oil and gas in the Powder River Basin Province.* U.S. Geological Survey Digital Data Series DDS–69–U, 93 p.

Aronson, J.L., and Hower, J.,. (1976). The mechanism of burial metamorphism of argillaceous sediments – 2: , . *Geological Society of America Bulletin, v. 87*, 738-744.

Bauluz, B. (2007). Illitization Processes: Series of Dioctahedral Clays and Mechanisms of Formation. *Sociedad Espanola de Mineralogia* .

Bauluz, B., Peacor, D. R., and Lopez, J. M. G. (2000). Transmission Electron Microscopy Study of Illitization in Pelites from the Iberian Range, Spain: layer-by-layer replacement? *Clays Clay Miner. 48,*, 374–384.

Beikman, H. M. (1962). *Geology of the Powder River Basin, Wyoming and Montana, with reference to subsurface disposal of radioactive wastes.* United State Geological Survey USGS Numbered Series 62-7.

Boles, J.R. and Franks, S.G. (1979). Clay Diagenesis in Wilcox Sandstones of Southwest Texas: Implications of Smectite Diagenesis on Sandstone Cementation. *Journal of Sedimentary Petrology. Vol. 49 No 1,* 0055-0070.

Brigatti M.F., Galan E., Theng, B.K.G. (2006). Structure and Mineralogy of Clay Minerals. In F. A. Bergaya, *Handbook of Clay Science* (pp. 21-68). Elsevier.

Bruce, C. (1984). Smectite Dehydration, its Relation to Structural Development and Hydrocarbon Accumulation in Northem Gulf of Mexico Basin. *American Association of Petroleum Geologists Bulletn' 68*, 673-683.

Burst, J. (1969). Diagenesis of Gulf Coast Clayey Sediments and I/S, Possible Relation to Hydrocarbon Migration. *American Association of Petroleum Geologiost, Bull. 53,*, 73-93.

Cartwright, J. A and Huuse, M. (2005). 3D seismic technology: the geological 'Hubble'. *Basin Research*, 17: 1-20.

Clayton, J. L., and R. T. Ryder,. (1984). Organic geochemistry of black shales and oils in the Minnelusa Formation (Permian and Pennsylvanian), Powder River Basin, Wyoming. *The Rocky Mountain Association of Geologist*, 231-252.

Craddock, W.H., Drake, R.M., II, Mars, J.C., Merrill, M.D., Warwick, P.D., Blondes, M.S., Gosai, M.A., Freeman, P.A., Cahan, S.M., DeVera, C.A., and Lohr, C.D.,. (2012). *Geologic framework for the national assessment of carbon dioxide storage resources—Powder River Basin, Wyoming, Montana, South Dakota, and Nebraska, chap. B of Warwick, P.D., and Corum, M.D., eds., Geologic framework for the national assessment of carbon* . U.S. Geological Survey Open-File Report 2012–1024–B, 30 p.

Cuadros J., and Linares J. . (1996). Experimental kinetic study of the smectite-to-illite transformation. . *Geochimica et Cosmochimica Acta, Vol. 60, No. 3,*, 439-453.

De Man, E. S. (2010). On the Nature and Chronostratigraphic Position of the Rupelian and Chattian Stratotypes in the Southern North Sea Basin. *Episodes, Vol. 33*.

Dolson, J. H., He, Z. and Horn, B.W. (2017). Advances and Perspectives on Stratigraphic Trap Exploration-Making the Subtle Trap Obvious. *AAPG Datapages, Search and Discovery Article #60054.*

Edenfield, M. E. (1998). *Kinetics of Smectite to Illite Transformation at Cerro Negro, New Mexico. A Thesis Presented in Partial Fulfillment of Requirements for the Degree of Master of Science.* Atlanta, Georgia: Georgia State University.

Elliott WC, Aronson JL, Matisoff G, Gautier DL. (1991). Ki- netics of the smectite to iltite transformation in the Denver basin: clay mineral, K/Ar, and mathematical model results. *Am Assoc Petrol Geol Bull 75*, 436-462.

Elliott, W. C. (1988). *Bentonite illitization in two contrasting cases: The denver basin and the southern appalachian basin.* Retrieved from https://www.proquest.com/dissertations-theses/bentonite-illitization-two-contrasting-cases/docview/303542049/se-2?accountid=11226.

Elliott, W.C., and Matisoff, G. (1996). Evaluation of Kinetic Models for the Smectite to Illite Transformation. *Clays and Clay Minerals*, Vol. 44, No. 1, 77-87.

Elliott, W.C., Edenfied, A.M., Wampler, J.M., Matisoff, G. and Long, P.E. (1999). The Kinetics of Smectite to Illite Transformation in Cretaceous Bentonites, Cerro Negro, New Mexico. *Clays and Clay Minerals, Vol. 47 No. 3*, 286-296.

Elliott, W.C., Wampler, J.M., Kadir, S., Külah, T., Connell, K.E., Önalgil, N., Erkoyun, H., . (2021). K-Ar age constraints on the sources of K minerals in bentonites of the Ankara-Çankırı Basin, Central Anatolia, Turkey. . *International Journal of Earth Sciences (Geol Rundsch). Springer Verlag 109(7),* , 2353-2367.

English, J. M., and Johnston, S. T. (2004). The Laramide Orogeny: What Were the Driving Forces? *International Geology Review, Vol. 46*, 833–838.

Eslinger, E., and Peaver, D.R. (1988). *Clay Minerals for Petroleum Geologists and Engineers.* Tulsa, OK,: SEPM (Society for Sedimentary Geology).

Faure, G., Mensing, T.M.,. (2005). *Isotopes: Principles and Applications Third Edition.* Hoboken, New Jersey: John Wiley and Sons.

Finn, T. (2021). *Stratigraphic cross sections of the Mowry Shale and associated strata in the Wind River Basin, Wyoming.* Reston, VA: USGS Numbered Series.

Finn, T. (2021,). Stratigraphic cross sections of the Mowry Shale and associated strata in the Wind River Basin, Wyoming:. *U.S. Geological Survey Scientific Investigations Map 3476*, 1 sheet,14-p. pamphlet,.

Ge, C. (2019). *DSpace@MIT.* Retrieved from MIT Open Access Article: https://hdl.handle.net/1721.1/121880

Gillot, P-V, Hildenbrand, A., Lefevre, J-C, Livade, C. (2006). The K/Ar Dating Method: Principle, Analytical Techniques and application to Holocene Volcanic Eruptions in Southern Italy. . *Acta Volcangologica. Vol. 18*, 55-66.

Green, H., Šegvić, B., Zanoni, G., Omodeo-Salé, S., & Adatte, T. (2020). Evaluation of shale source rocks and clay mineral diagenesis in the permian basin, USA: Inferences on basin thermal maturity and source rock potential. . *Geosciences, 10(10)*, 381.

Hoffman, J., & Hower, J. (1979). Clay Mineral Assemblages as Low Grade Metamorphic Geothermometers: Application to the Thrust Faulted Disturbed Belt Of Montana, U.S.A. *Society for Sedimentary Geology SEPM*.

Hower, J. (1981). X-ray diffraction of mixed layer clay minerals. In e. EJ. Longstaffe, *In Clays and the Resource Geologist* (pp. 39-59). Mineralogical Society of Canada Short Course Handbook.

Hower, J., Eslinger, E. V., Hower, M. E., and Perry, E. A. (1976). Mechanism ofburial metamorphism ofargillaceous sediments: . *Mineralogical and chemical evidence: Geol. Soc. Amer. Bull. 87*, 725-737.

Huang, W. L., Longo, J. M., and Pevear, D. V. (1993). An Experimentally Derived Kinetic Model for Smectite-to-Illite Conversion and its Use as a Geothermometer. *Clays Clay Miner. 41*, 162–177.

Huertas, F. J. (2007). Transformation reactions in phyllosilicates at low temperature: experimental approach . *Sociedad Espanola de Mineralogia*.

Huff, W. (1962). Mineralogy of Ordovician K-bentonites in Kentucky. *Clays and Clay Minerals,v. 11,*, 200-209.

Jackson, M. L. (1979). , *Soil Chemical Analysis-Advanced Course, A Manual of Methods Useful for Instruction and Research in Soil Chemistry, Physical Chemistry of Soils, Soil Fertility, and Soil Genesis.* Published by the Author.

Jiang, S. (2012).). *Clay minerals from the perspective of oil and gas exploration. Clay minerals in nature-their characterization, modification and application.*

Jiao, Z. S. and Surdam, R. C. (1993). Low-Permeability Rocks, Capillary Seals, and Pressure Compartment Boundaries in the Cretaceous Section of the Powder River Basin. *WGA, 2005 - Jubilee Anniversary Field Conference Guidebook: Wyoming Geology, Past, Present, and Future,*. Laramie, Wyomming: Wyoming Geology Association.

Kadir, S., Külah, T., Erkoyun, H., Önalgil, N., Eren, M., Elliott, W.C., . (2021). Mineralogy, geochemistry, and genesis of bentonites in the Upper Cretaceous pyroclastics of the Bereketli member of the Reşadiye Formation, Reşadiye, (Tokat), Turkey. .*Applied Clay Science.* , v. 204,106024.

Kelley, S. (2002). K-Ar and Ar-Ar Dating. *Reviews in Mineralogy and Geochemistry*, 785-818.

Lázaro, B. B. (2007). Illitization processes: Series of dioctahedral clays and mechanisms of formation . *Seminarios de la Sociedad Española de Mineralogía. Vol. 3*.

Lee, M. J. (1985). K/Ar dating of time of gas emplacement in Rotliegendes sandstone. *Netherlands. AAPG Bulletin, v. 69,,* , 1381 1385.

Lichtner, T. D., Toner, R. N., Wrage, J. M., and Lynds R. M. (2020). *Upper Cretaceous Strata in the Powder River Basin: Formation Tops Database, Structure and Thickness Contour Maps, and Associated Well Data.* Wyoming State Geological Survey Open File Report 2020-9, 50 p.

Lynch, L. E. (19979). Burial Diagenesis of Illite/Smectite in Shales and The Origins of Authigenic Quartz and Secondary Porosity in Sandstones. *Geochimica et Cosmochimica Acta, Vol. 61,* 1995-2006.

Lynds, R. M. (2013). Geologic storage assessment of carbon dioxide (CO2) in the Laramide basins of Wyoming. *Wyoming State Geological Survey Technical Memorandum No. 3,* (p. 200 P.). Laramie: Wyoming State Geological Survey.

Magara, K. (1975). Reevaluation of Montmorillonite Dehydration as Cause of Ahnormal Pressure and Hydrocarbon Migratton. *Bull. Am. Assoc. Pet. Geol., 59,* 292-302.

Mao, S. A and Journel, A.G. (1999). Conditional 3D simulation of lithofacies with 2D seismic data. *Computers & Geosciences 25(7),* 845-862.

Merewether, E. (1996). Stratigraphy and tectonic implica-tions of Upper Cretaceous rocks in the Powder River Basin, northeastern Wyoming and southeastern Montana. *U.S. Geological Survey Bulletin 1917–T,* 92.

Moore, D.M and Reynolds, R.C. (1997). *X-Ray Diffraction and the Identification and Analysis of Clay Minerals.* New York: Oxford University Press.

Murshed, N. (2021). *"Clay Mineralogy And Geochemistry Of Pleistocene Sediments From Paleolake Olduvai, Tanzania." Thesis, Georgia State University.* https://scholarworks.gsu.edu/geosciences_theses/152.

Nadeau, P., Wilson, M., McHardy, W., & Tait, J. (1985). The conversion of smectite to illite during diagenesis: Evidence from some illitic clays from bentonites and sandstones. *Mineralogical Magazine, 49 (352)*, 393-400.

Newman, A.C. and Brown, G. (1987). The chemical constitution of clays. *Chemistry of Clays and Clay Minerals*, 1– 128.

Nixon, R. P. (1973). Oil Source Beds in Cretaceous Mowry Shale of Northwestern Interior United States. *AAPG Bulletin, 57 (1)*, 136-161.

Odom, I. E. (1984). Smectite Clay Minerals: Properties and Use. *Philosophical Transactions of the Royal Society of London. Series A, Mathematical and Physical Sciences*, 391-409 .

Oliver, J. (1986). Fluids Expelled Tectonically from Orogenic Belt: Their Role In Hydrocarbon Migration and other Geologic Phenomena. *Geology. V 14*, 99-102.

Osborn, S. G. (2006). *The Timing and Causes of Illite Formation in the Cretaceous Marias River Shale, Disturbed Belt, Montana Marias River Shale, Disturbed Belt, Mont.* Atlanta, Georgia: scholarworks.gsu.edu.

Pevear, D. R. (1999). Illite and hydrocarbon exploration . *National Academy of Sciences colloquium ‘‘Geology, Mineralogy, and Human Welfare,’*, 3440–344.

Pollastro, R. M. (1993). Considerations And Applications Of The Illite/Smectite Geothermometer In Hydrocarbon-Bearing Rocks Of Miocene To Mississippian Age. *Clays and Clay Minerals, Vol. 41*, 119-133.

Pytte, A. (1982). *The kinetics of the smectite to illite reaction in contact metamorphic shales.* New Hampshire: Dartmouth College, Hanover,.

Pytte, A.M., and Reynolds, R.C. (1989). (1989). *The Thermal Transformation of Smectite to Illite. In M. T. In: Naeser N.D., Thermal History of Sedimentary Basins.* New York: NY: Springer.

Rahman, M. W., Olson, R. K., Symcox, C. W., & Bingham, S. (2016). Geochemistry of Cretaceous Oils and Source Rocks in the Powder River Basin. *In Unconventional Resources Technology Conference,* (pp. 496-508). San Antonio, Texas,: Society of Exploration Geophysicists, American Association of Petroleum Geologists, Society of Petroleum Engineers.

Roberts, N. R. L., Finn, T. M., Lewan, M. D., and Kirschbaum, M. A.,. (2007). *Burial history, thermal maturity, and oil and gas generation history of petroleum systems in the Wind River Basin Province, central Wyoming: Chapter 6 in Petroleum systems and geologic assessment of oil and gas resources in the Wind River Basin Province, .* Reston, VA: USGS Numbered Series.

Sharp, W. N and White A. M. (1956). *Geology of the Pumpkin Buttes Area of the Powder River Basin, Campel and Johnson Counties Wyoming.* Denver: United States of Interior Geological Survey.

Soares, J. and Webb, C. (2018). Evolving Exploration Methods in the Hydrocarbon Play Within the Patchawarra Formation on the Western Flank, Cooper Basin. *ASEG Extended Abstracts*, 1-8.

Stefanov, Y. (2018). Illite/smectite diagenesis and thermal evolution of Lower Cretaceous–Paleogene successions in the Dolna Kamchiya Depression, Eastern Bulgaria. *GEOLOGICAL BALCANICA, ,* 3-21.

Stephens, E. C., Anderson, J. R., Gullet-Young, C., Wampler, J. M., Elliott, W. C.,. (2007). Age of the Ocmulgee Limestone (Georgia Coastal Plain) Based on Revised Methodology for the K-Ar Age of Glaucony. *Southeastern Geology*, 15-24.

Stevens, T., Palk, C., Carter, A. Lu, H., Clift, P.D. (2010). Assessing the provenance of loess and desert sediments in northern China using U-Pb dating and morphology of detrital zircons: . *Geological Society of America Bulletin, v. 122*, 1331-1344.

Stroker, T. M. (2009). *K-Ar Dating of Authigenic Illites: Integrating the Diagenic History of the Fluvial William Fork Formation, Mesa Verde Group, Piceance Basin, NW Colorado. Thesis, Colorado School of Mines.* Denver, Colorado: mountainscholar.org.

Stroker, T. M., Harris, N. B., Elliott, W. C., Wampler, J. C.,. (2013). Diagenesis of a tight gas sand reservoir: Upper Cretaceous Mesaverde Group, Piceance Basin, Colorado. *Marine and Petroleum Geology, Volume 40.*, 48-68.

Surdam, R.C., Jiao, Z., De Bruin, R.H., and Bentley, R.D. (2010). *Shale Gas Potential of the Mowry Shale in Wyoming Laramide Basins.* Colorado: Wyoming State Geological Survey Challenges in Geologic Resource Development .

Whitney, G. and Northrop, H. R. (1988). Experimental in- vestigation of the smectite to illite reaction: Dual reaction mechanisms and oxygen-isotope systematics. *Amer. Mineral. 73*, 77-90.

Zhang, F., Lenton, T. M., Rey, A., Romaniello, S. J., Chen, X., Planavsky, N. J., Clarkson, M. O., Dahl, T. W., Lau, K. V., Wang, W., Li, Z., Zhao, M., Isson, T., Algeo, T. J., Anbar, A. D. (2020). Uranium isotopes in marine carbonates as a global ocean paleoredox proxy: A critical review. *Geochimica et Cosmochimica Acta,*, 27-49.

Zheng, X-Y., Beard, B.L., Elliott, W.C., Johnson, C.M., 2020, Tracing diagenetic smectite-illite transition using stable K isotopes: Goldschmidt Conference Honolulu, HI. ***G****oldschmidt Abstracts*, 2020 3186.

Zielinski, R. A. (1983). The Mobility of Uranium and other Elements during Alteration Of Rhyolite Ash To Montmorillonite: A Case Study in the Troublesome Formation, Colorado, U.S.A. *Chemical Geology*, 185-204.

APPENDICES

Appendix A: X-ray Analyses

Appendix A.1 Method: Sample Preparation and Procedure

Steps	Procedure	Duration
Soaking of sample	20-30 grams of bentonite samples were soaked in deionized (DI) water	14 days
Disaggregation of sample	Mild crushing and disaggregation of samples in DI water in a mortar and pestle followed, in order to reduce large clumps and increase clay content	
Sample Treatment and Removal of Carbonate Cements, Gross Organic Matter and Iron (III) Oxides	First, samples were treated with Sodium Acetate-Acetic Acid Buffer (CH_3COOH + CH_3COONa) pH = 5, at 50°C water bath heating to remove carbonate cement. Followed by hydrogen peroxide (H_2O_2) treatment of samples to remove gross organic matter at 50°C water bath heating. Removal of Iron (III) oxide (Fe_2O_3) from Bentonite with Sodium Citrate ($Na_3C_6H_5O_7$), Sodium Bicarbonate ($NaHCO_3$) and Sodium Dithionite ($Na_2O_4S_2$) at 50°C water bath heating.	4 - 24 hours 30 minutes 25-30 minutes
Separation of Clay from Silt and Sand	> 50-micron Sand was the first to be separated from clay using the time settling technique. 2 – 20-micron grain size silt was then separated from the clay via the same technique. < 2-micron clay was finally separated and retrieved using the time settling method, flocculated and centrifuged to get clay concentrate.	45 – 60 seconds 5 - 5.5 minutes 8 hours

Mounting < 2-micron clay fraction on clean Petrographic glass slide	Using a pipette, 1 ml < 2-micron clay was mounted on a petrographic glass slide. Allowed to air-dried overnight and ready for X-Ray Diffraction Analysis	 6 - 12 hours
X-Ray Diffraction Analyses of Air-dried and Ethylene Glycol Solvated oriented mount clay	Air-dried, < 2-micron Oriented mount clay was scanned using X-Ray Diffractometer with the following specification; Cu radiation (45 kV, 40 mA), Ni-filter from 2- 40 degrees two theta at a speed of 1 degree two theta per two minutes. Samples kept in ethylene glycol vapor for 24 hours were also scanned using X-Ray Diffractometer with the same specifications	1.10 hours 24 – 25.10 hours

Appendix A.2 X-Ray Diffraction Patterns.

The patterns were labeled with specific d-spacings (Glycol Solvated, Air Dried and Heated). X-Ray Diffraction Patterns for the Mowry Bentonites Samples.

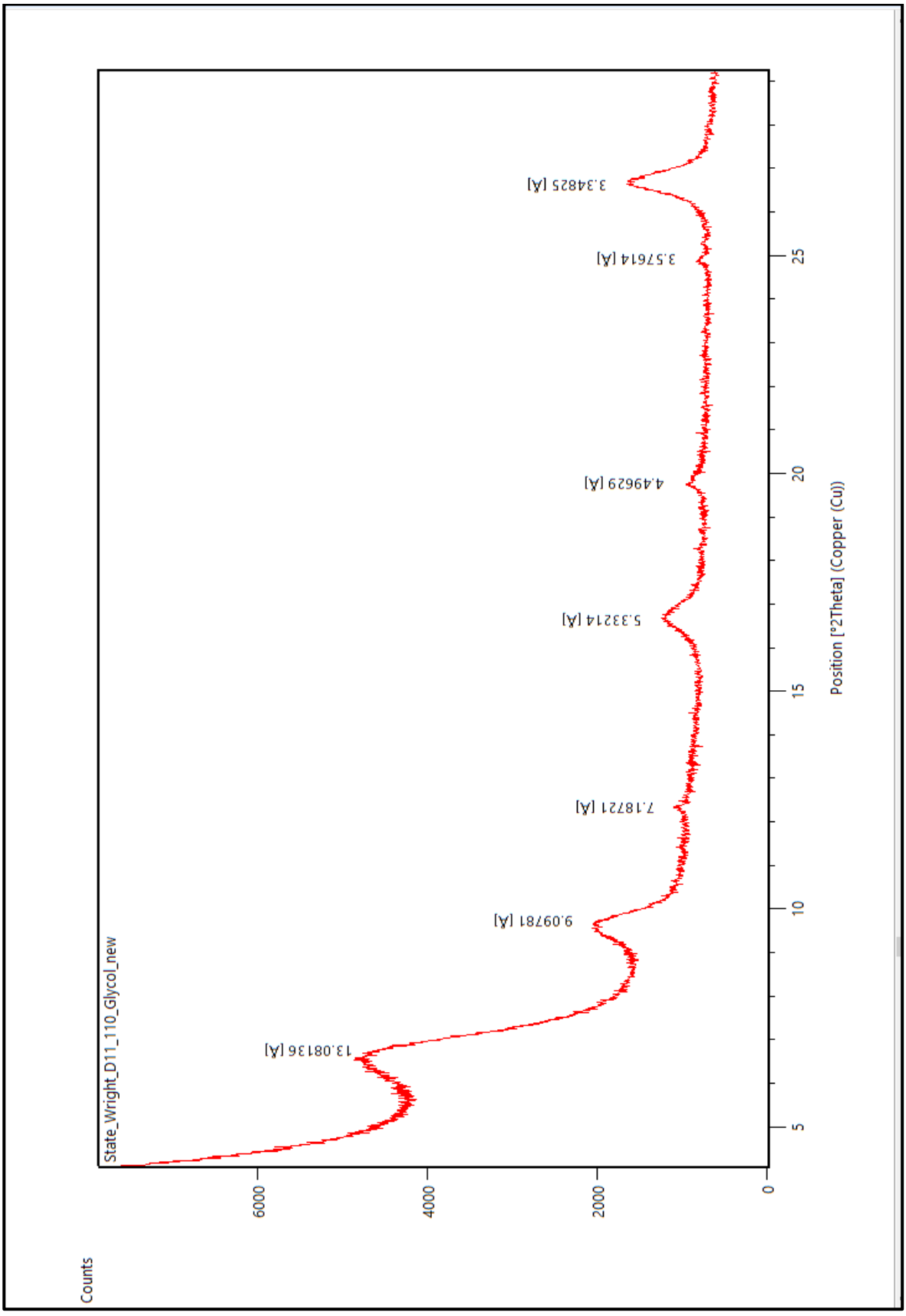
State_Wright_D11_110_Glycol_new
13.08136 [Å]
9.09781 [Å]
7.18721 [Å]
5.33214 [Å]
4.49629 [Å]
3.57614 [Å]
3.34825 [Å]
Counts
0
2000
4000
6000
5
10
15
20
25
Position [°2Theta] (Copper (Cu))

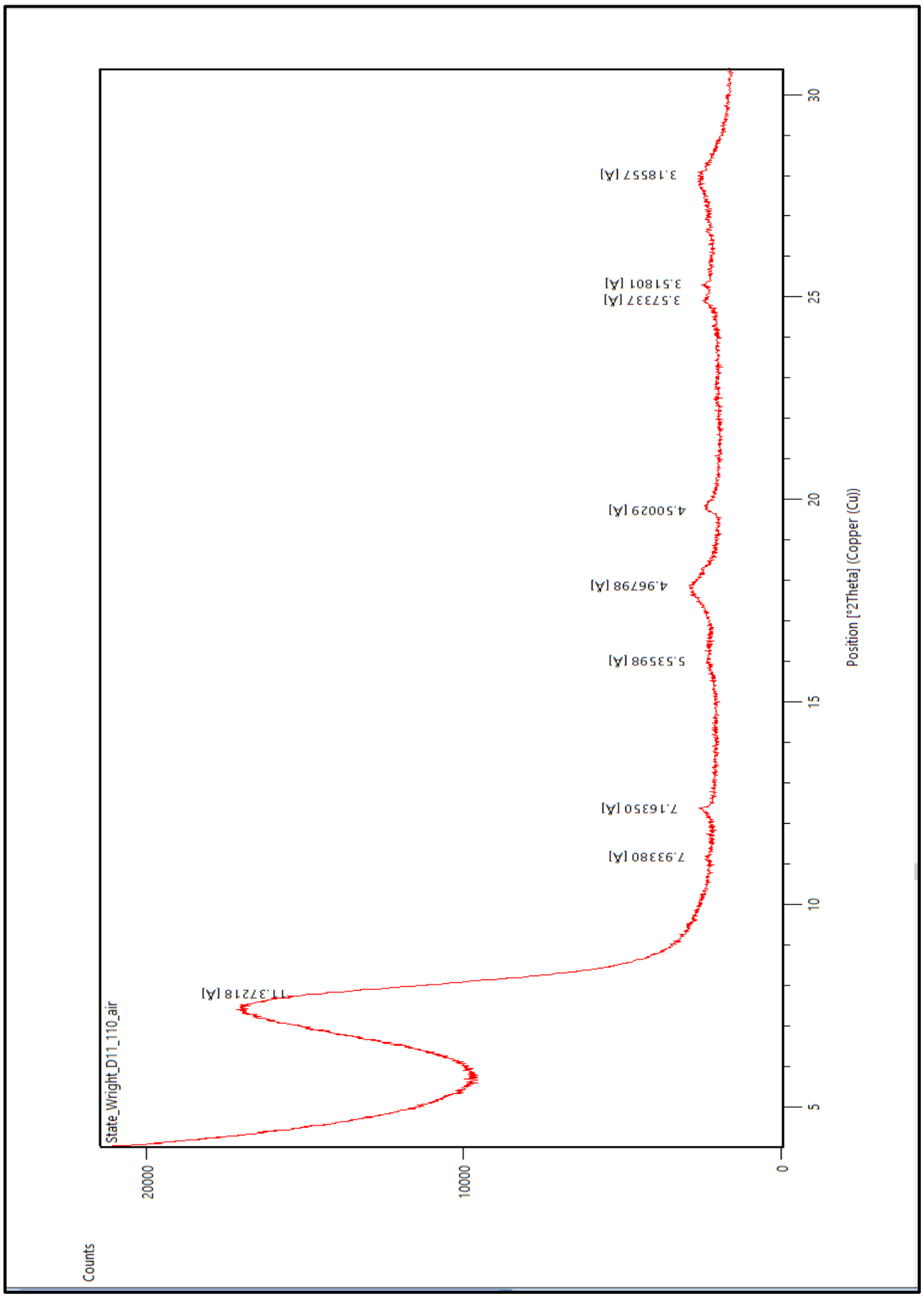
State_Wright_D11_110_air
11.372218 [Å]
7.933801 [Å]
7.163501 [Å]
5.535981 [Å]
4.967981 [Å]
4.500291 [Å]
3.573371 [Å]
3.518011 [Å]
3.185571 [Å]
Counts
20000
10000
0
5
10
15
20
25
30
Position [°2Theta] (Copper (Cu))

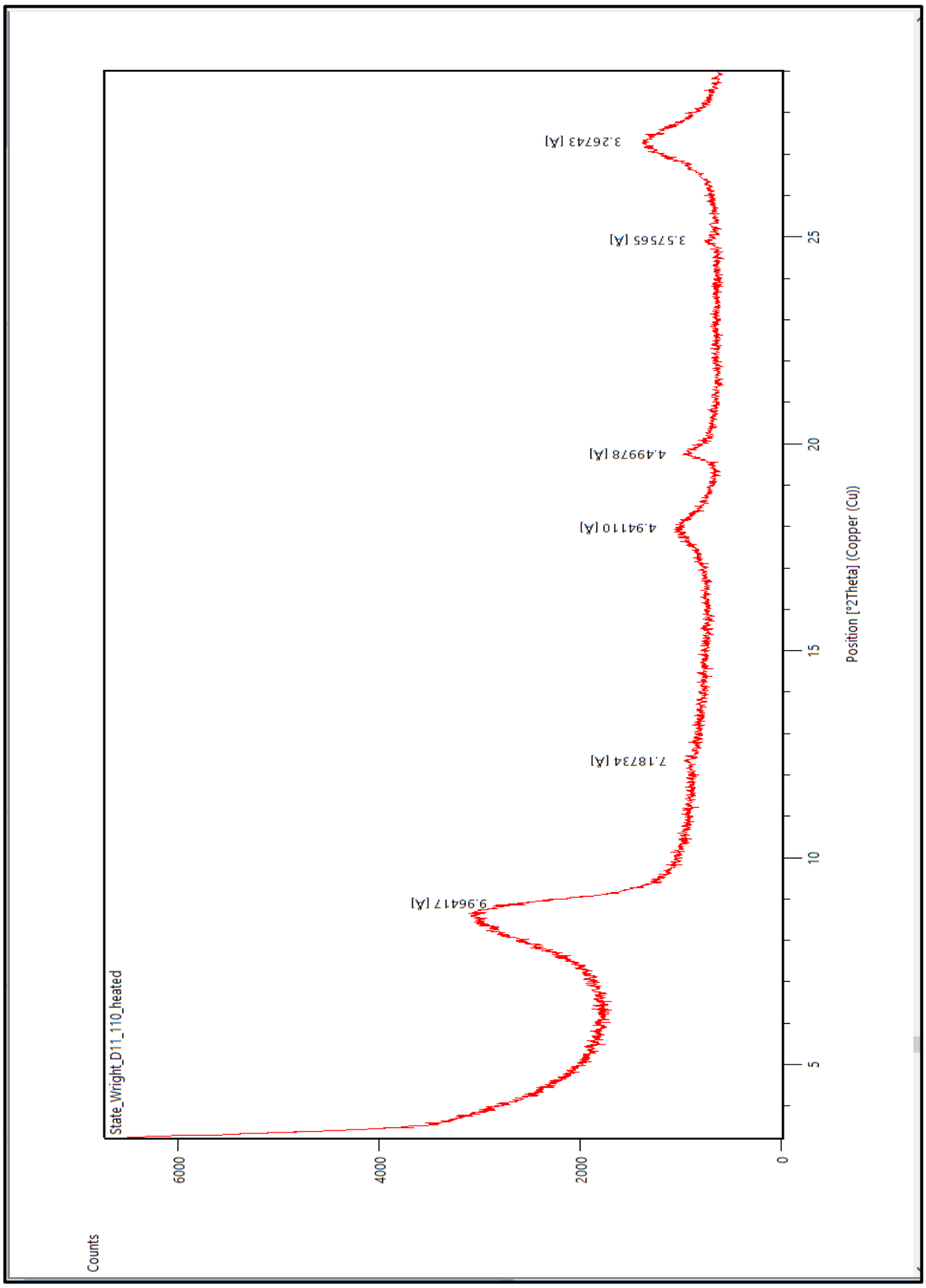
State_Wright_D11_110_heated
Counts
6000
4000
2000
0
5
10
15
20
25
Position [°2Theta] (Copper (Cu))
9.96417 [Å]
7.18734 [Å]
4.94110 [Å]
4.49978 [Å]
3.57565 [Å]
3.26743 [Å]

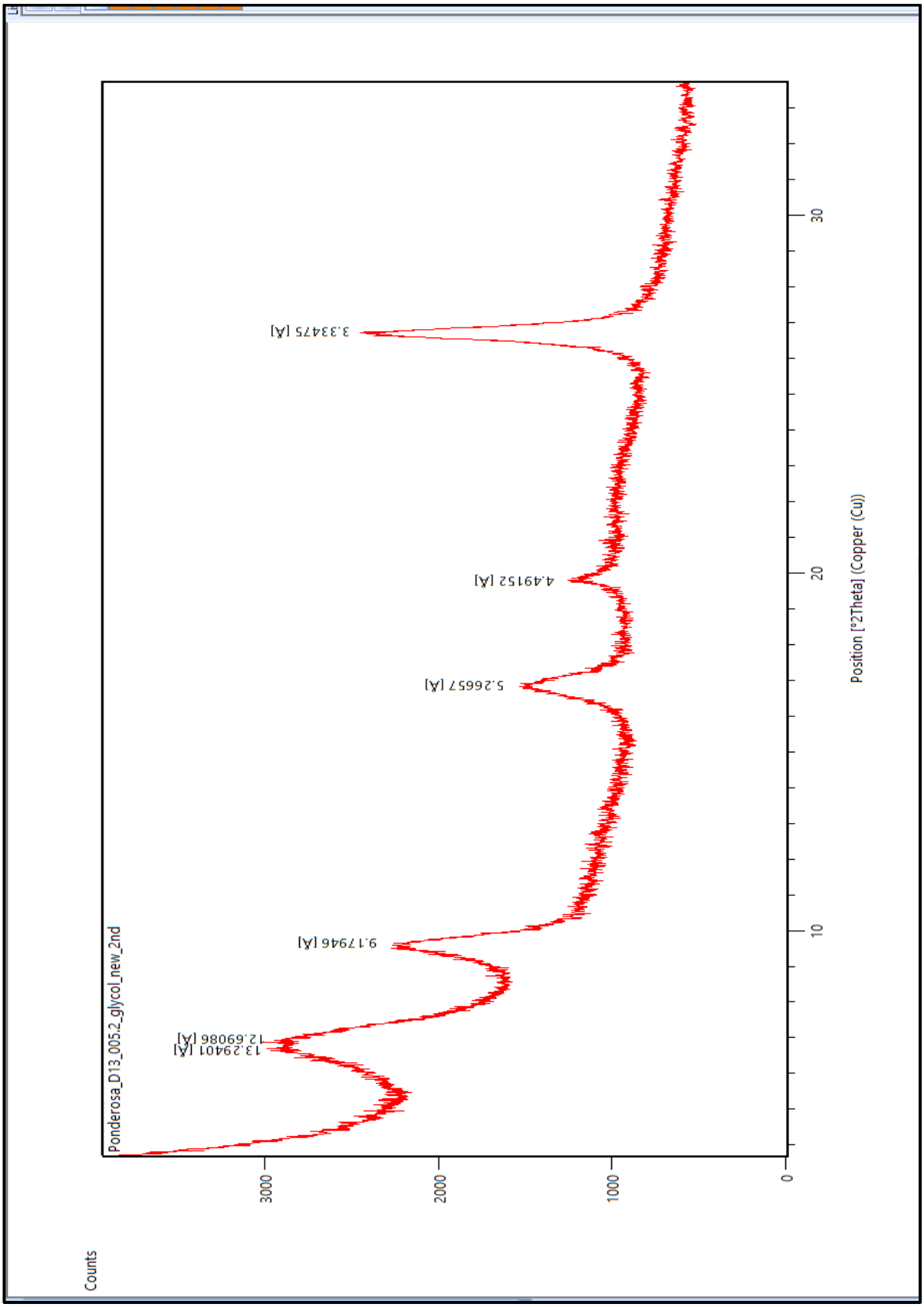
Ponderosa_D13_005.2_glycol_new_2nd
Counts
Position [°2Theta] (Copper (Cu))
0
1000
2000
3000
10
20
30
13.29401 [Å]
12.69086 [Å]
9.17946 [Å]
5.26657 [Å]
4.49152 [Å]
3.33475 [Å]

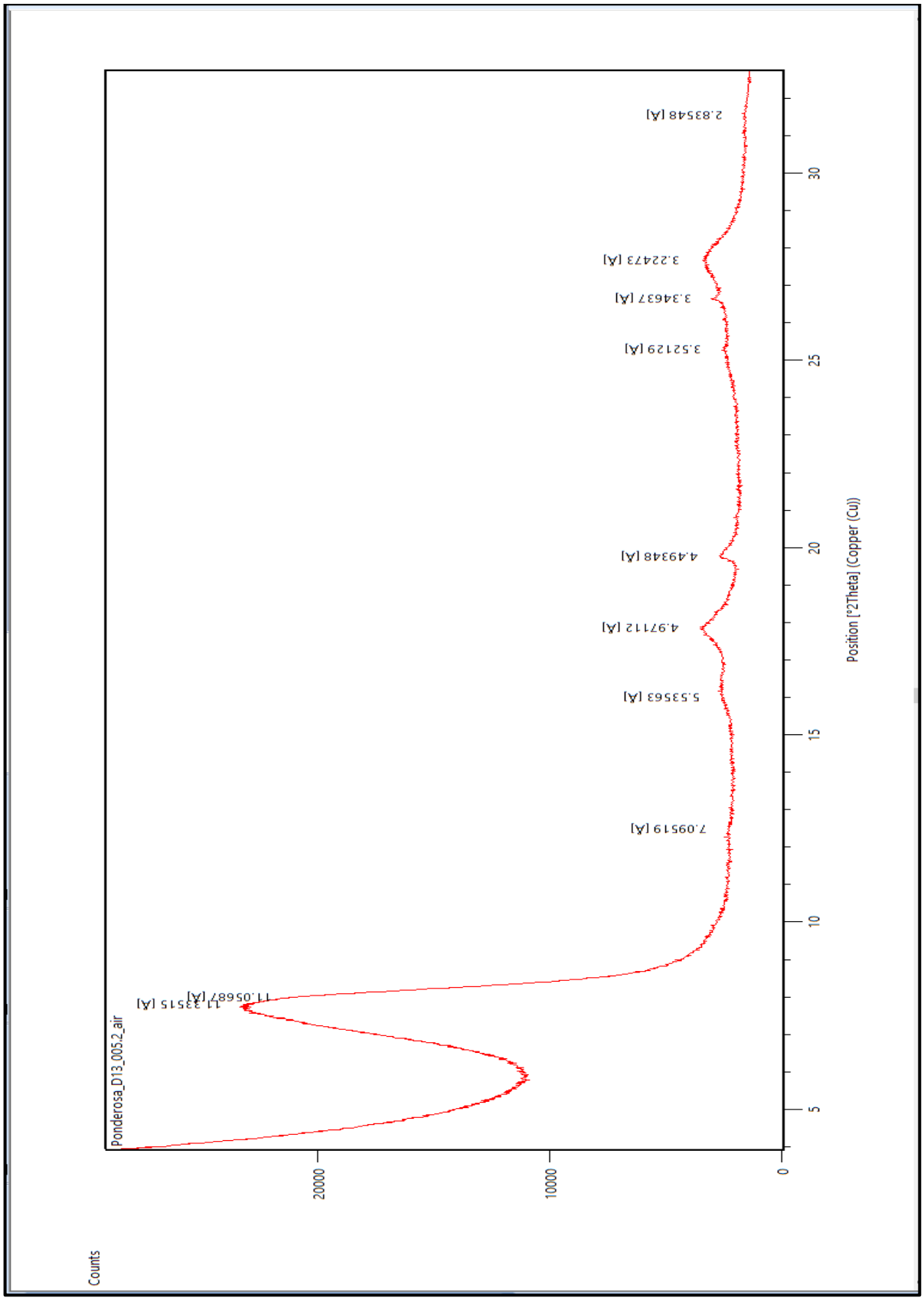
Counts
20000
10000
0
Ponderosa_D13_005.2_air
11.33515 [Å]
11.05687 [Å]
7.09519 [Å]
5.53563 [Å]
4.97112 [Å]
4.49348 [Å]
3.52129 [Å]
3.34637 [Å]
3.22473 [Å]
2.83548 [Å]
5
10
15
20
25
30
Position [°2Theta] (Copper (Cu))

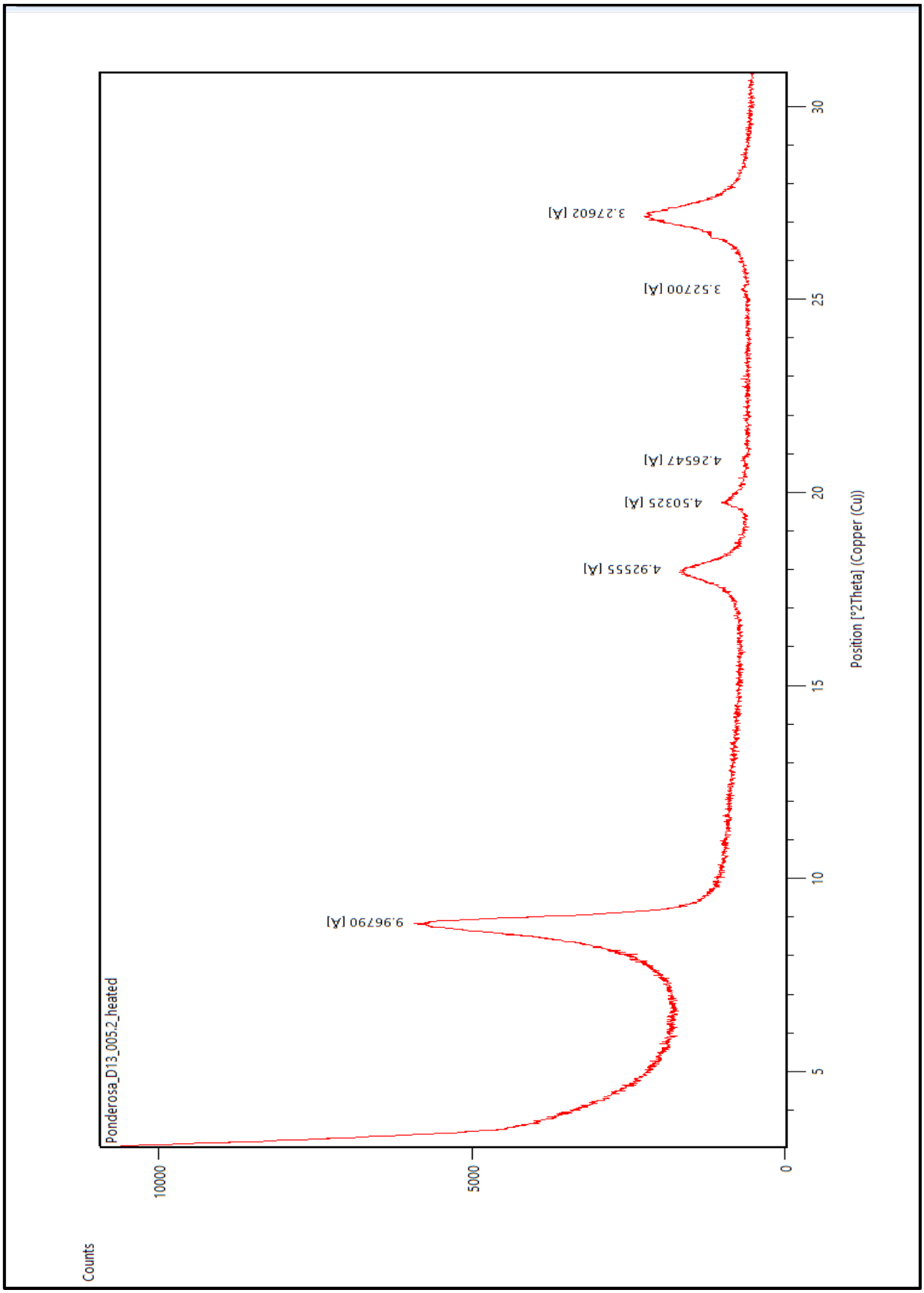
Counts
10000
5000
0
Ponderosa_D13_005.2_heated
9.96790 [Å]
4.92555 [Å]
4.50325 [Å]
4.26547 [Å]
3.52700 [Å]
3.27602 [Å]
5
10
15
20
25
30
Position [°2Theta] (Copper (Cu))

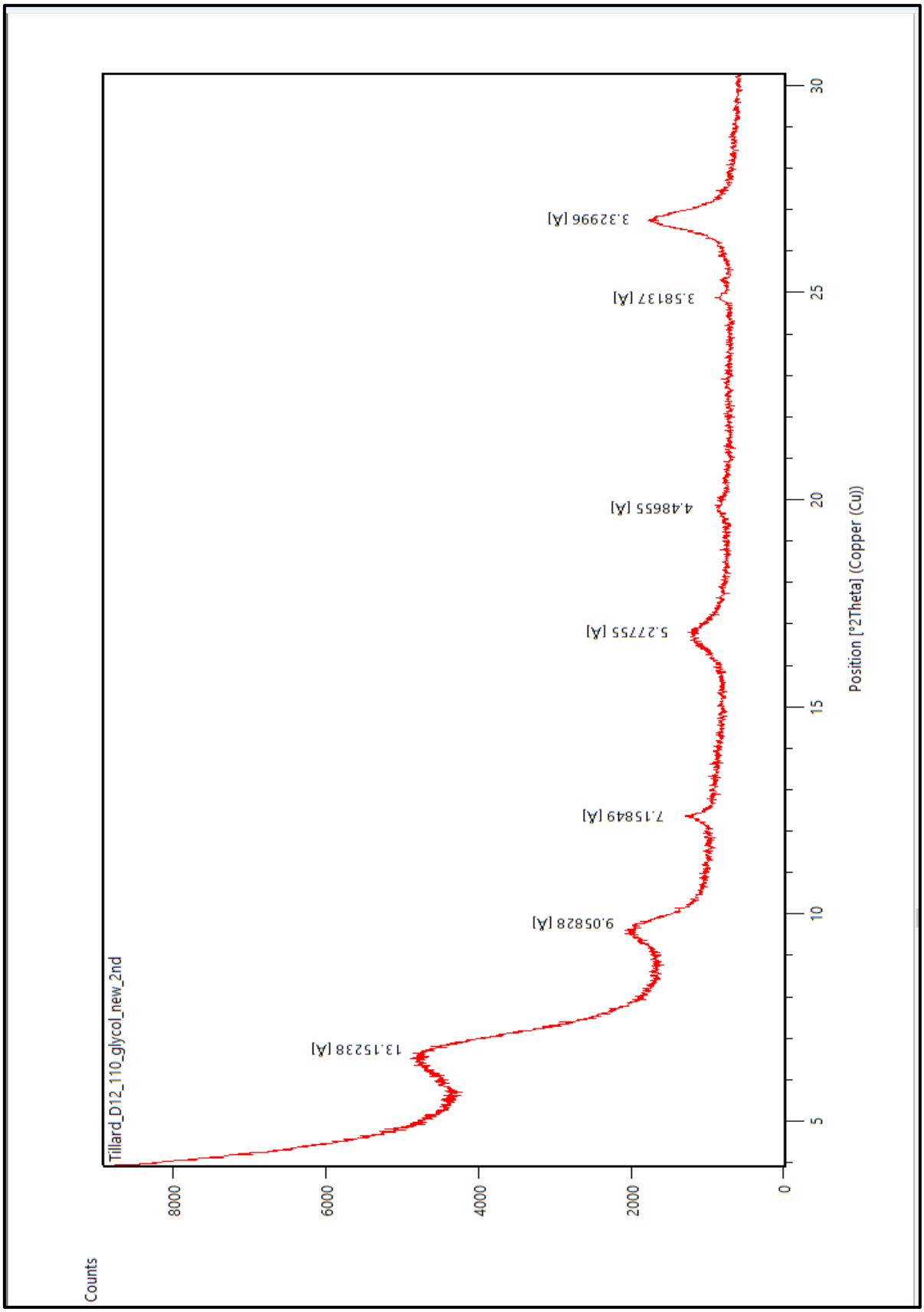
Counts
8000
6000
4000
2000
0
Tillard_D12_110_glycol_new_2nd
13.15238 [Å]
9.05828 [Å]
7.15849 [Å]
5.27755 [Å]
4.48655 [Å]
3.58137 [Å]
3.32996 [Å]
5
10
15
20
25
30
Position [°2Theta] (Copper (Cu))

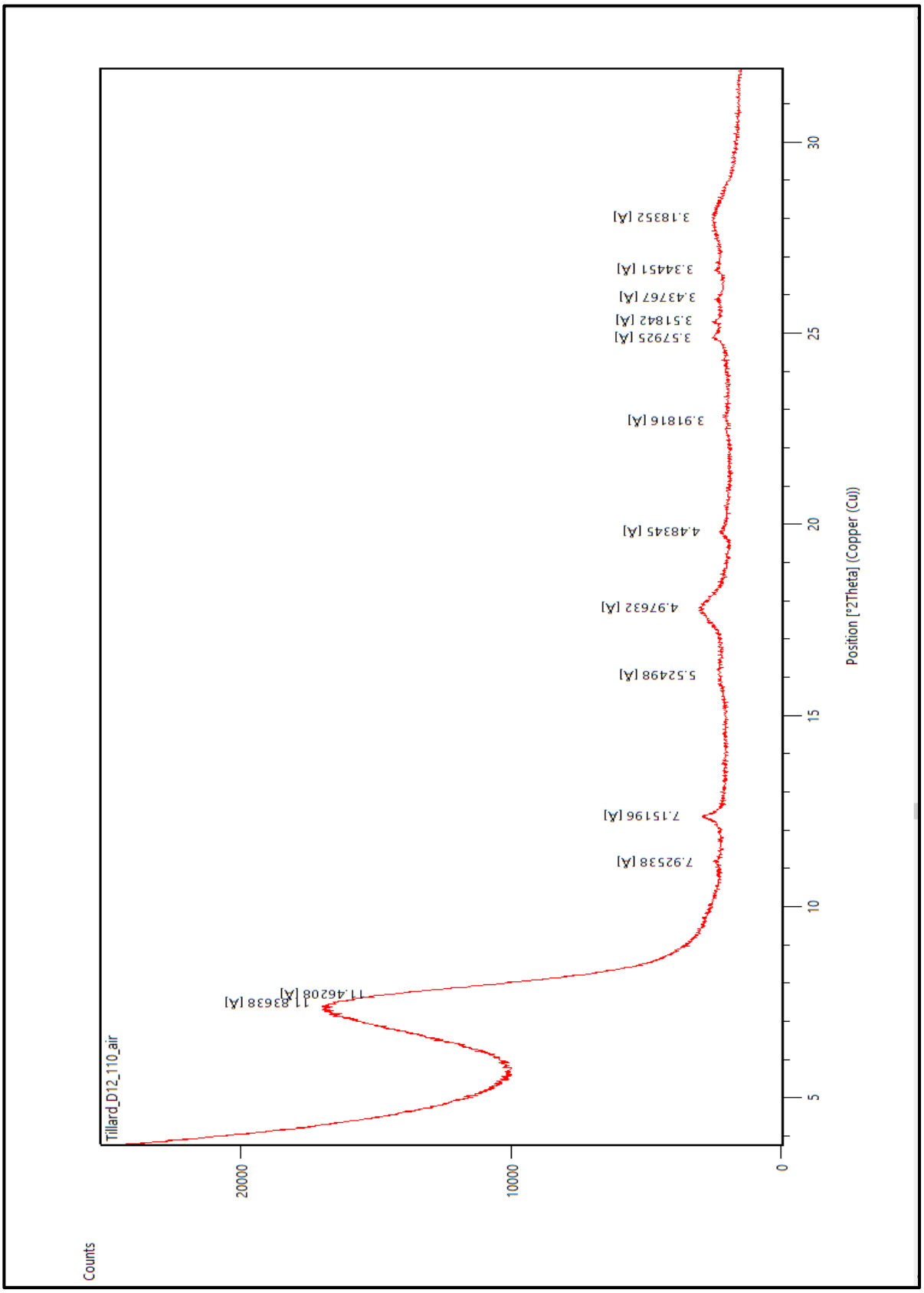
Tillard_D12_110_air
Counts
20000
10000
0
5
10
15
20
25
30
Position [°2Theta] (Copper (Cu))
11.83638 [Å]
11.46208 [Å]
7.92538 [Å]
7.15196 [Å]
5.52498 [Å]
4.97632 [Å]
4.48345 [Å]
3.91816 [Å]
3.57925 [Å]
3.51842 [Å]
3.43767 [Å]
3.34451 [Å]
3.18352 [Å]

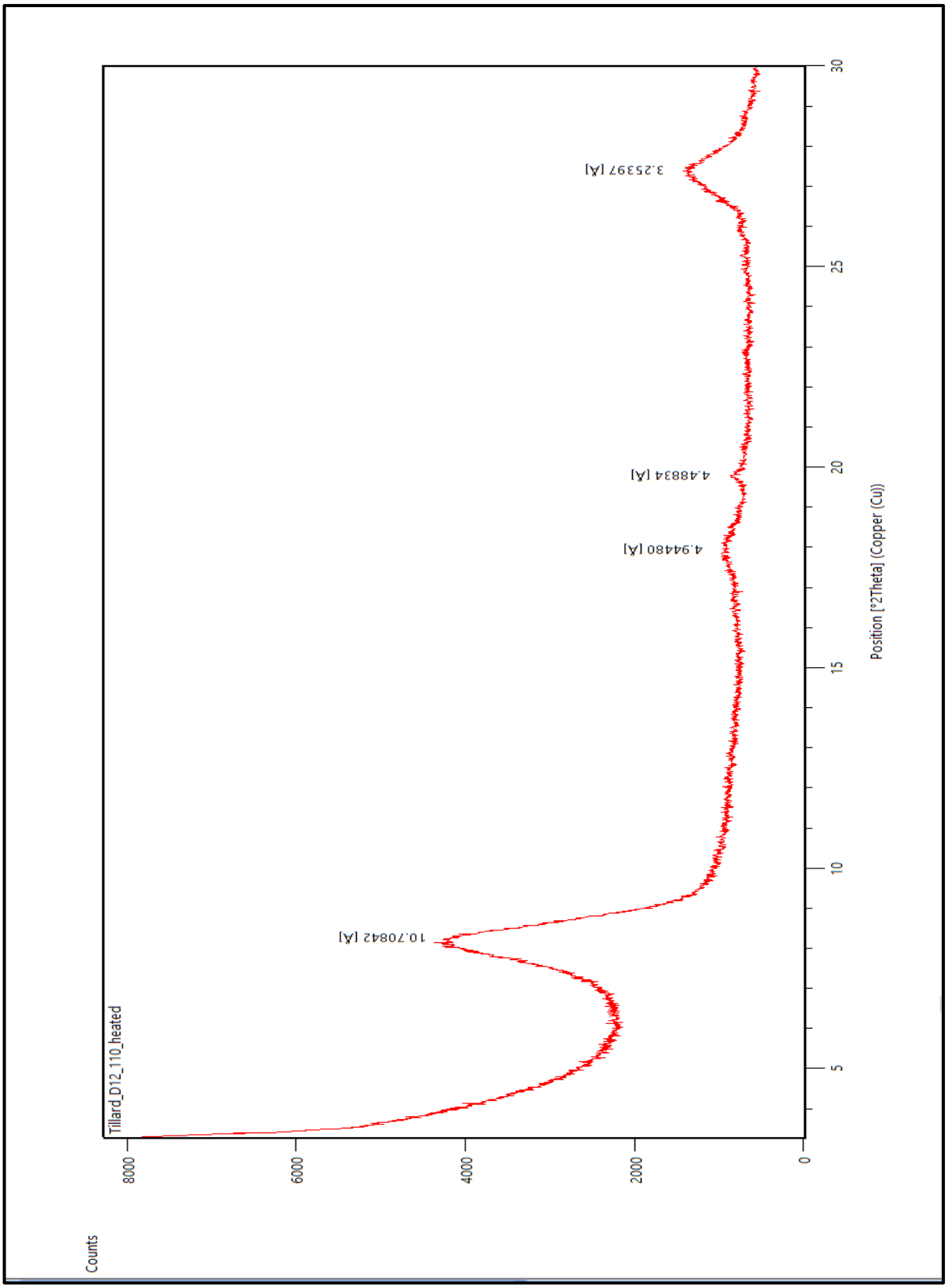
Tillard_D12_110_heated
Counts
8000
6000
4000
2000
0
5
10
15
20
25
30
Position [°2Theta] (Copper (Cu))
10.70842 [Å]
4.94480 [Å]
4.48834 [Å]
3.25397 [Å]

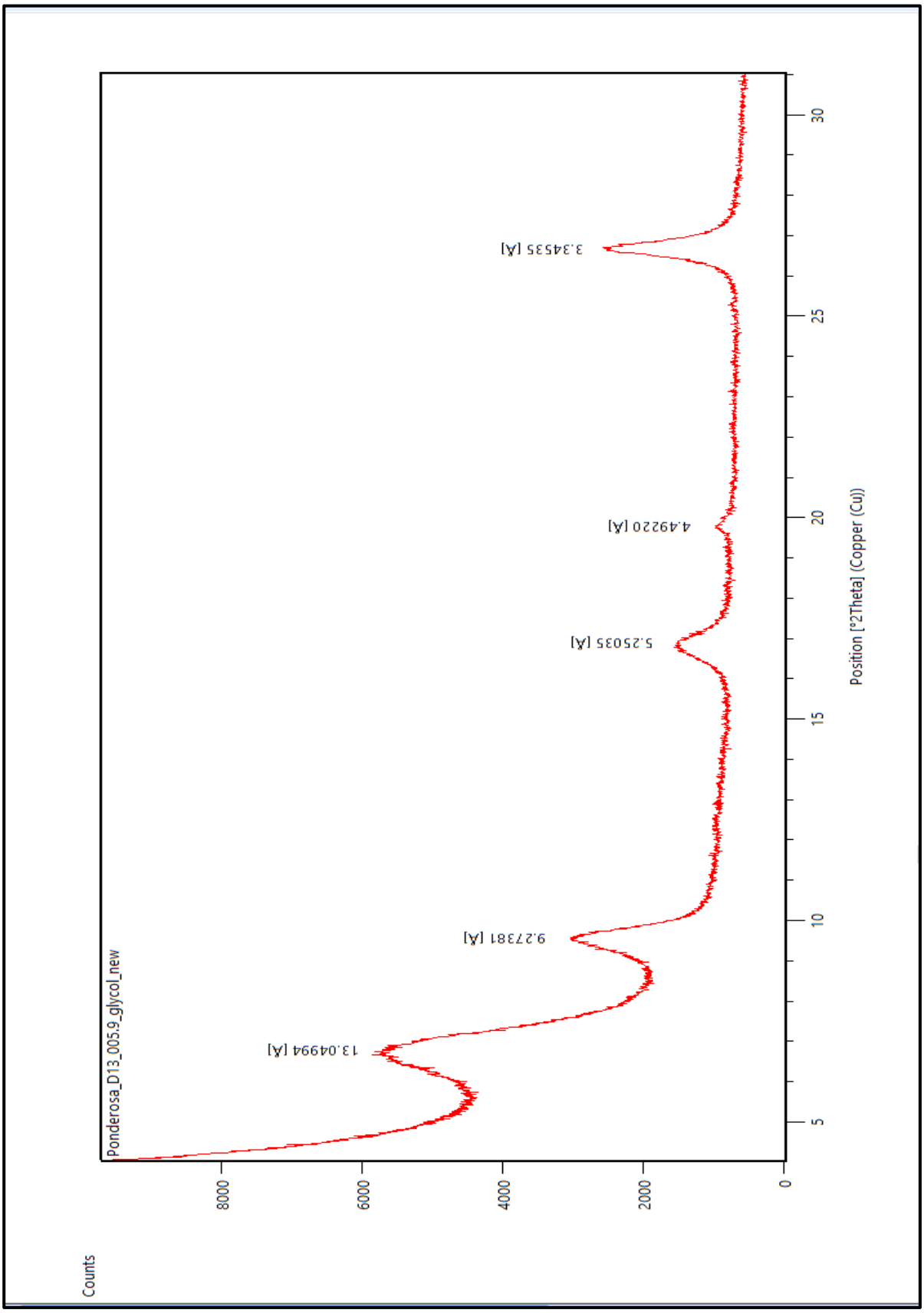
Ponderosa_D13_005.9_glycol_new
Counts
0
2000
4000
6000
8000
5
10
15
20
25
30
Position [°2Theta] (Copper (Cu))
13.04994 [Å]
9.27381 [Å]
5.25035 [Å]
4.49220 [Å]
3.34535 [Å]

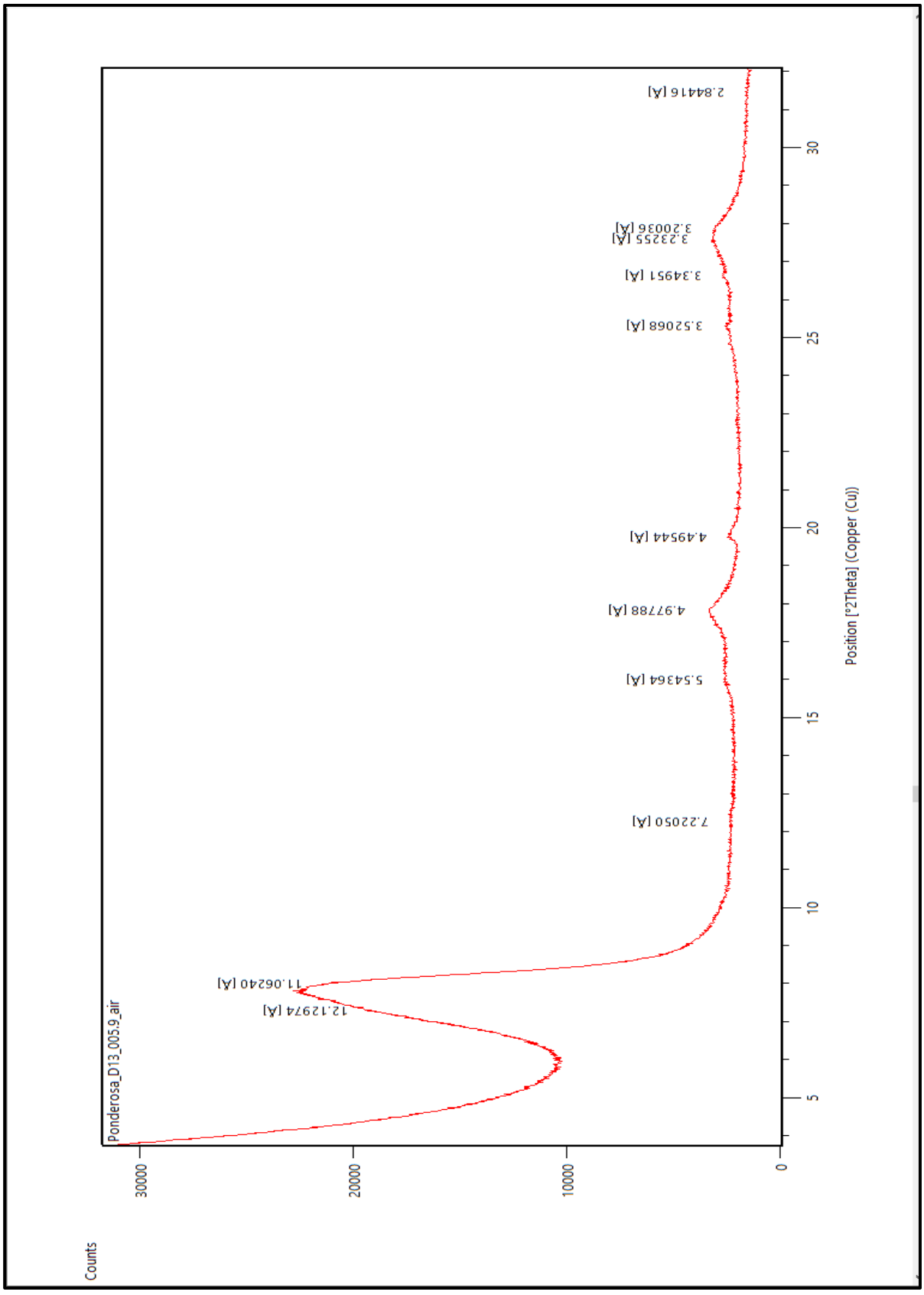
Ponderosa_D13_005.9_air
Counts
30000
20000
10000
0
5
10
15
20
25
30
Position [°2Theta] (Copper (Cu))
11.06240 [Å]
12.12974 [Å]
7.22050 [Å]
5.54364 [Å]
4.97788 [Å]
4.49544 [Å]
3.52068 [Å]
3.34951 [Å]
3.23255 [Å]
3.20036 [Å]
2.84416 [Å]

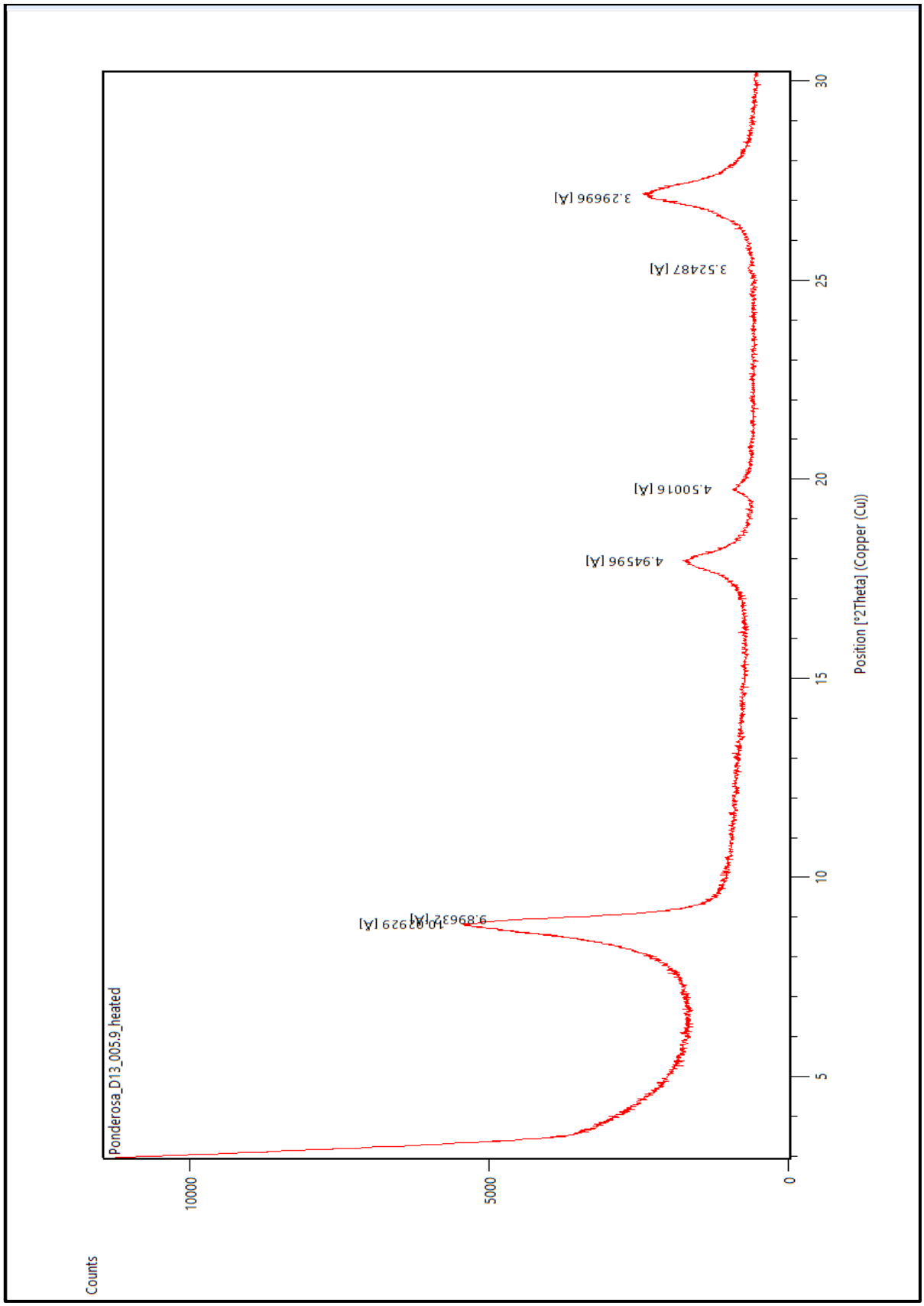
Counts
10000
5000
0
Ponderosa_D13_005.9_heated
9.89632 [Å]
10.02929 [Å]
4.94596 [Å]
4.50016 [Å]
3.52487 [Å]
3.29696 [Å]
5
10
15
20
25
30
Position [°2Theta] (Copper (Cu))

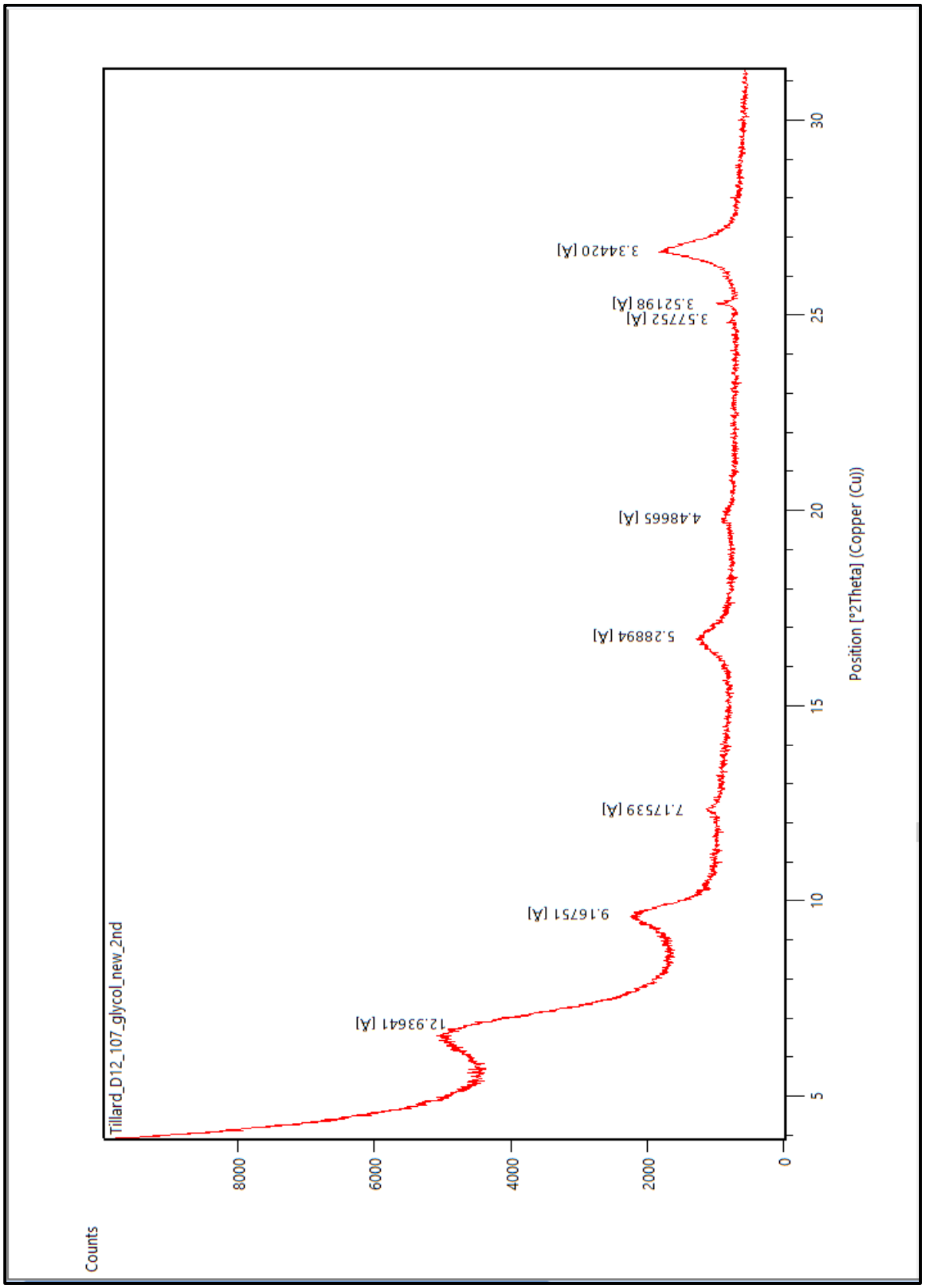
Tillard_D12_107_glycol_new_2nd
Counts
0
2000
4000
6000
8000
5
10
15
20
25
30
Position [°2Theta] (Copper (Cu))
12.93641 [Å]
9.16751 [Å]
7.17539 [Å]
5.28894 [Å]
4.48665 [Å]
3.57752 [Å]
3.52198 [Å]
3.34420 [Å]

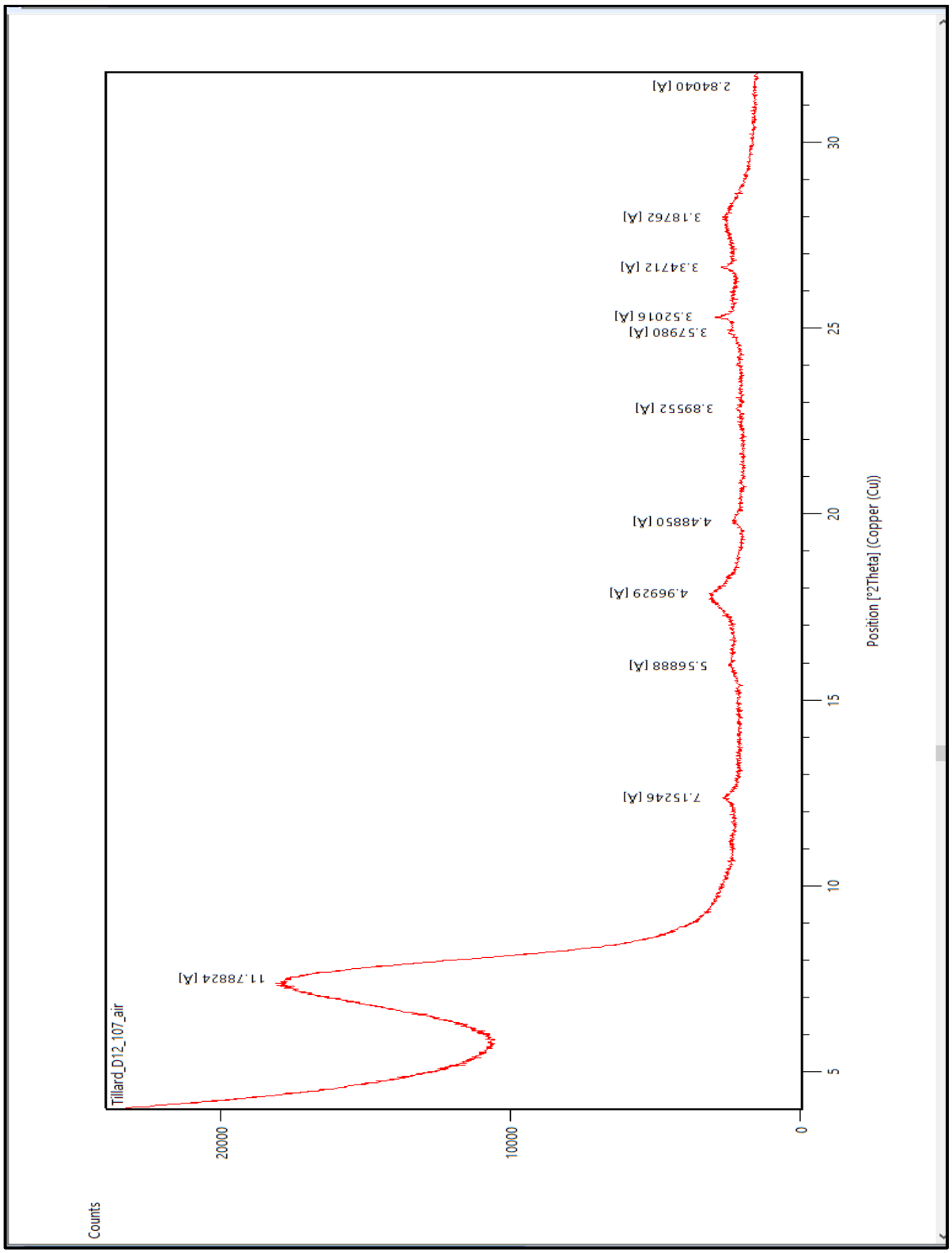
Counts
20000
10000
0
Tillard_D12_107_air
11.78824 [Å]
7.15246 [Å]
5.56888 [Å]
4.96929 [Å]
4.48850 [Å]
3.89552 [Å]
3.57980 [Å]
3.52016 [Å]
3.34712 [Å]
3.18762 [Å]
2.84040 [Å]
5
10
15
20
25
30
Position [°2Theta] (Copper (Cu))

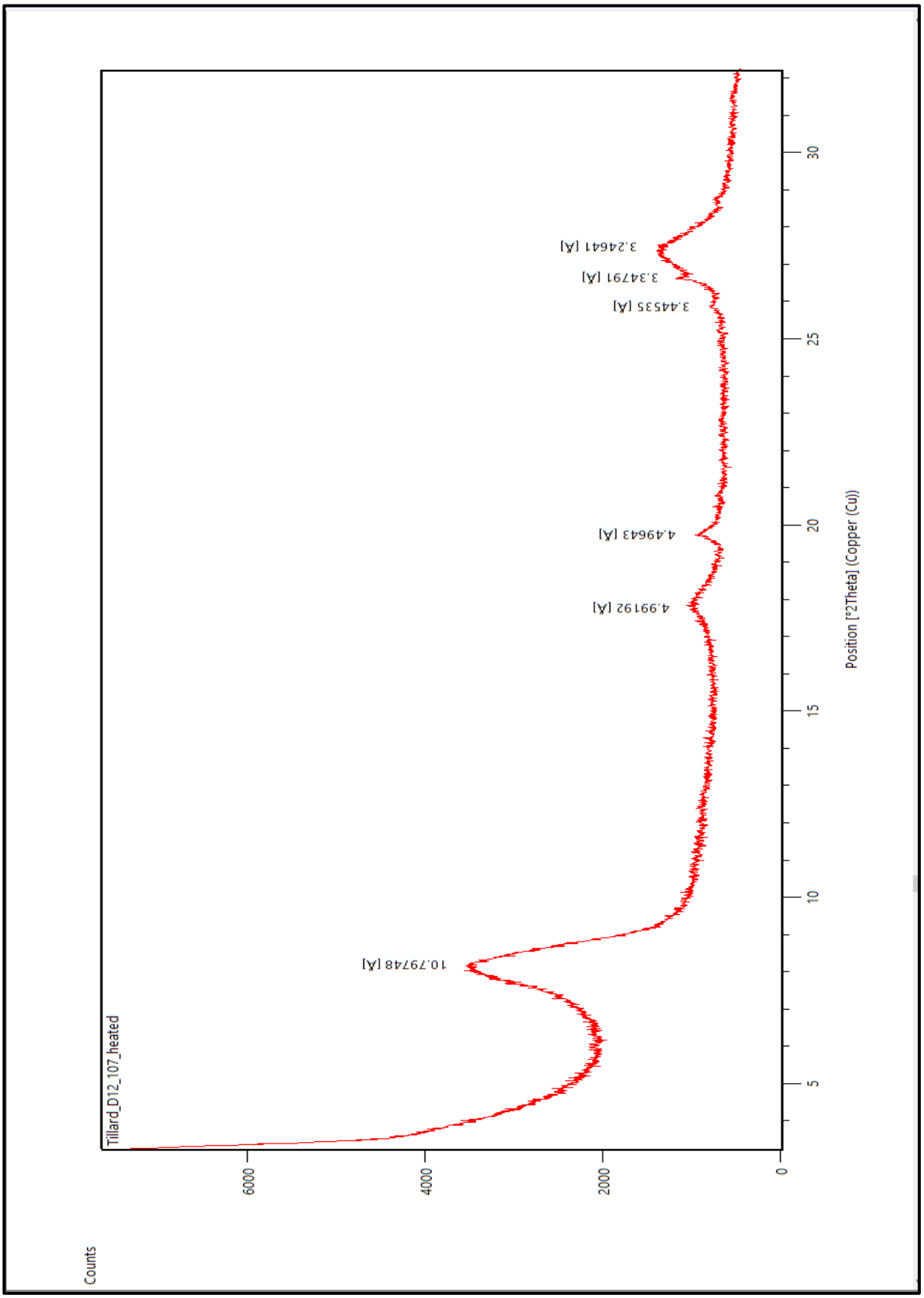
Counts
6000
4000
2000
0
Tillard_D12_107_heated
10.79748 [Å]
4.99192 [Å]
4.49643 [Å]
3.44535 [Å]
3.34791 [Å]
3.24641 [Å]
5
10
15
20
25
30
Position [°2Theta] (Copper (Cu))

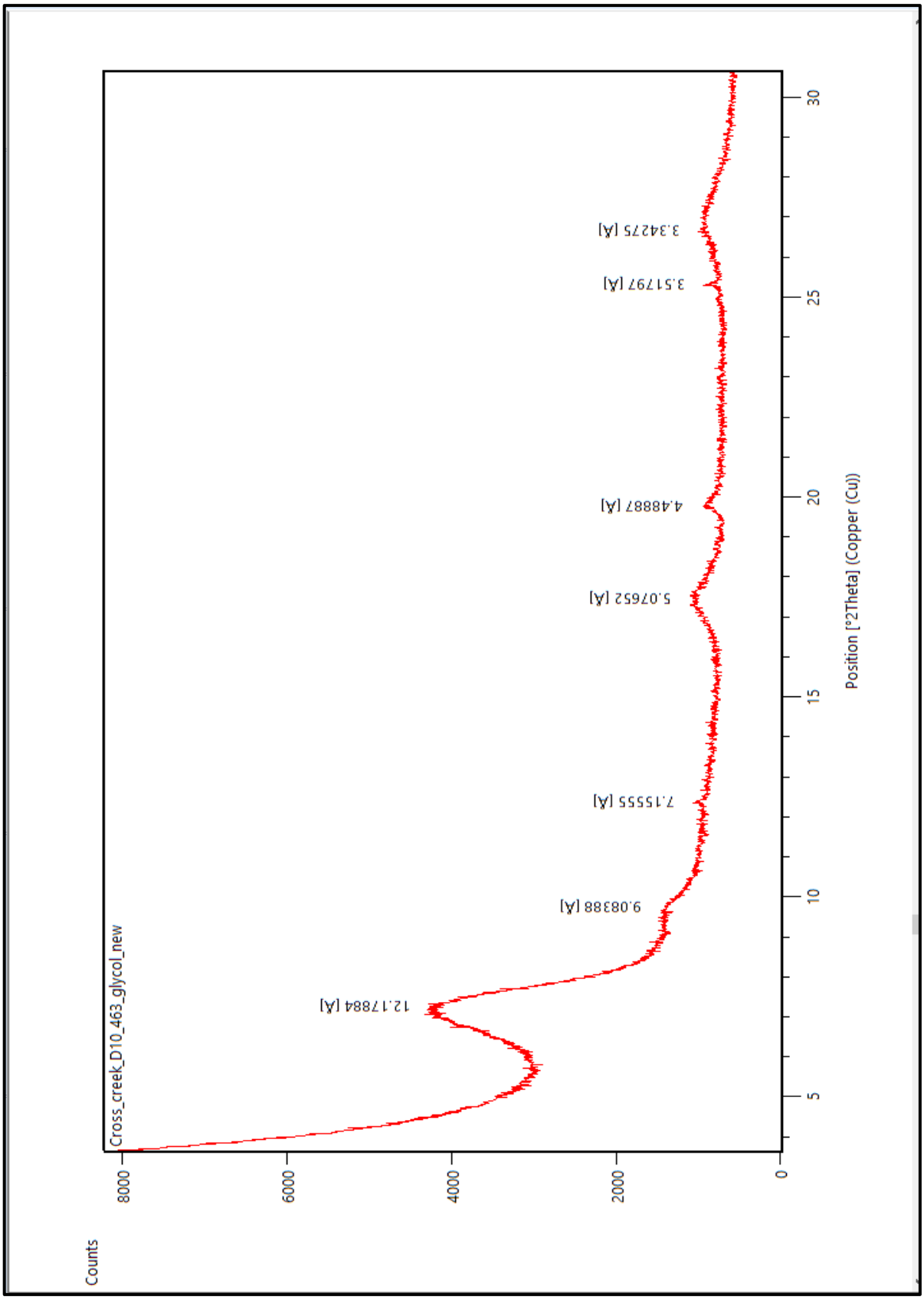
Counts
8000
6000
4000
2000
0
Cross_creek_D10_463_glycol_new
12.17884 [Å]
9.08388 [Å]
7.15555 [Å]
5.07652 [Å]
4.48887 [Å]
3.51797 [Å]
3.34275 [Å]
5
10
15
20
25
30
Position [°2Theta] (Copper (Cu))

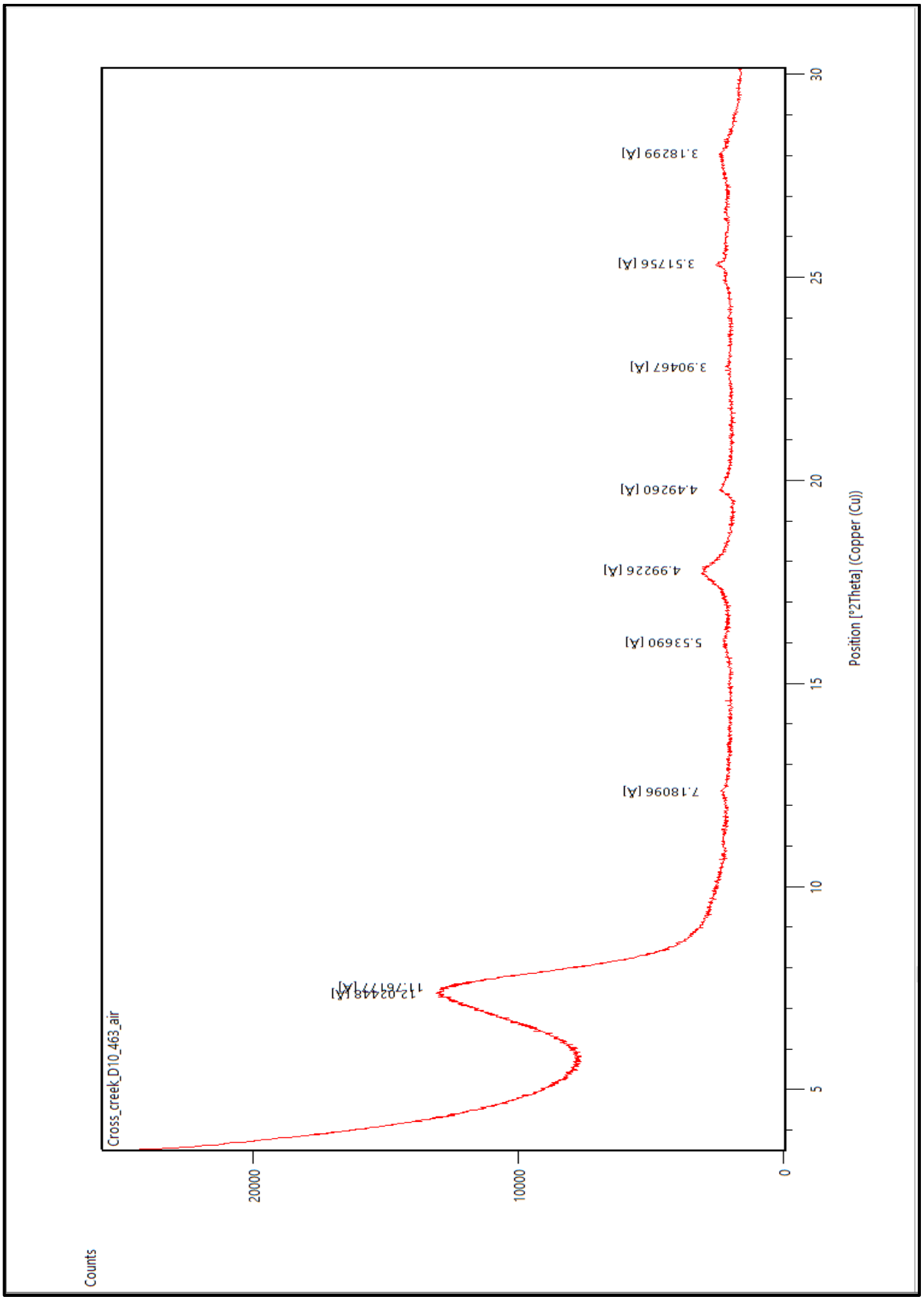
Counts
20000
10000
0
Cross_creek_D10_463_air
12.02448 [Å]
11.76177 [Å]
7.18096 [Å]
5.53690 [Å]
4.99226 [Å]
4.49260 [Å]
3.90467 [Å]
3.51756 [Å]
3.18299 [Å]
5
10
15
20
25
30
Position [°2Theta] (Copper (Cu))

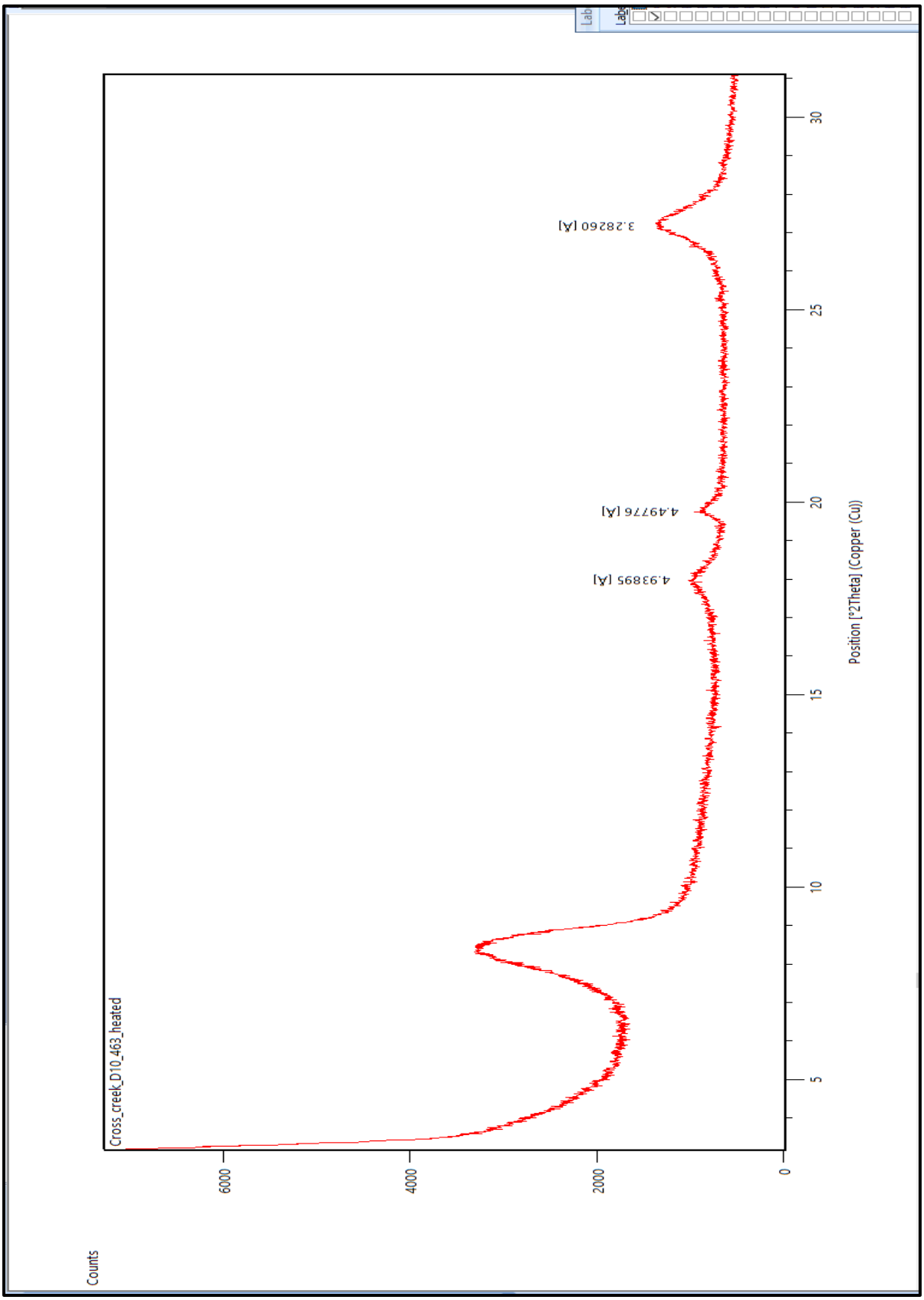
Cross_creek_D10_463_heated
Counts
6000
4000
2000
0
5
10
15
20
25
30
Position [°2Theta] (Copper (Cu))
3.28260 [Å]
4.49776 [Å]
4.93895 [Å]

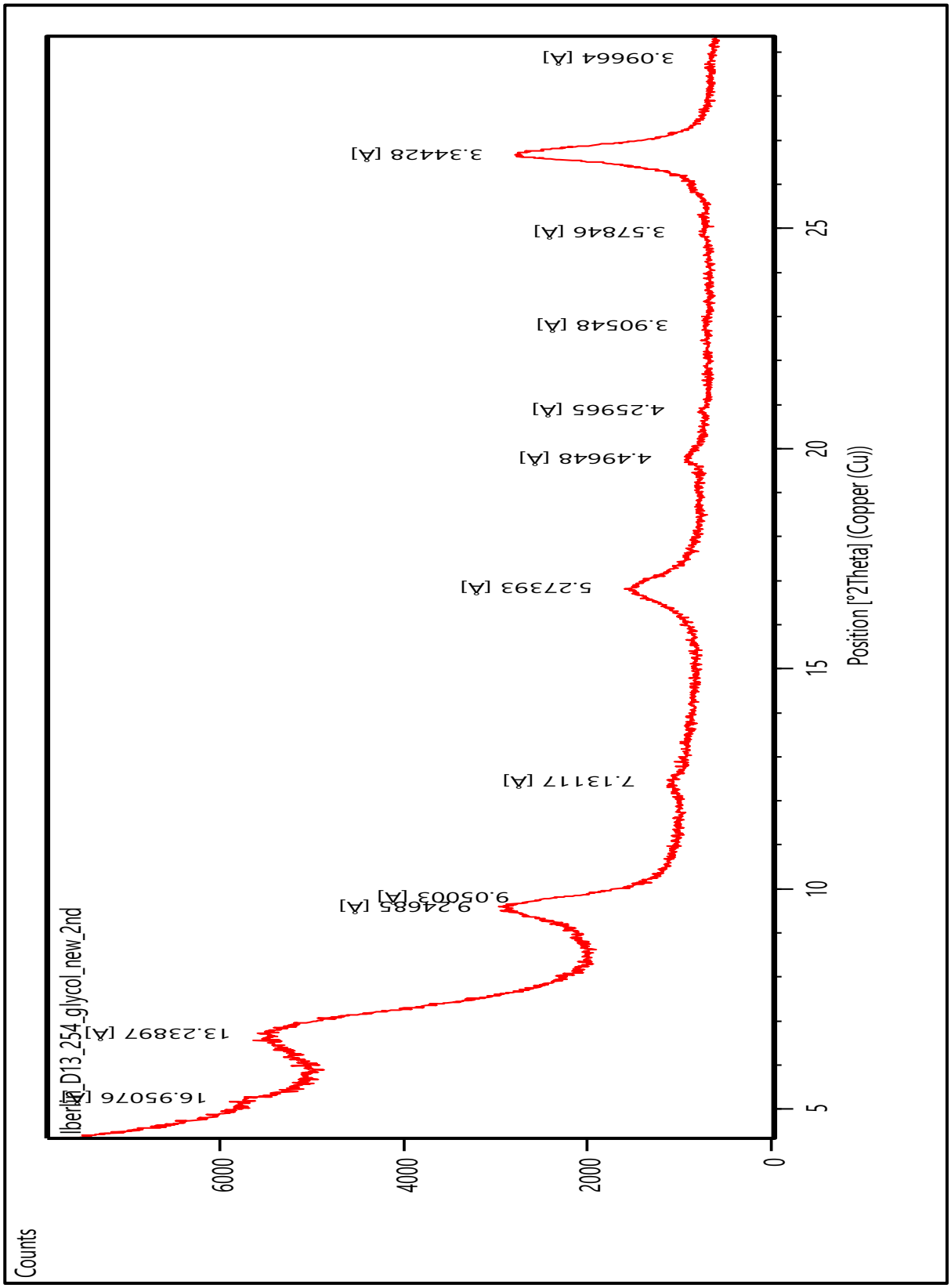
Counts
6000
4000
2000
0
5
10
15
20
25
Position [°2Theta] (Copper (Cu))
16.95076 [Å]
13.23897 [Å]
9.24685 [Å]
9.05003 [Å]
7.13117 [Å]
5.27393 [Å]
4.49648 [Å]
4.25965 [Å]
3.90548 [Å]
3.57846 [Å]
3.34428 [Å]
3.09664 [Å]

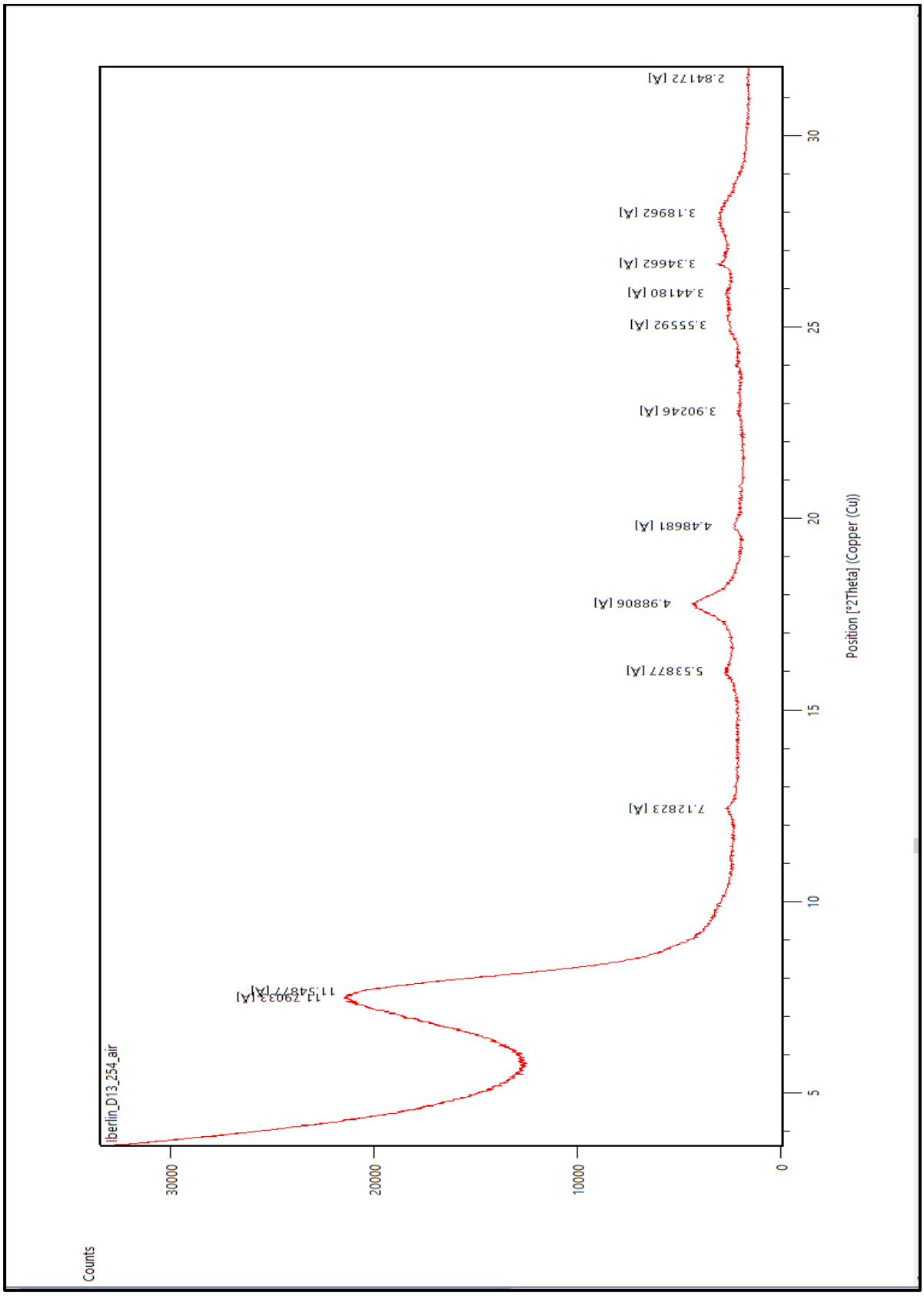
Counts
30000
20000
10000
0
Iberlin_D13_254_air
11.548777 [Å]
11.729033 [Å]
7.12823 [Å]
5.53877 [Å]
4.98806 [Å]
4.48681 [Å]
3.90246 [Å]
3.55592 [Å]
3.44180 [Å]
3.34662 [Å]
3.18962 [Å]
2.84172 [Å]
5
10
15
20
25
30
Position [°2Theta] (Copper (Cu))

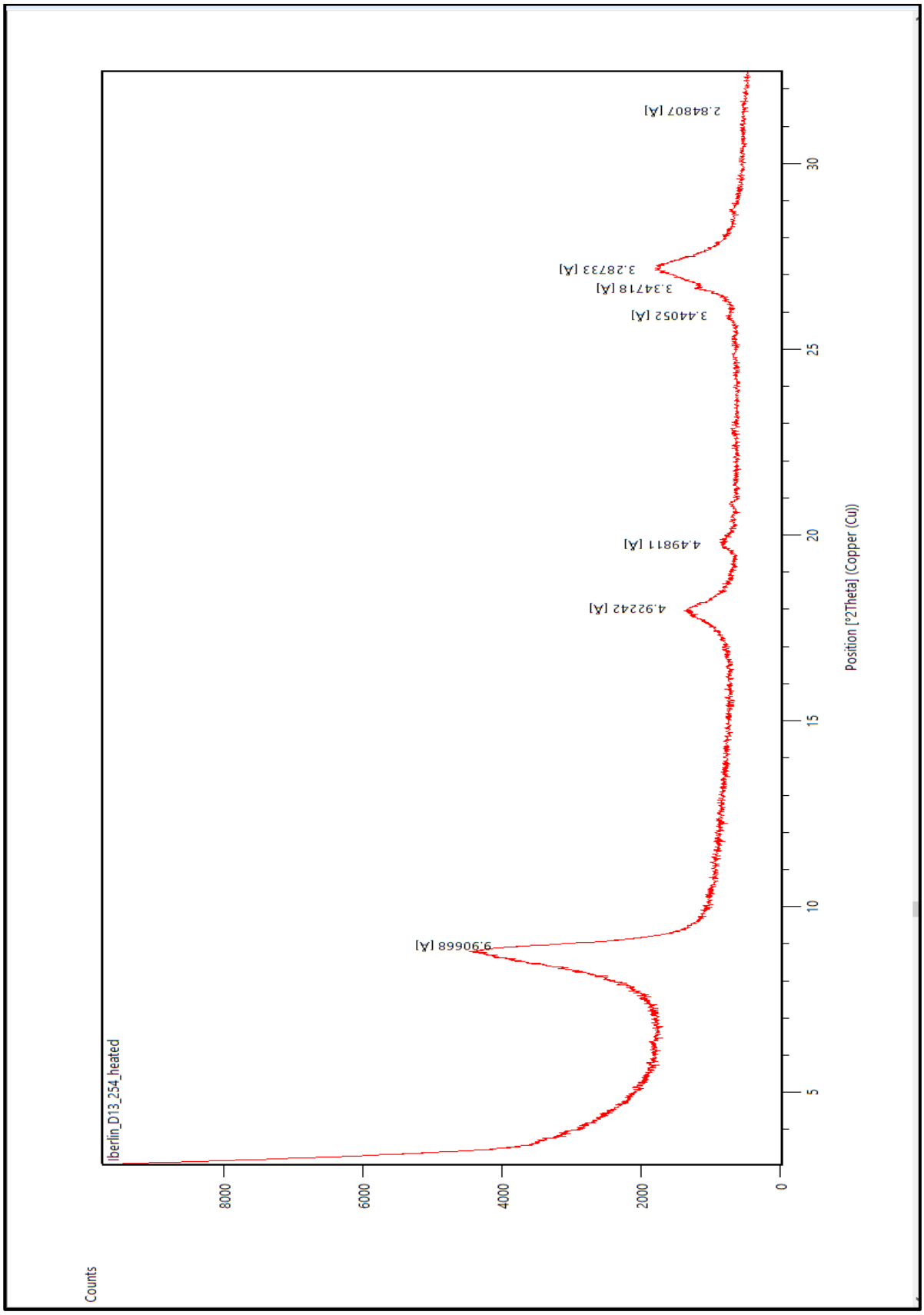
Iberlin_D13_254_heated
Counts
0
2000
4000
6000
8000
5
10
15
20
25
30
Position [°2Theta] (Copper (Cu))
9.90668 [Å]
4.92242 [Å]
4.49811 [Å]
3.44052 [Å]
3.34718 [Å]
3.28733 [Å]
2.84807 [Å]

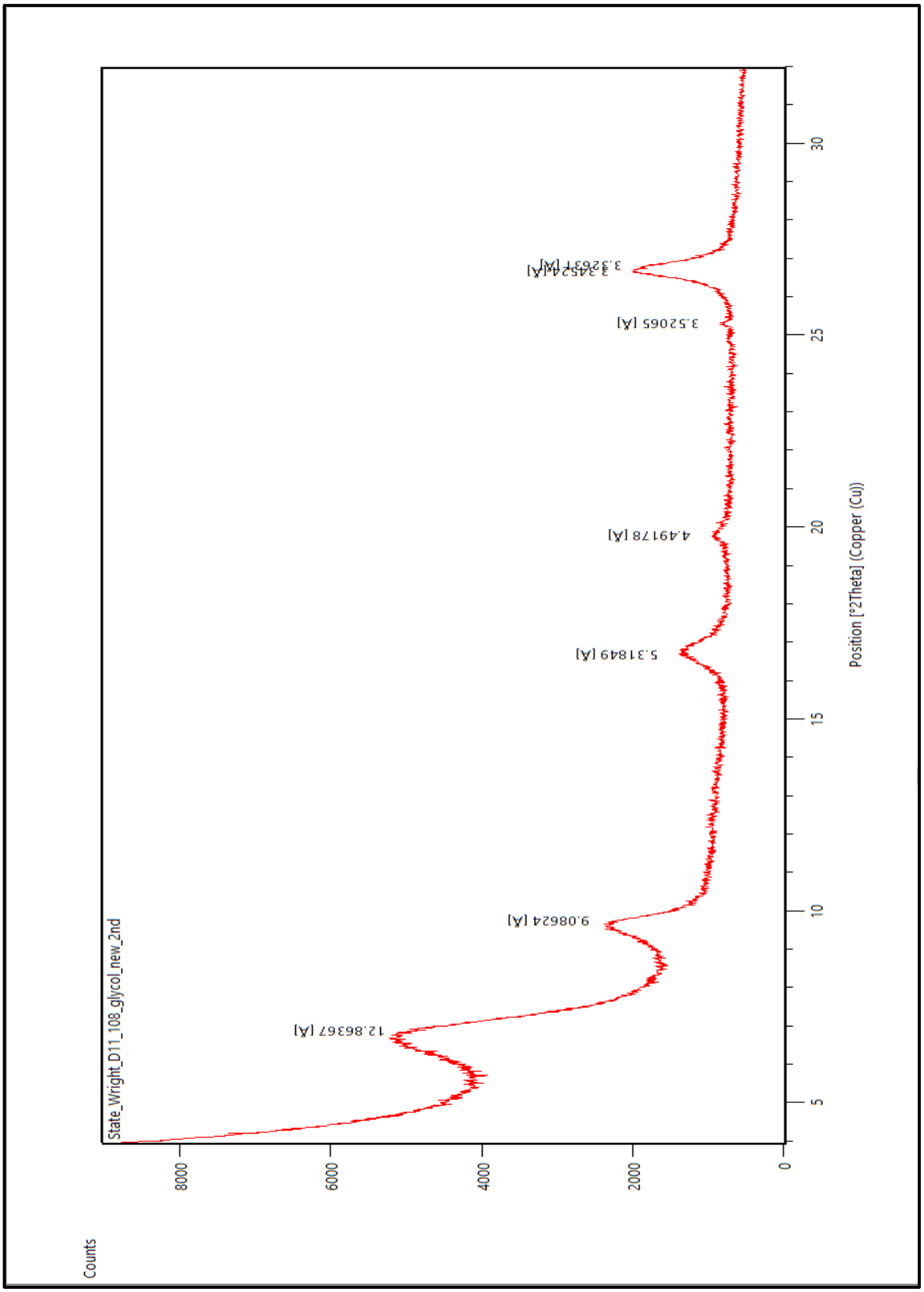
State_Wright_D11_108_glycol_new_2nd
Counts
8000
6000
4000
2000
0
5
10
15
20
25
30
Position [°2Theta] (Copper (Cu))
12.86367 [Å]
9.08624 [Å]
5.31849 [Å]
4.49178 [Å]
3.52065 [Å]
3.34524 [Å]
3.32637 [Å]

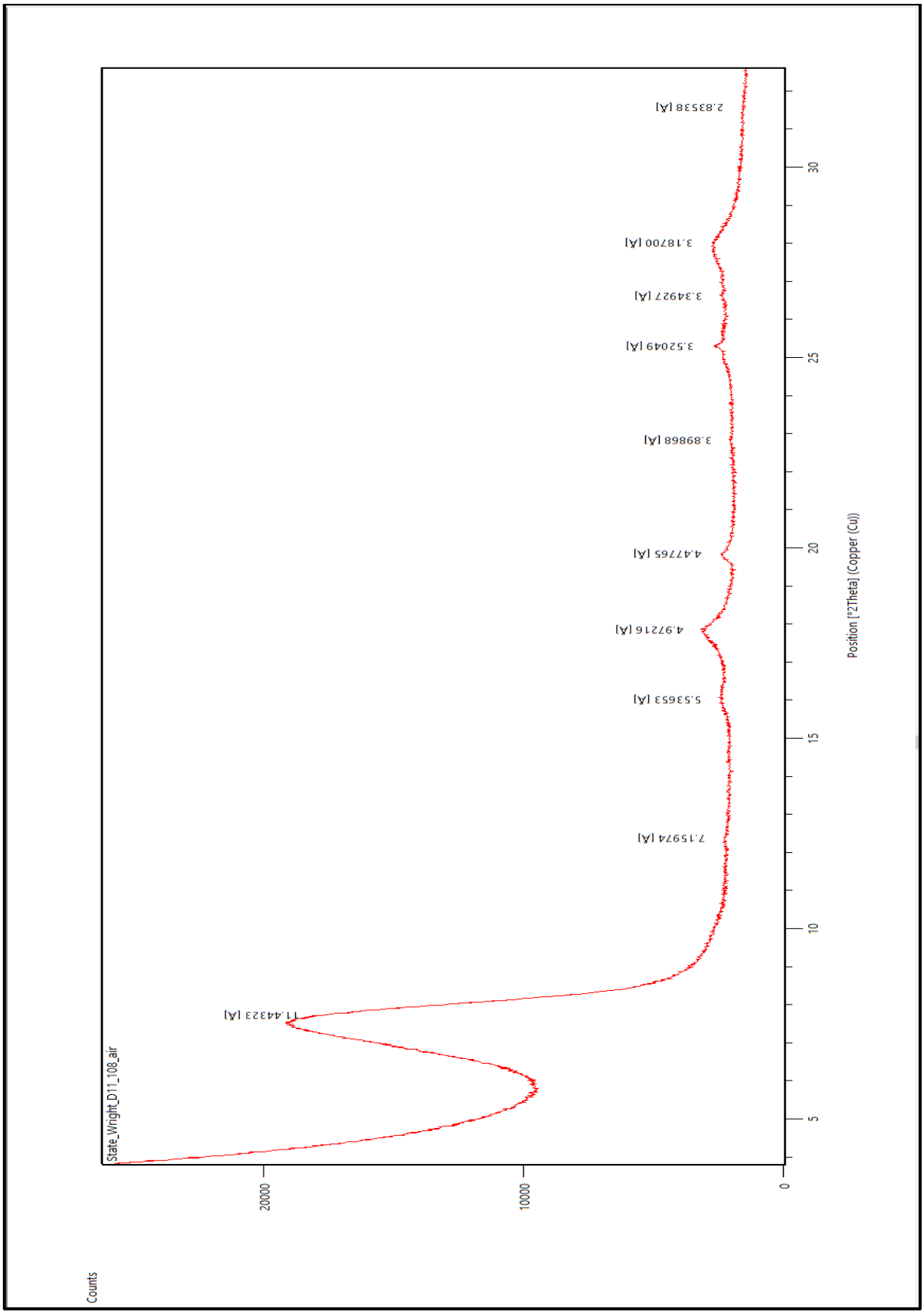
State_Wright_D11_108_air
Counts
20000
10000
0
5
10
15
20
25
30
Position [°2Theta] (Copper (Cu))
11.44323 [Å]
7.15974 [Å]
5.53653 [Å]
4.97216 [Å]
4.47765 [Å]
3.89868 [Å]
3.52049 [Å]
3.34927 [Å]
3.18700 [Å]
2.83538 [Å]

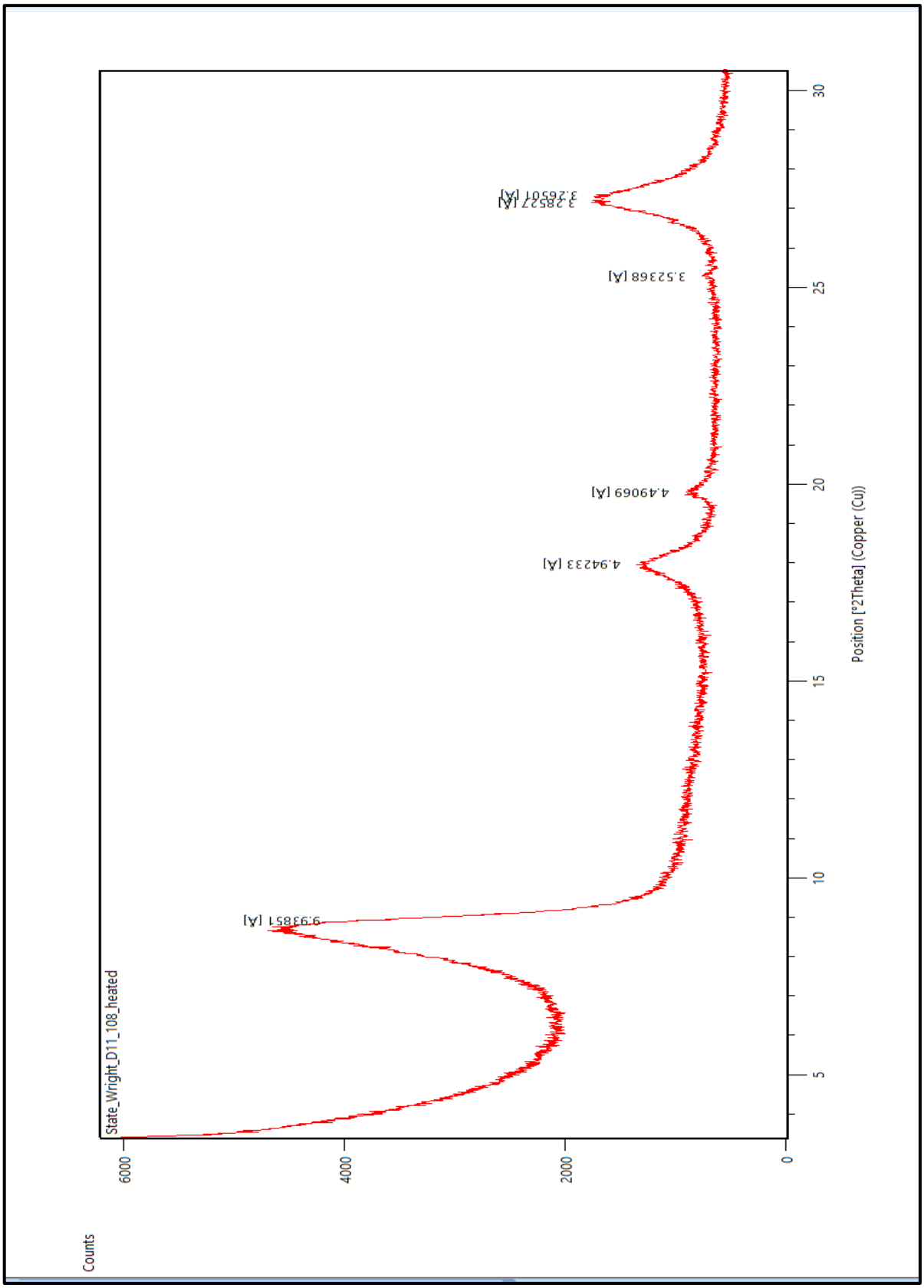
State_Wright_D11_108_heated
Counts
6000
4000
2000
0
9.93851 [Å]
4.94233 [Å]
4.49069 [Å]
3.52368 [Å]
3.28527 [Å]
3.26501 [Å]
5
10
15
20
25
30
Position [°2Theta] (Copper (Cu))

Appendix A.3: X-Ray Diffraction Patterns for the Mowry Reworked Bentonites.

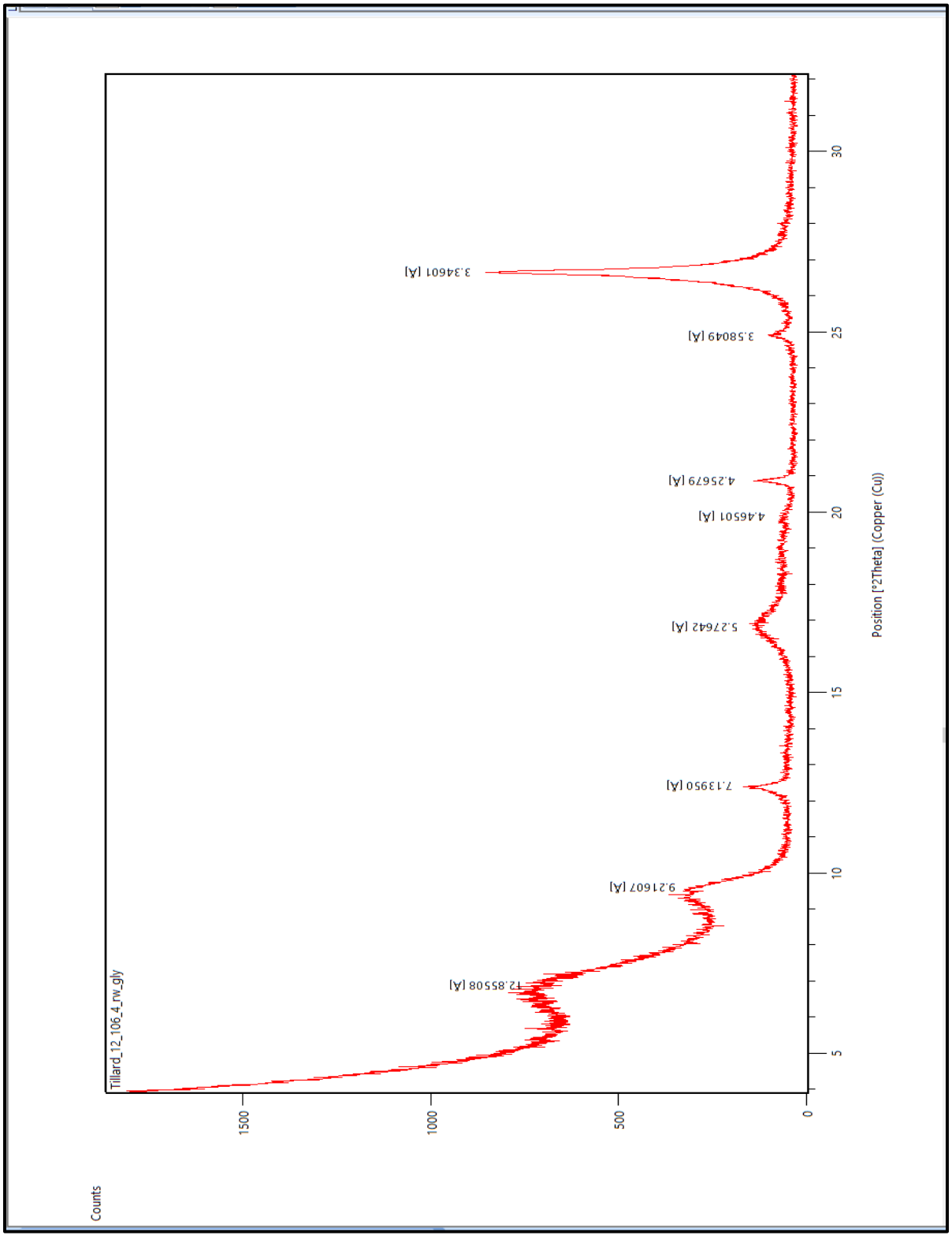

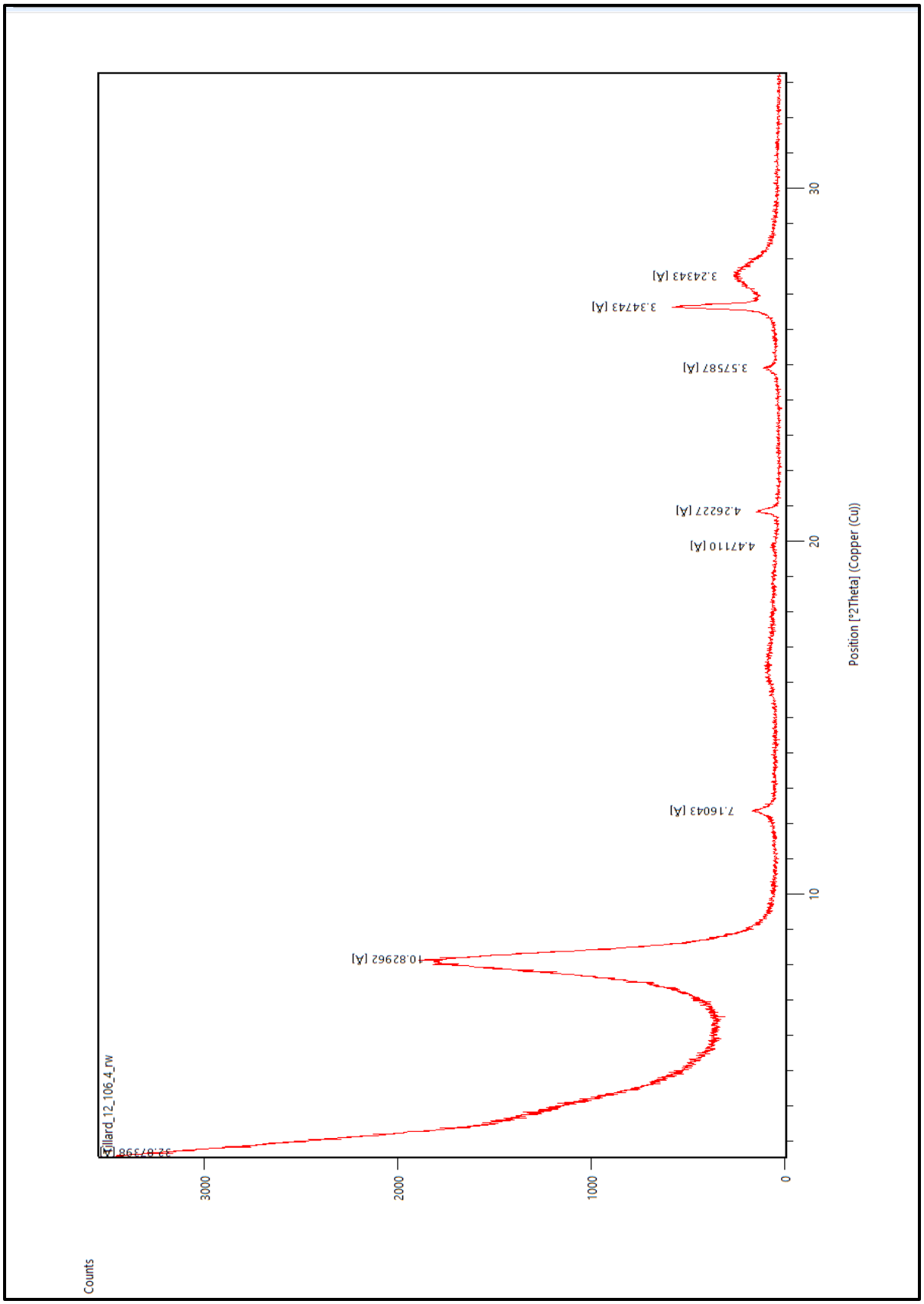
Counts
3000
2000
1000
0
10
20
30
Position [°2Theta] (Copper (Cu))
Tillard_12_106_4_rw
32.87598 [Å]
10.82962 [Å]
7.16043 [Å]
4.47110 [Å]
4.26227 [Å]
3.57587 [Å]
3.34743 [Å]
3.24343 [Å]

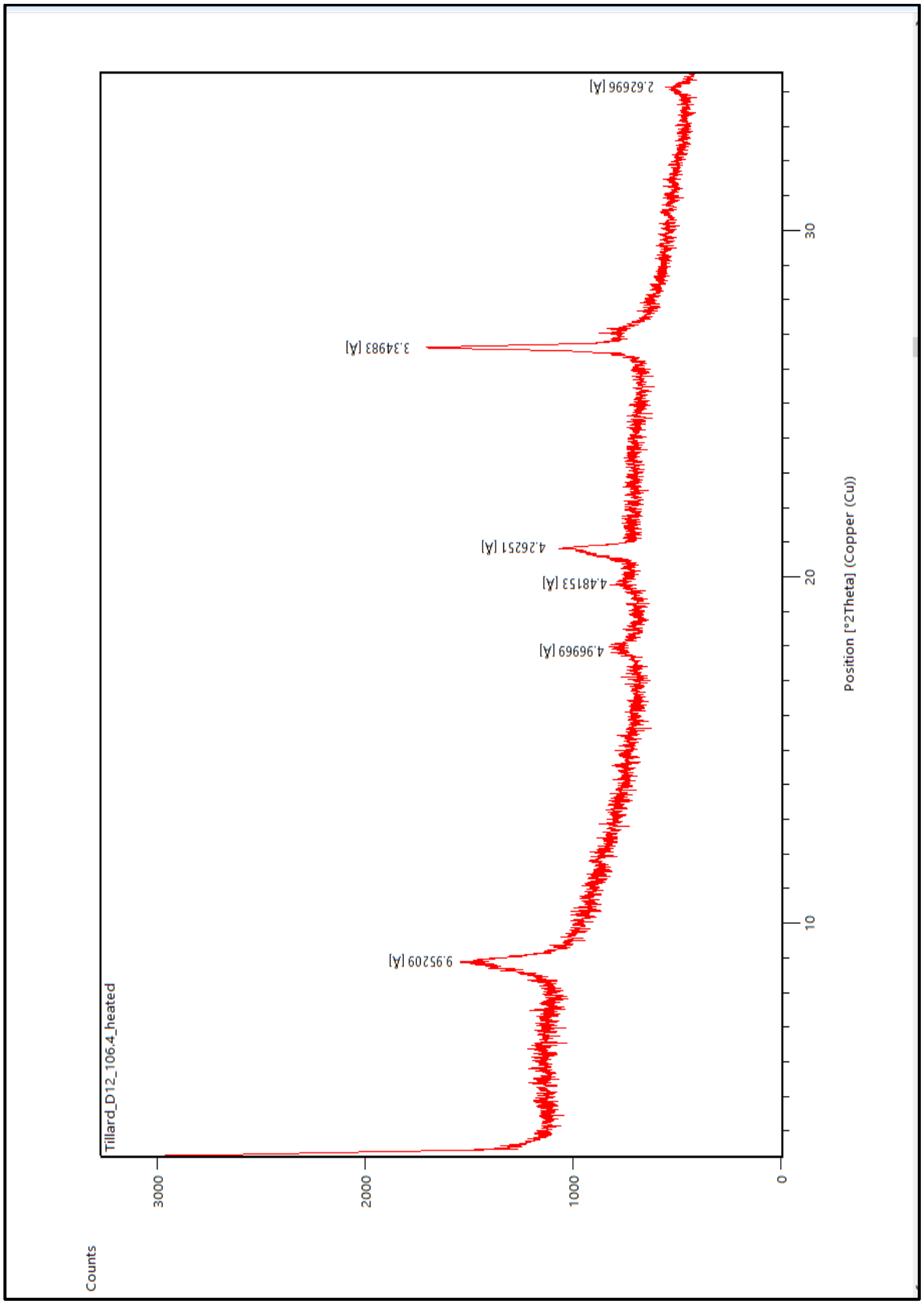
Tillard_D12_106.4_heated
Counts
3000
2000
1000
0
10
20
30
Position [°2Theta] (Copper (Cu))
9.95209 [Å]
4.96969 [Å]
4.48153 [Å]
4.26251 [Å]
3.34983 [Å]
2.62696 [Å]

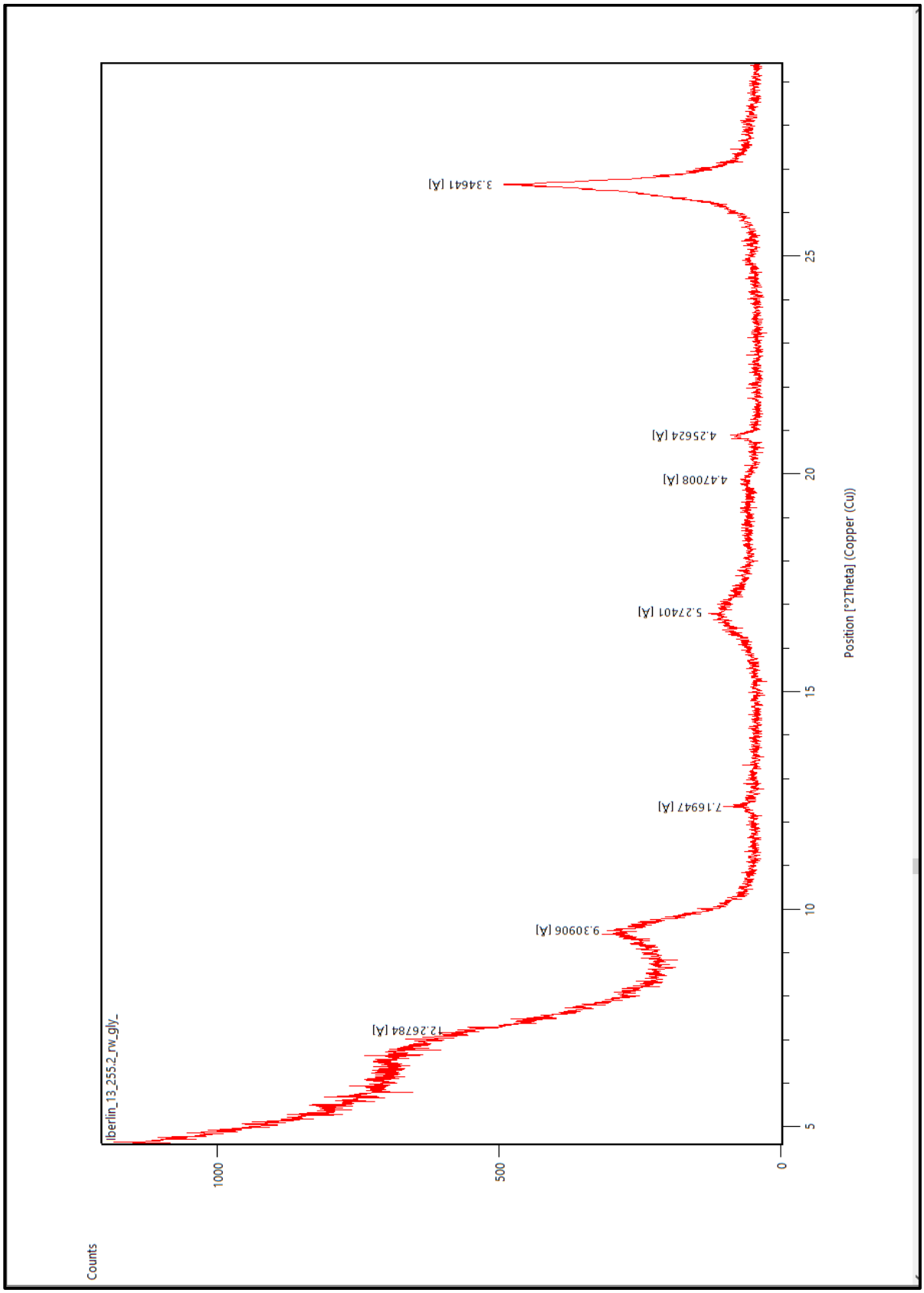
Counts
1000
500
0
5
10
15
20
25
Position [°2Theta] (Copper (Cu))
Iberlin_13_255.2_rw_gly_
12.26784 [Å]
9.30906 [Å]
7.16947 [Å]
5.27401 [Å]
4.47008 [Å]
4.25624 [Å]
3.34641 [Å]

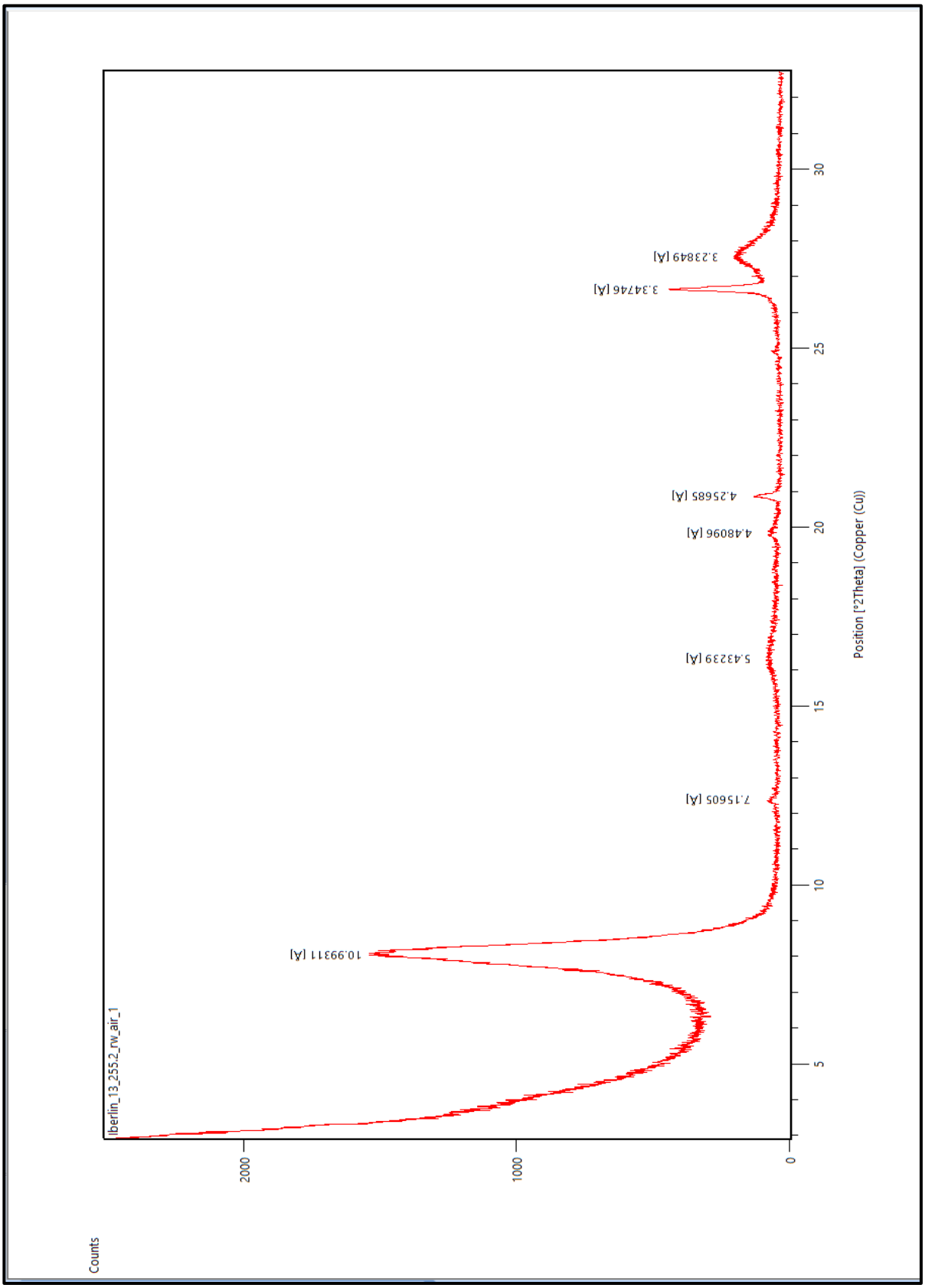
Counts
2000
1000
0
Iberlin_13_255.2_rw_air_1
10.99311 [Å]
7.15605 [Å]
5.43239 [Å]
4.48096 [Å]
4.25685 [Å]
3.34746 [Å]
3.23849 [Å]
5
10
15
20
25
30
Position [°2Theta] (Copper (Cu))

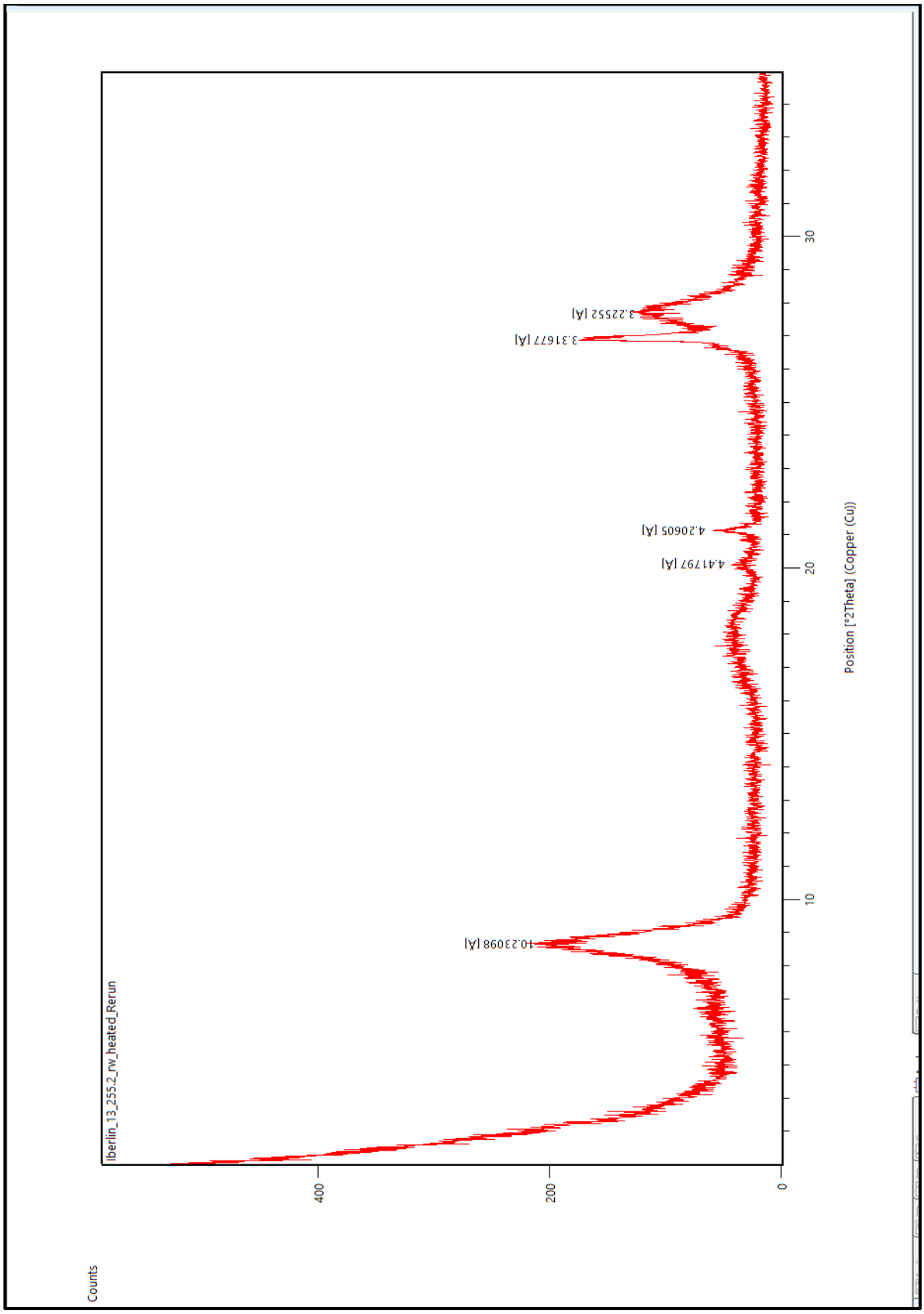
Counts
0
200
400
10
20
30
Position [°2Theta] (Copper (Cu))
Iberlin_13_255.2_rw_heated_Rerun
10.23098 [Å]
4.41797 [Å]
4.20605 [Å]
3.31677 [Å]
3.22552 [Å]

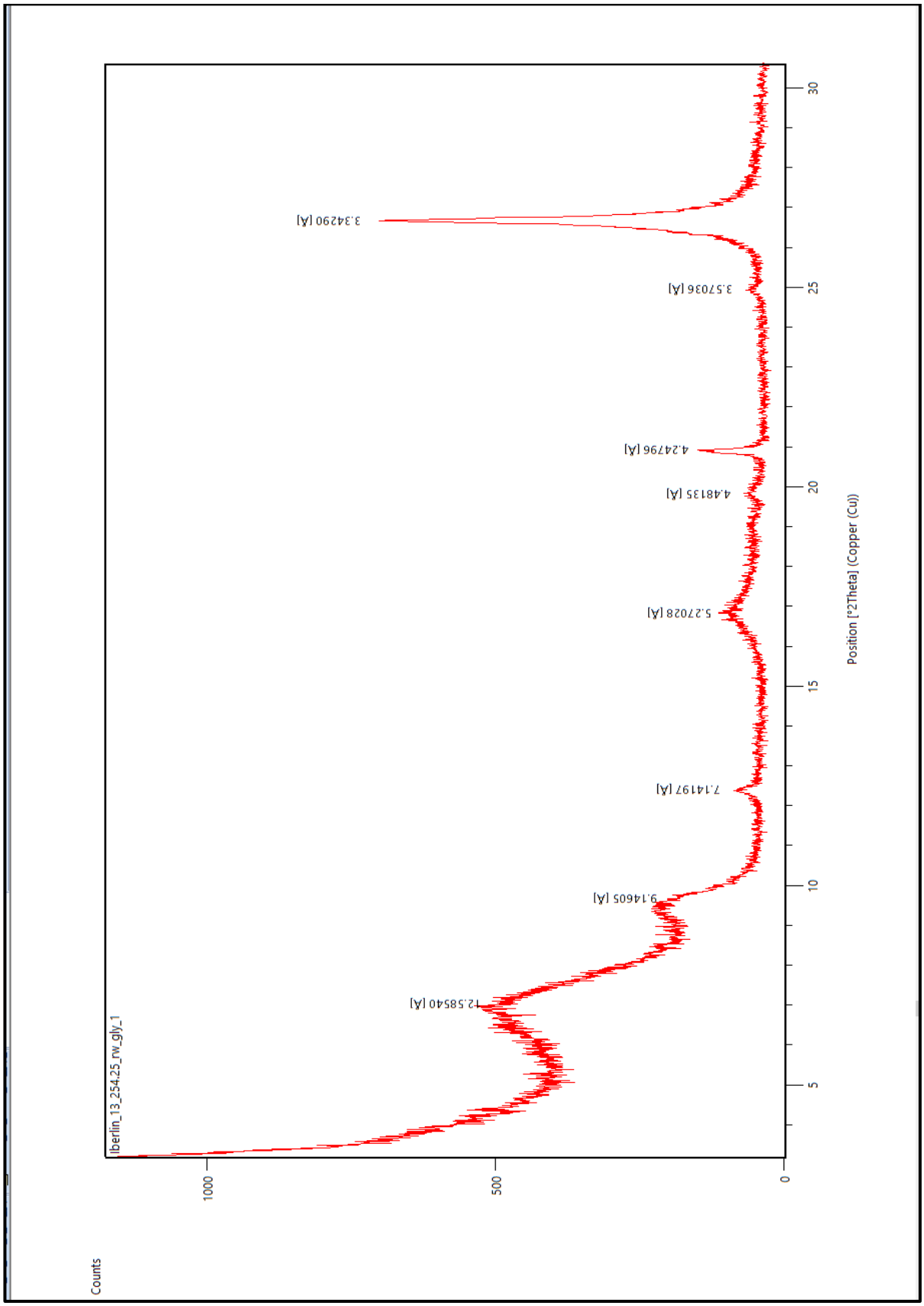
Counts
1000
500
0
Iberlin_13_254.25_rw_gly_1
12.58540 [Å]
9.14605 [Å]
7.14197 [Å]
5.27028 [Å]
4.48135 [Å]
4.24796 [Å]
3.57036 [Å]
3.34290 [Å]
5
10
15
20
25
30
Position [°2Theta] (Copper (Cu))

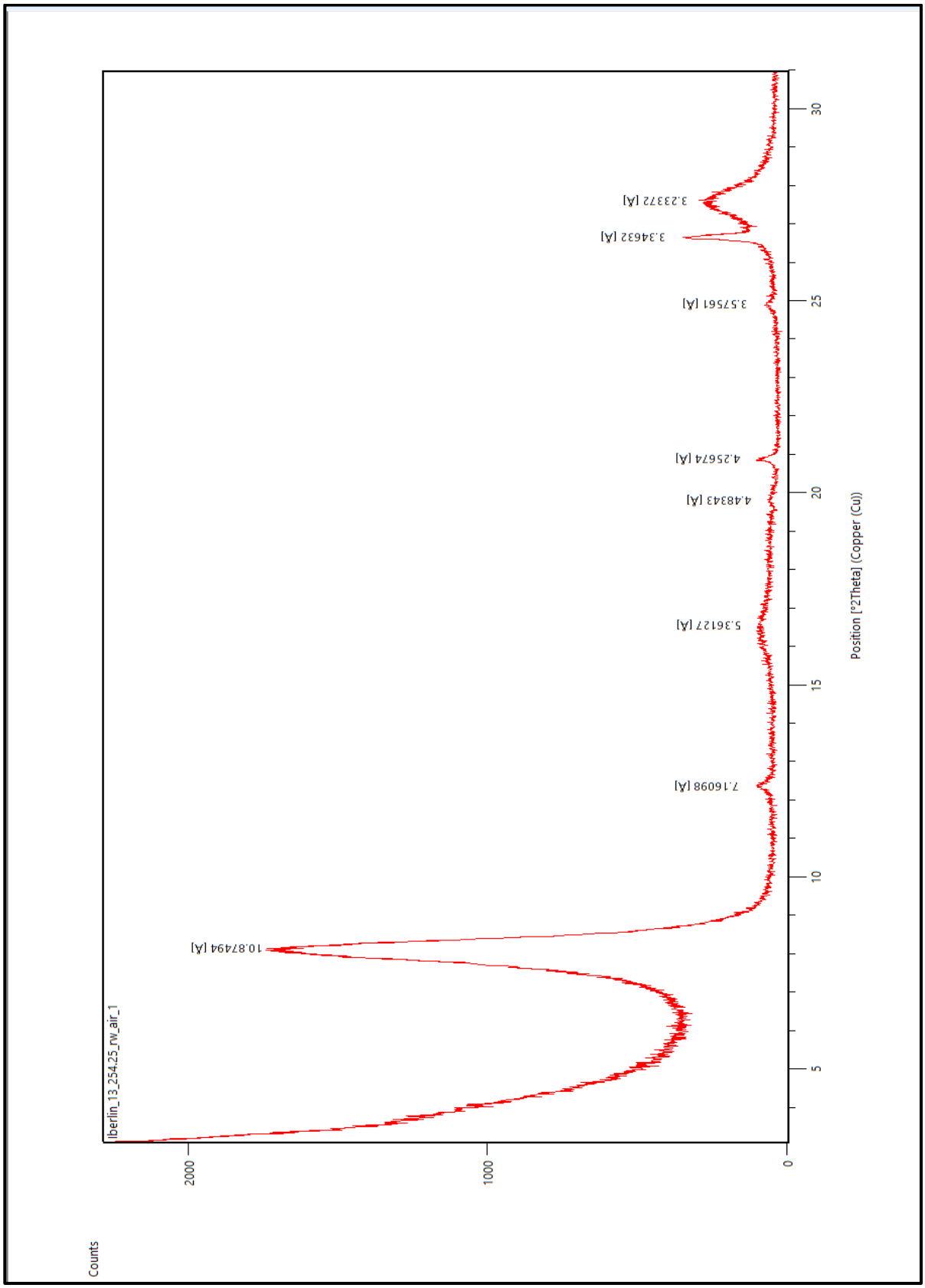
Counts
2000
1000
0
Iberlin_13_254.25_rw_air_1
10.87494 [Å]
7.16098 [Å]
5.36127 [Å]
4.48343 [Å]
4.25674 [Å]
3.57561 [Å]
3.34632 [Å]
3.23372 [Å]
5
10
15
20
25
30
Position [°2Theta] (Copper (Cu))

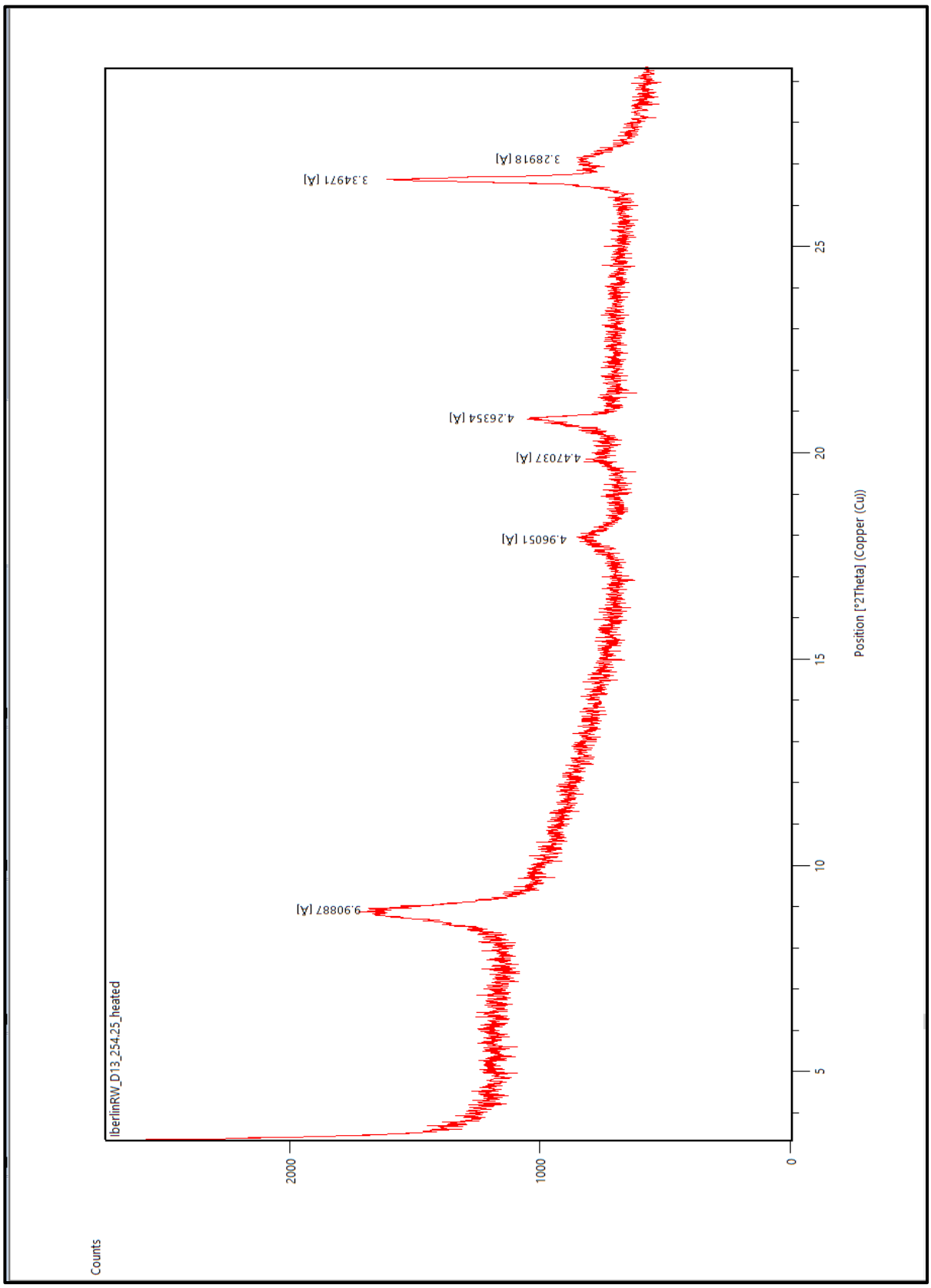
Counts
2000
1000
0
5
10
15
20
25
Position [°2Theta] (Copper (Cu))
IberiinRW_D13_254.25_heated
9.90887 [Å]
4.96051 [Å]
4.47037 [Å]
4.26354 [Å]
3.34971 [Å]
3.28918 [Å]

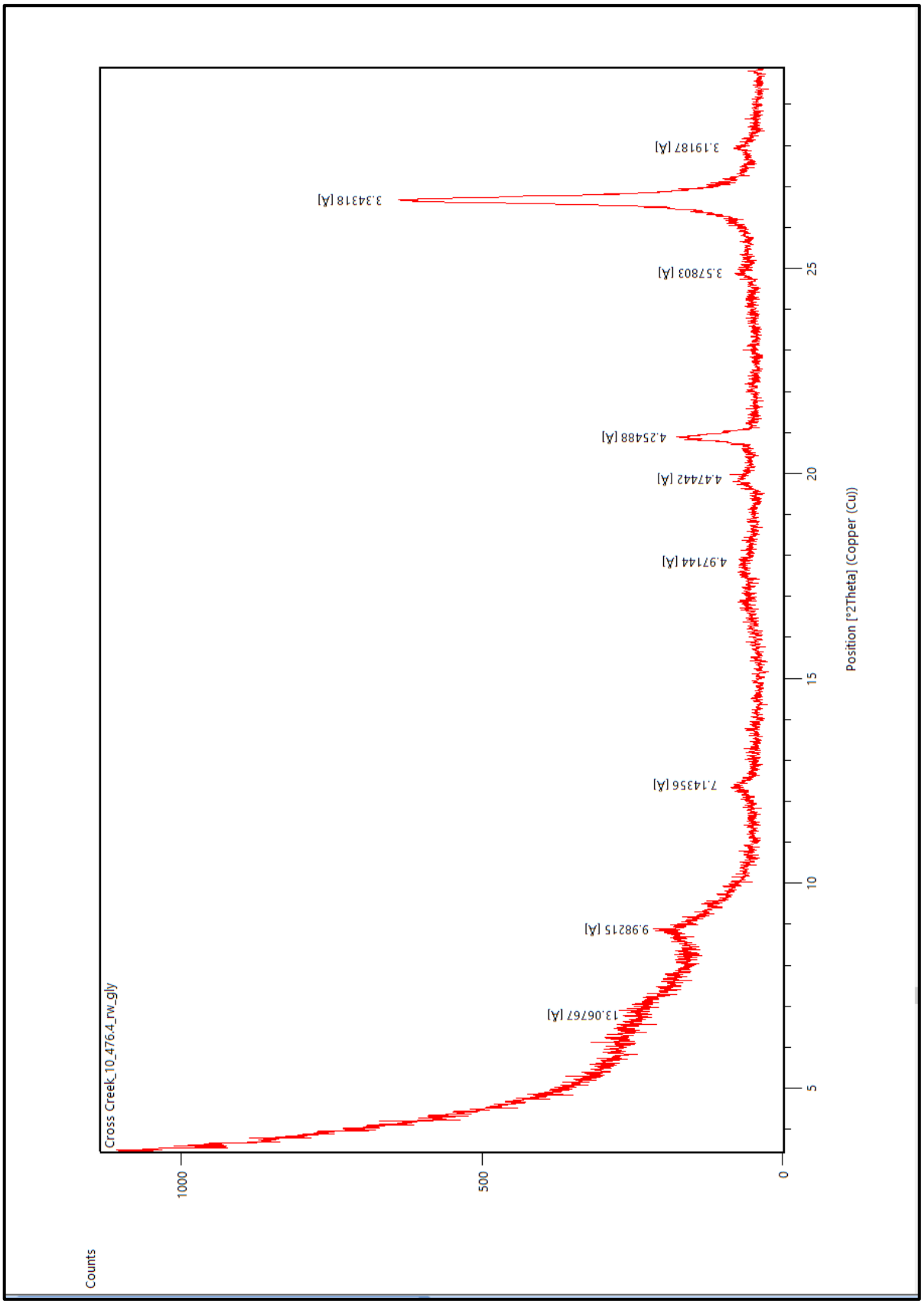
Counts
1000
500
0
Cross Creek_10_476.4_rw_gly
13.06767 [Å]
9.98215 [Å]
7.14356 [Å]
4.97144 [Å]
4.47442 [Å]
4.25488 [Å]
3.57803 [Å]
3.34318 [Å]
3.19187 [Å]
5
10
15
20
25
Position [°2Theta] (Copper (Cu))

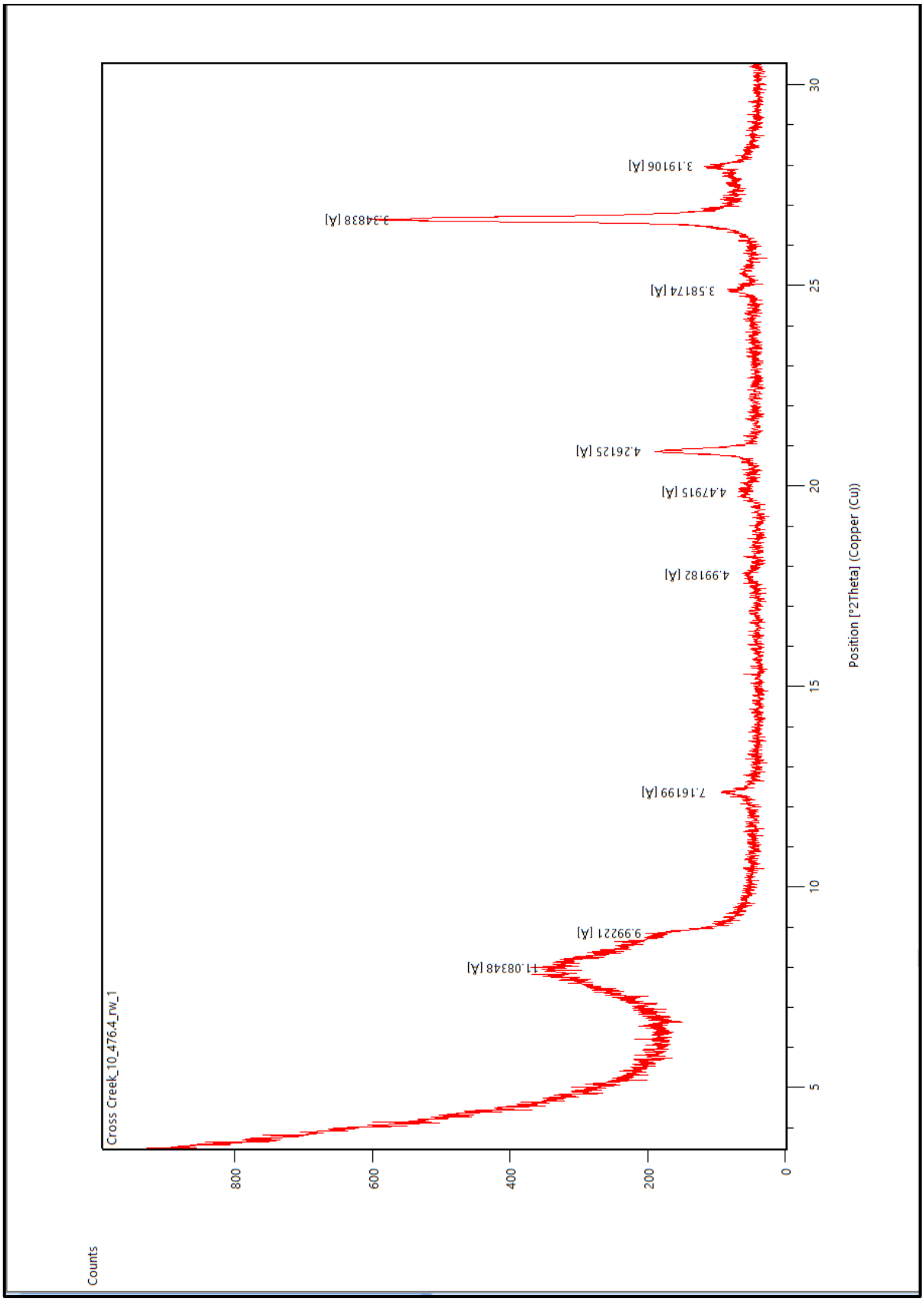
Counts
Cross Creek_10_476.4_rw_1
11.08348 [Å]
9.99221 [Å]
7.16199 [Å]
4.99182 [Å]
4.47915 [Å]
4.26125 [Å]
3.58174 [Å]
3.34838 [Å]
3.19106 [Å]
Position [°2Theta] (Copper (Cu))

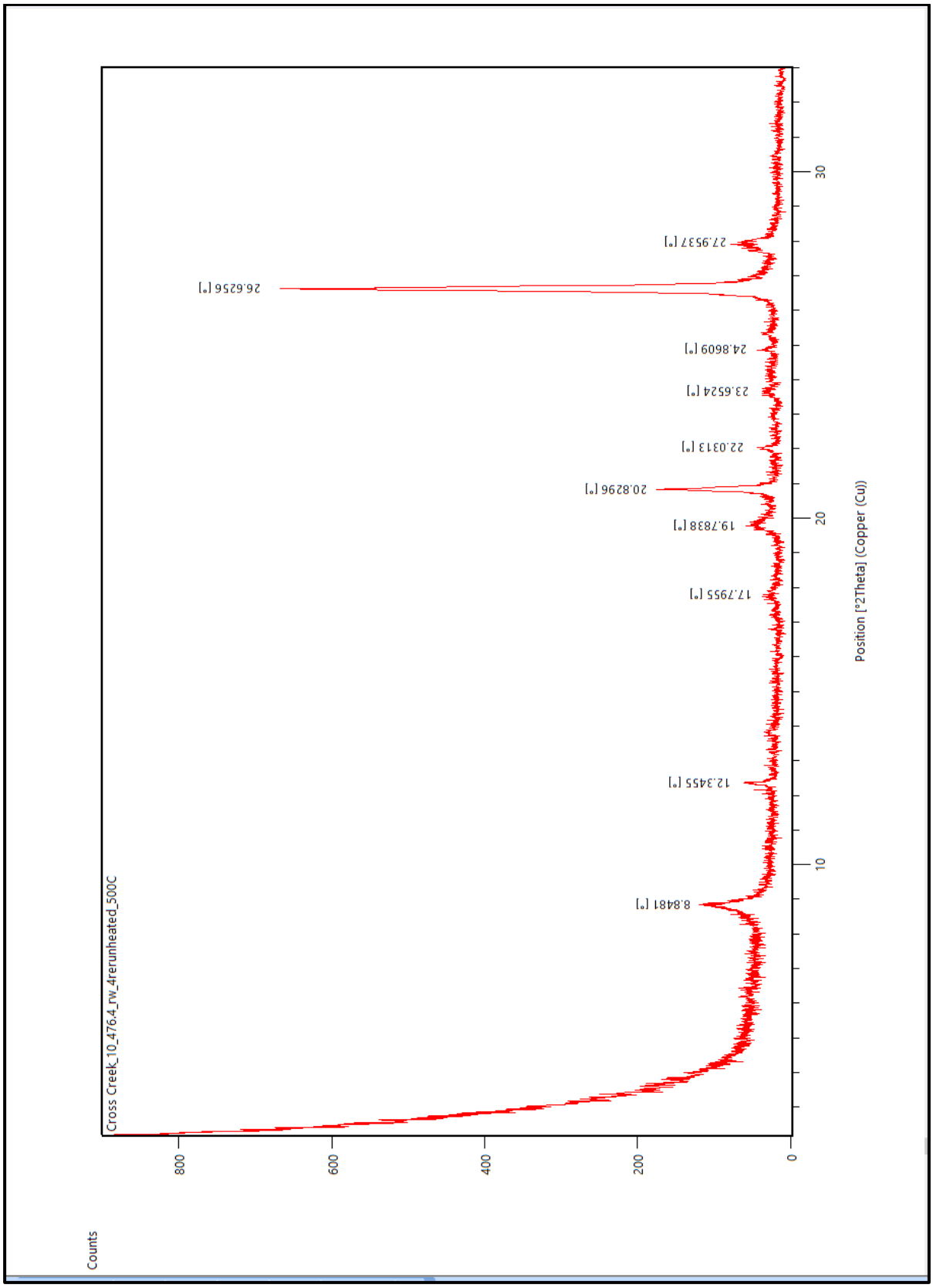
Cross Creek_10_476.4_rw_4rerunheated_500C
Counts
0
200
400
600
800
10
20
30
Position [°2Theta] (Copper (Cu))
8.8481 [°]
12.3455 [°]
17.7955 [°]
19.7838 [°]
20.8296 [°]
22.0313 [°]
23.6524 [°]
24.8609 [°]
26.6256 [°]
27.9537 [°]

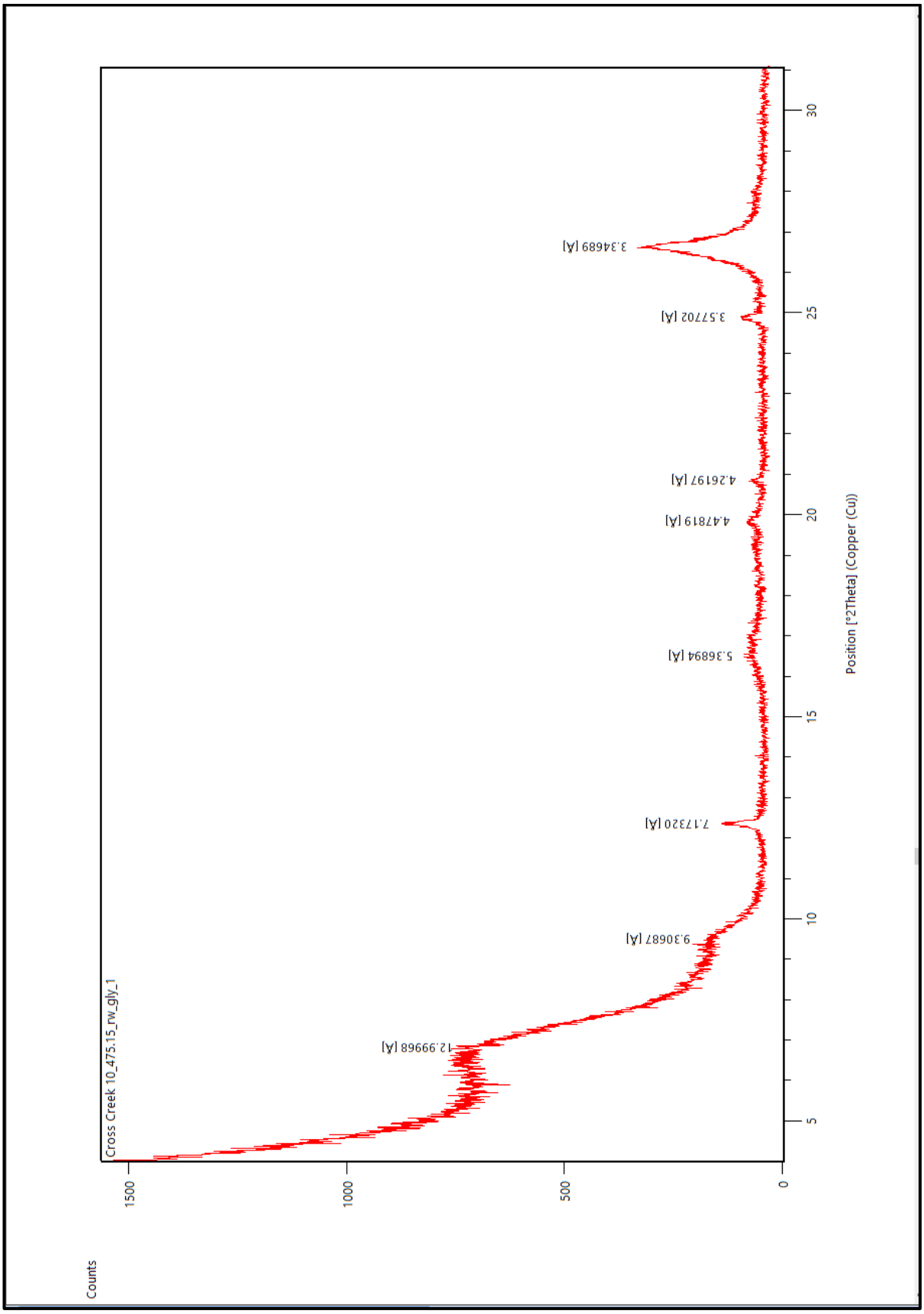
Cross Creek 10_475.15_rw_gly_1
Counts
0
500
1000
1500
5
10
15
20
25
30
Position [°2Theta] (Copper (Cu))
12.99968 [Å]
9.30687 [Å]
7.17320 [Å]
5.36894 [Å]
4.47819 [Å]
4.26197 [Å]
3.57702 [Å]
3.34689 [Å]

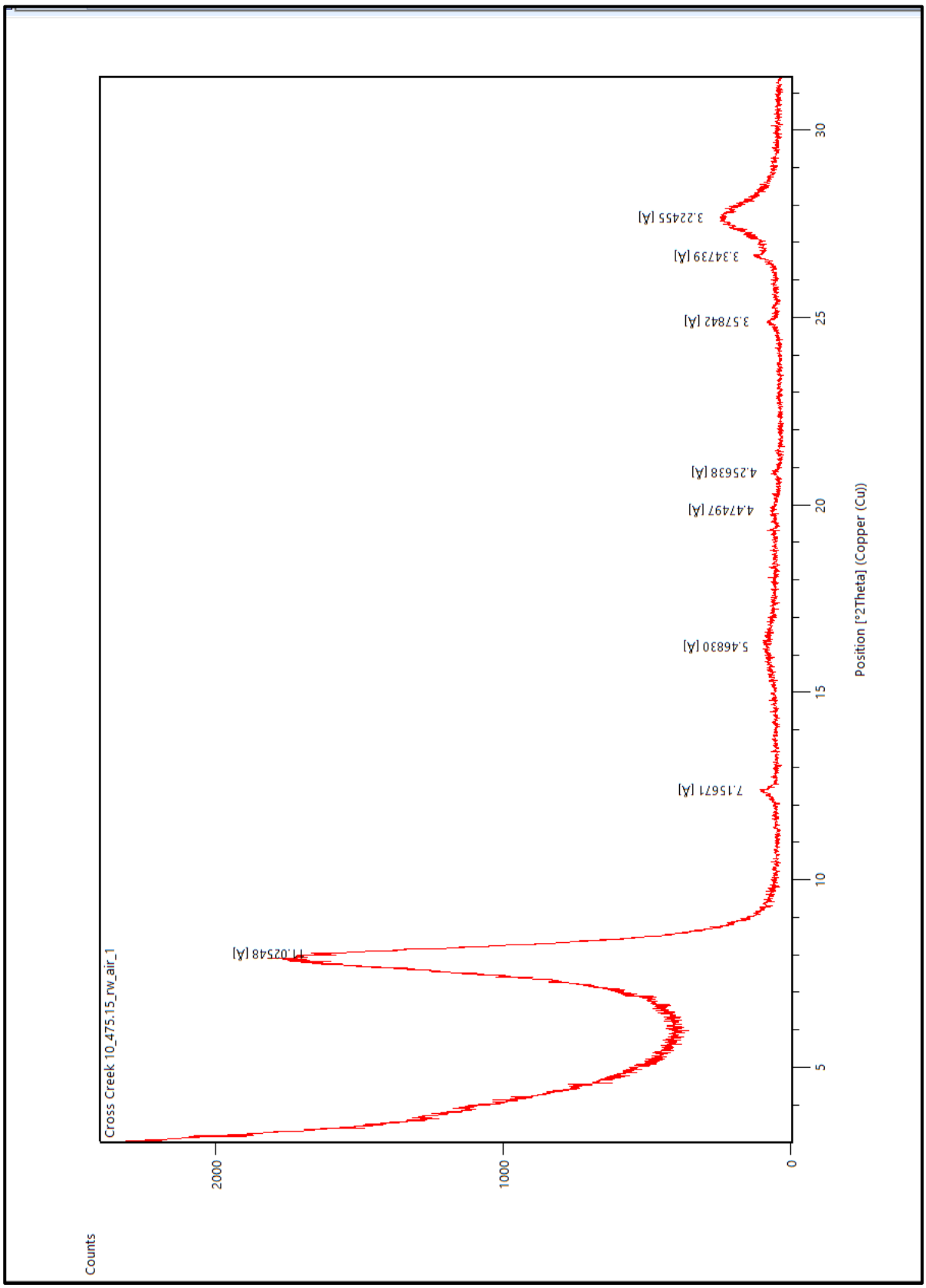
Cross Creek 10_475.15_rw_air_1
Counts
2000
1000
0
5
10
15
20
25
30
Position [°2Theta] (Copper (Cu))
11.02548 [Å]
7.15671 [Å]
5.46830 [Å]
4.47497 [Å]
4.25638 [Å]
3.57842 [Å]
3.34739 [Å]
3.22455 [Å]

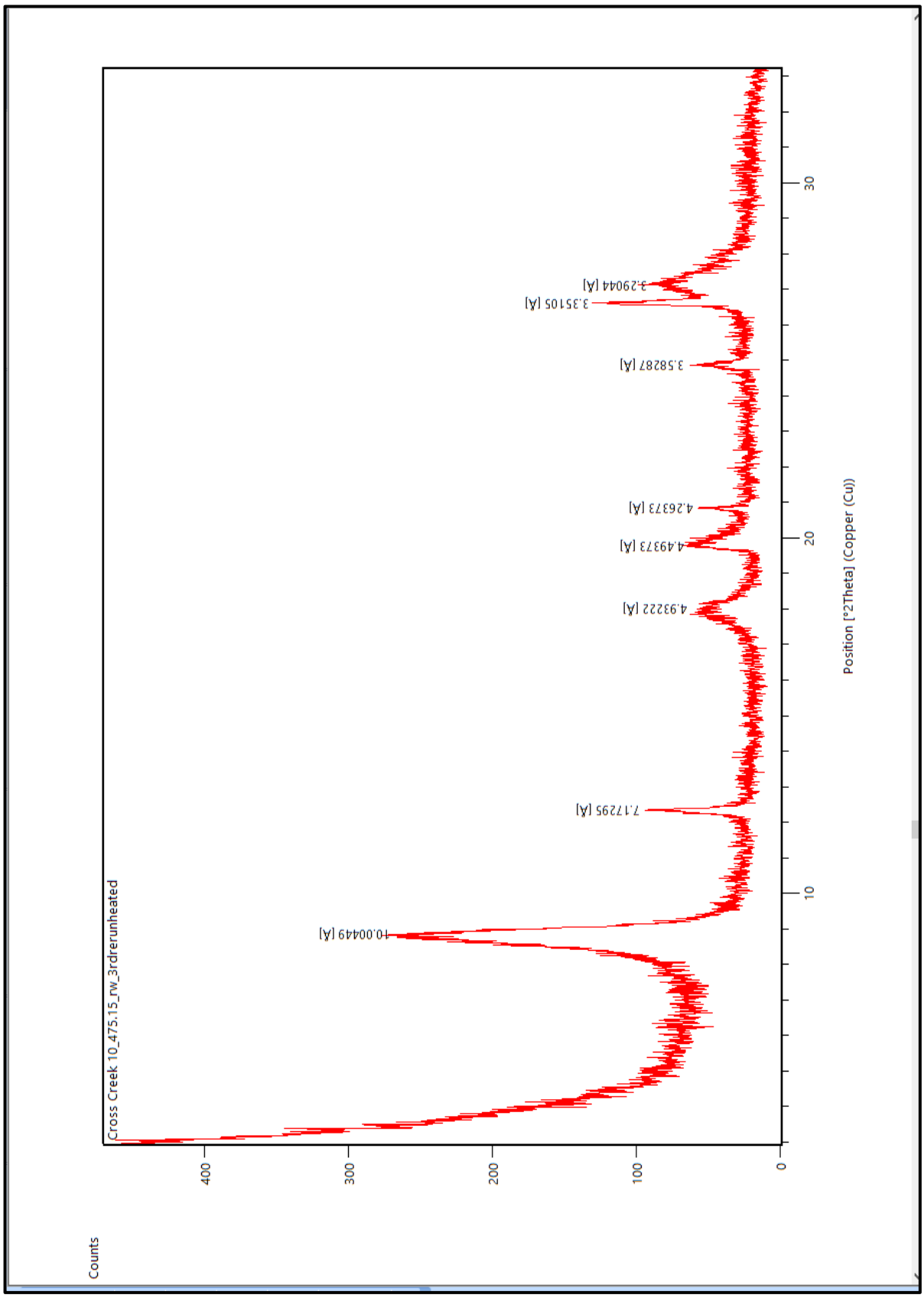
Cross Creek 10_475.15_rw_3rdrerunheated
Counts
0
100
200
300
400
10
20
30
Position [°2Theta] (Copper (Cu))
10.00449 [Å]
7.17295 [Å]
4.93222 [Å]
4.49373 [Å]
4.26373 [Å]
3.58287 [Å]
3.35105 [Å]
3.29044 [Å]

Appendix B: K-Ar Method

B1 Sample Preparation and Procedure for K-Ar Analyses

The steps for the preparation and procedure for K-Ar Analyses follows Prof. Marion Wampler (Rtd.) prepared guide book.

Steps	Procedures
Weighing Single Test Portions	16 to 27 mg of powdered, < 2-micron clay fraction of bentonites placed in copper foil capsules were weighed using a Mettler micro-analytical balance. The capsules containing the test portions were placed in vacuum overnight to remove adsorbed moisture from the clay. The capsules plus test portions were re-weighed and recorded.
^{40}Ar Extraction and Measurements.	Test portion in capsules were heated to 1000 °C in a high vacuum extraction line connected to a computerized mass spectrometer using an external wire-wound heater. Traces of CO_2, H_2O and other gases present in the extraction line were systematically trapped and removed by liquid nitrogen and heated titanium. The argon mixture of ^{36}Ar, ^{38}Ar, and ^{40}Ar is then released to the MS-10 mass spectrometer for scanning and isotopic analysis. The result of the Ar analysis is recorded and saved as a text file on the computer.
Preparation of Clay for Potassium Measurement after Argon Extraction	The capsules with its contents were removed from the Ar extraction line, re-weighed, recorded and kept in a labelled fluorocarbon container.

	1 ml acid mixtures of concentrated HF and HNO_3 were added for the digestion of the capsules plus the test portions in the fluorocarbon container. The labelled containers were gently heated (< 100 ̊C) until the samples were digested. The containers were opened in a fume hood to allow evaporation of SiF_4, HF and HNO_3 left in the samples. The samples were diluted with Cs diluting solution and transferred to a pre-weighed (appropriately labelled) 125 ml polyethylene bottle filled to the bottle neck. Measurement of K content was done using Atomic-Absorption Spectroscopy. The data from the K-Ar analyses were used in the calculations and determination of the age of illite present in the I-S mixed layer.

B 2: Extraction and measurement of argon from clay

This procedure is for extraction and measurement of argon from a clay test portion by heating at ~1000°C, which allows the test portion to be used also for potassium determination. If the argon is to be extracted by fusion of the clay, which would require that a separate test portion be used for the potassium determination, a different procedure (Gas Extraction by Fusion and Measurement of Argon) is to be followed.

Setup Checklist

Use this checklist to ensure that the extraction line and mass spectrometer are correctly set up for argon extraction from clay and for isotope dilution and mass spectrometry.

1. Turbomolecular pump running	*Valves R1 and R2 should be open when the turbomolecular pump is running.*
2. Liquid nitrogen on trap DT-2	

3. Valves D1, D2, T0, T1, T3, F2, and S0 open	
4. Valves F1, T2, T4, and S1 closed	*Other valves, V1, C2, A1, A2, S2, S3, and S4, are normally closed. Their status need not be checked.*
5. Titanium heaters TF-0, TF-1, and TF-2 hot	*The titanium heaters should have been hot for at least 15 minutes before proceeding. This is to ensure that they have been well degassed.*
6. P1 less than 20 mTorr and P2 less than 1 mTorr	*These values are guidelines that are easily met if the system has been well degassed and there are no leaks.*
7. Mass spectrometer on and set to $m/z = 40$ (at or very near the red 40 mark)	*The signal at m/z = 40 should be low on the 0.1×10^{-11} A range, as it will be if the system has been well degassed and there are no leaks.*
8. 6423 data-reader program ready for use	*Run 6273.exe to start the program.*

Argon Extraction and Cleanup	
1. Prepare a spike by checking that S1 is tightly closed <u>and then</u> opening S2.	***The underlining is to emphasize that S1 and S2 must not be both open at the same time.***
2. Wait one-half minute and then close S2 tightly. If a reduced spike is to be used, do the following as well: a. Close S0. b. Open S1. c. Wait one-half minute and then close S1 and open S0.	*S2 must be closed tightly to prevent argon from leaking through it at a significant rate. (The old valve no longer seals perfectly.)* *If a reduced spike is prepared, a three-minute period is needed after S0 is opened for all the ^{38}Ar not used in the reduced spike to be pumped away. That period must elapse before step 6 is executed.*
3. Move the capsule to be heated into the position where it will be heated.	*Any previously heated material must have been removed from that position. Do not put the heater over the new material yet.*
4. Put liquid nitrogen in the cold finger of trap MT-1.	*When the liquid nitrogen has become stable, it should occupy about one-half of the cold finger.*
5. Put liquid nitrogen, in a small Dewar flask, around MT-1.	*The level of liquid nitrogen in the Dewar flask should be a little below that in the cold finger.*

6. Close valve T0.	*This important step isolates the extraction line from the pumps.*
7. Center the heater over the capsule to be heated.	
8. See that input to the chart recorder is from gauge P1.	*Recorder input is from the P1 gauge when the input switch has been turned clockwise.*
9. Turn on power to the heater at 9.0 VAC.	*Control the voltage with a variable transformer.*
10. Release the spike by closing S2 tightly and then opening S1. *Record the spike number, C2-xxxx [C2R-xxxx for a reduced spike], on the chart.*	***The underlining is to emphasize that S1 and S2 must not be both open at the same time.***
11. At intervals of one minute or longer, raise the heater voltage in steps of 1.0 VAC.	*Observe P1 to monitor the release of gases from the clay. (P1 will respond to gases that are much more abundant than argon.)*
12. When the maximum heater voltage has been reached, turn off power to the titanium heater TF-0.	*The maximum heater voltage, sufficient for a temperature of about 1000°C, currently is 14.0 VAC. Do not use a voltage above 14.0 VAC.*
13. Wait at least 10 minutes, and then turn off power to the heater.	*Experience has shown that 10 minutes at 1000°C is sufficient for complete extraction of argon from clay-sized phyllosilicates.*
14. Wait one minute and then turn off power to the titanium heater TF-1.	*P1 should decrease as the titanium cools.*
15. Wait, if necessary, until P1 <20 mTorr, and then put liquid nitrogen on charcoal CC-1.	*Make sure the liquid nitrogen level is above the glass wool above the charcoal.*
16. Put a little liquid nitrogen in the cold finger of trap MT-2.	*The liquid nitrogen level in the cold finger need not be higher than 1 cm.*
17. Move the liquid nitrogen surrounding MT-1 to MT-2.	*You may wash the outside of MT-1 with ethanol to see the ice ring(s) from the volatiles condensed on the cold finger.*
18. Remove liquid nitrogen from the cold finger of MT-1 by inserting a large Teflon stirring rod into the cold finger to heat the liquid nitrogen.	*Any argon that may have been trapped in ice on the cold finger of MT-1 will be released when the ice evaporates as the cold finger warms.*
19. Observe P1 as CO_2, first, and then water evaporate from the MT-1 cold finger and move to the MT-2 cold finger. Wait until P1 <20 mTorr before proceeding.	*Virtually all the argon will have been adsorbed by the charcoal by the time all the water has moved to the MT-2 cold finger.*

20. Check that at least five minutes have elapsed since charcoal CC-1 and then close valve T1.	
21. Remove the liquid nitrogen from CC-1.	*Be very careful not to break the glass when removing the liquid nitrogen from the charcoal.*
22. Switch the chart recorder input from the P1 signal to the electrometer signal.	*Turn the recorder-input switch counterclockwise.*

Argon Transfer

Follow only the steps in the left-hand column, below, unless there is a reason that less than the maximum amount of argon be transferred to the mass spectrometer. In that case, follow only the steps on the right.

Usual Argon Transfer	**Alternative Argon Transfer**
1. Check that argon has been evacuated from the mass spectrometer, as indicated by a signal at $m/z = 40$ that is low on the 0.1×10^{-11} A range.	1. Check that argon has been evacuated from the mass spectrometer, as indicated by a signal at $m/z = 40$ that is low on the 0.1×10^{-11} A range.
2. Enter an identifying file name for the digital record and start digital recording.	2. Enter an identifying file name for the digital record and start digital recording.
3. Close valve D2.	3. Close valve D2.
4. Turn off power to TF-2.	4. Turn off power to TF-2.
5. Set the electrometer to the 10×10^{-11} A range.	2. Close valve T3 and open valve T2.
3. Open valve T2. Watch the signal at $m/z = 40$ and change the electrometer range as necessary.	3. Wait one minute, then close valve T2.
4. Wait two minutes and then close T2.	4. Set the electrometer to the 10×10^{-11} A range.
	5. Open valve T3. Watch the signal at $m/z = 40$ and change the electrometer range as necessary.

If after either transfer procedure, too much argon for measurement is in the mass spectrometer, a special procedure not written here must be used to reduce the amount of argon without isotopic fractionation.

Isotopic Analysis Of Argon	
1. Set the mass selector to the red 33 mark, set the electrometer to the 0.1×10^{-11} A range, and scan over $m/z = 36$ and $m/z = 37$ to confirm that the baseline will be low enough for accurate measurement of these two peaks.	*Early in an isotopic analysis, it is normal for the baseline to decrease in level and in slope as the cooling titanium in TF-2 absorbs hydrogen. The sloping baseline is due mostly to Ar^+ and CO_2^+ ions scattered by collision with H_2 and other gas molecules.*
2. Take a set of measurements of the argon isotopes, by scanning upward through the mass range from the red 33 mark to beyond the red 40 mark, changing the electrometer range as necessary.	*In a typical argon isotopic analysis, the range will need to be changed from 0.1×10^{-11} A to 1×10^{-11} A for the $m/z = 38$ peak. Change the range when the signal begins to rise sharply as the 38 peak is approached. Another change will typically be needed for the $m/z = 40$ peak.*
3. Return the scanner to the red 33 mark, change to the 0.1×10^{-11} A range, and scan upward again, this time continuing the scan past the red 44 mark. Change the electrometer range as necessary.	*This longer scan will provide useful information about the signals at $m/z = 42$ and 44. As the signal goes down after the $m/z = 40$, peak, change to a more sensitive electrometer range for the small 42 peak and be prepared to change again for the 44 peak.*
4. Take a third scan, through at least $m/z = 40$.	
5. Stop digital recording.	
6. Stop the scanner, set the electrometer to the range used for the 40 peak, and set the mass selector to the red 40 mark.	

Extraction Line Setup *The extraction line setup need be done only if another argon extraction is to be done before daily shutdown.*	
1. Open valve T0.	
2. Remove the liquid nitrogen from around MT-2 and any liquid nitrogen remaining in its cold finger.	*Insert a large Teflon stirring rod into the cold finger to warm it.*
3. Turn on power to TF-1.	

4. Open valve T1.	
Wait at least ten minutes for the extraction line to become fully evacuated and for TF-1 to become hot before beginning "Argon Extraction and Cleanup" (above) for the next sample.	

Mass Spectrometer Setup *The mass spectrometer setup need be done only if another isotopic analysis is to be done before daily shutdown.*	
1. Turn on power to titanium heater TF-2.	
2. Check that the mass selector is set to m/e = 40.	*The electrometer should be set to a range appropriate for the signal.*
3. Check that liquid nitrogen is on trap DT-2.	
4. Open valve D2.	*After a few minutes, the signal at m/z = 40 should be low on the 0.1×10^{-11} A range.*

B 3 Extraction Line Daily Startup

9. Begin the daily chart record as follows: a. (Optional) Advance the chart and remove the record of previous work. b. Turn the chart drive on, at a speed of 30 cm/h or less. c. Put the pen in place and lower it to record. d. Record the date, time, analyst (optional), and chart speed.	*Use the chart to keep a written record of subsequent activity. If the analyst is careful to record all changes in chart speed (preferably along the left side of the chart), the chart will provide a useful time record of the work.* *If the recorder is on STBY, change to REC.* *The steps following this one are written on the assumption that the rough pump has been running at least overnight, valves R1 an R2 are open.*
10. Read and record the pressure, P0, in the rough pumping line.	*P0 should be less than 300 millitorr. A value persistently greater than that indicates either a leak or too much volatile material in the molecular sieve trap (which could be cooled to solve that problem).*

11. Read and record the pressure, P1, in the argon extraction line.	*The value of P1provides information about the state of the extraction line that may be important.*
12. Read and record the pressure, P2, in the line between valve D2 and trap DT-2.	*The value of P2 before the trap DT-2 is cooled provides information about the state of the pumping line that may be important.*
13. Start the turbomolecular pump.	
14. Check that the valves T2, T4, and V1 are closed.	
15. After the turbomolecular pump has reached full speed, 75 K RPM, put liquid nitrogen on the trap DT-2.	*Any water in the small Dewar flask should be removed before the liquid nitrogen is put in it. P2 should be at or near zero soon after the trap is cooled.*
16. Turn on the mass spectrometer as follows: a. Release the zero check button of the electrometer and set the electrometer to the 10×10^{-11} A range. b. Set the mass selector on the MS-10 to the red 36 mark. c. On the MS-10 control panel, turn the Mains switch on and the Filament switch on.	*The position where m/z=40 will be near but not necessarily exactly at the "red 36" mark.* *A signal should appear in about 20 s. Argon invariably accumulates in the mass spectrometer overnight.*
17. Adjust the mass selector as necessary to the top of the $m/z = 40$ peak.	*If there is no signal, likely because there is too much gas in the mass spectrometer, go to the next step.*
18. Open valve D2.	*The driver should be turned counterclockwise two full turns.*
19. Open valve T3.	*The signal at m/z = 40 should decrease (but there may be a transient increase initially).*
20. Turn power on to the titanium heaters (TF-1 and TF-2).	*The signal at m/z = 40 will increase temporarily as the titanium degasses. Allow 20 minutes for degassing before beginning an argon extraction.*

21. Open the valves D1 (if closed) and T0 (if closed).	*Observe P1 and P2 as these valves are opened. If P2 rises, it should return to near zero within a minute or so. The response of P1 will depend largely on how much water was in the extraction line before valve T0 was opened.*
22. Open the valve, F1 or F2, that leads to the part of the line where argon extractions are to occur, if it is not already open.	*The other valve, F1 or F2, should be closed.* *Observe P1 and P2.*
23. Open valve T1.	*Observe P1 and P2.*

B 3 Extraction Line Daily Shutdown

1. Turn off the mass spectrometer as follows: a. On the MS-10 control panel, turn the Filament and Mains switches off. b. Depress the zero check button of the electrometer.	*The shutdown procedures are for the typical situation in which a day's work ends as an isotopic analysis of argon is completed.* *The electrometer is not to be turned off, unless the entire system is to be shut down for a long time.*
2. Check that valve T2 is closed. Close valve T3. Close valve D2 if it is not already closed.	*It is not necessary that the argon from the last isotopic analysis be pumped out of the mass spectrometer before shutdown. There will be plenty of time for that on the next work day.*
3. Check that valves S1 and A1 are closed. Then close valve S0.	*Having these valves closed during periods of inactivity is important to the integrity of the reference gases.*
4. If valve T1 is open, close it.	
5. Stop the turbomolecular pump.	*The screen will show "Ready for local soft start."*
6. Stop the recorder as follows. a. Chart speed = off.	*The recorder is not normally turned off overnight. Optionally, it may be put on standby (STBY).*

b. Lift the pen, remove it, and put the cap over its tip.	*The analyst may choose to remove the chart paper having the record of the day's work, or not.*